Differential Alternative Splicing of a Novel *FGFR3* Variant Involved in African American Prostate Cancer Disparities

by Jacqueline Leigh Olender Moy

B.S. in Biology, May 2011, Northeastern University

A Dissertation submitted to

The Faculty of
The Columbian College of Arts & Sciences
of The George Washington University
in partial fulfillment of the requirements
for the degree of Doctor of Philosophy

May 19, 2019

Dissertation directed by

Norman H. Lee
Professor of Pharmacology and Physiology
and of Biochemistry and Molecular Medicine

The Columbian College of Arts and Sciences of The George Washington University certifies that Jacqueline Leigh Olender Moy has passed the Final Examination for the degree of Doctor of Philosophy as of April 5, 2019. This is the final and approved form of the dissertation.

Differential Alternative Splicing of a Novel *FGFR3* Variant Involved in African American Prostate Cancer Disparities

Jacqueline Leigh Olender Moy

Dissertation Research Committee:

Norman H. Lee, Professor of Pharmacology & Physiology and of Biochemistry and Molecular Medicine, Dissertation Director

Susan Ceryak, Associate Professor of Pharmacology & Physiology, Committee Member

Katherine Kennedy, Professor of Pharmacology & Physiology, Committee Member

© Copyright 2019 by Jacqueline Leigh Olender Moy
All rights reserved

Acknowledgements

First and foremost, I would like to thank my mentor, Dr. Norman H. Lee. Thank you for welcoming me into your lab and introducing me to the world of health disparities. I am grateful for your patience, guidance, understanding, and support over the last five years. I would not be the scientist I am today without you constantly challenging me and believing in me. Thank you for surrounding me with lab mates, past and present, with whom I have had the opportunity to learn from and collaborate, including Dr. Bi-Dar Wang, Dr. Kristen Ceniccola, Kenny Ngyuen, Kaitlin Garofano, Tessa Knox, Chaimae Samtal, and Emily Sun.

I would like to thank my committee members, Dr. Katherine Kennedy, Dr. Susan Ceryak, and Dr. Patricia Latham. Your continued support and enthusiasm for my project has meant the world to me and I appreciate all your guidance and direction. Thank you to Dr. Bernard Kwabi-Addo for serving as my outside examiner.

Science does not occur in isolation and this project is no exception. To all the collaborators who have contributed to this study, Dr. Bi-Dar Wang, Kenny Ngyuen, Dr. Anelia Horvath, Dr. Lana Garmire, Dr. Anastas Popratiloff, Dr. Patricia Latham, Dr. Sylvia Silver, Dr. Ramez Andrawis, and Emily Sun: I could not have done it without you.

A big thank you to the IBS staff who work tirelessly behind the scenes. Thank you to Dr. Linda Werling for seeing the potential within me and creating such a supportive environment. Thank you to Marc Wittlif, Julie Zhu, and Colleen Kennedy for helping me navigate all the non-science requirements of a graduate student.

I have had the privilege of having amazing mentors in my life who have supported and inspired me. To Mrs. Bank, my high school AP Biology teacher who

introduced me to the exciting world of science: You encouraged me pursue a career in biomedical science and my life would not be the same with the enthusiasm and opportunities I experienced in your class. Dr. Phyllis Strauss: Thank you for opening up your lab to a very, very inexperienced college freshman and teaching me the fundamentals I would need to succeed as a scientist. Thank you to Dr. Wendy Smith and Dr. Srikanth Subrimanian for showing me how great working in a collaborative environment with amazing scientists and people can be. Thank you to Dr. Martin Wright and Dr. Julie Su for bringing me onboard your team as an undergraduate co-op student and later as an employee. Your mentorship, guidance, and encouragement made working at Adnexus an incredible learning experience for me.

I would also like to acknowledge all those who supported me outside of the lab throughout my graduate work. A huge hug and thank you to all ladies near and far who went through graduate school alongside me: Jacquelyn Hanson, Tamar Ledoux, Sarah Deasy, Stephanie Perkail, and Eshini Panditharatna. Nancy Forbes, Jacquie Gertz, and Britt Aguilar: Our monthly AWIS mentoring meetings were a lifeline during the last three years. I am so lucky to support and be supported by intelligent and kind women in science. Thank you to Tara Mason and Lauren Philbrick for your constant encouragement and friendship.

I owe my greatest acknowledgements to my family. Thank you to Zack and Sophie for your love and companionship. Gram, thank you for your unconditional love and support. I am indebted to Allie, Amanda, Dom, and Tim for making DC feel like a home. There's nothing quite like sisters and I am lucky enough to have two. To my parents, Jim and Leslee, thank you for always being there for me and encouraging me to

pursue my dreams. And finally, a special thank you to my husband, Jeff. Thank you for believing in me even when I did not always believe in myself. Thank you for being the best (long distance) partner I could have ever asked for.

Abstract of Dissertation

Differential Alternative Splicing of a Novel *FGFR3* Variant Involved in African American Prostate Cancer Disparities

Prostate cancer (PCa) is the most diagnosed cancer in men and the second leading cause of male cancer-related deaths annually in the United States (Siegel, Miller, and Jemal 2019). Despite increased screening and decreasing mortality rates of PCa, African American (AA) men have significantly higher rates of PCa incidence, high-risk cancer, and mortality compared to European American (EA) men (Cooperberg 2013). AA men are 1.7 times more likely to be diagnosed with PCa (DeSantis et al. 2016; Kelly et al. 2017). Additionally, the mortality ratio of AA compared to EA PCa patients (2.4 to 1) is the largest of any other malignancy in the United States (Rebbeck 2017a). Even after adjusting for clinical and epidemiological factors, AA men still have significantly higher occurrence and mortality rates, suggesting differences in biology and genetics may be playing a role in this disparate disease burden (Evans et al. 2008; Tyson and Castle 2014).

Alternative splicing (AS) is the major mechanism for post-transcriptional regulation of gene expression, mRNA diversity, and protein modification. While AS has been shown to play a role in PCa development and progression, a link between AS and PCa health disparities has been largely unexplored. Recently, a novel splice variant of the fibroblast growth factor receptor 3 (*FGFR3*), a known proto-oncogene, was identified as a possible candidate for differential AS (dAS) in AA PCa (Wang et al. 2017). Here, we aim to clone and functionally characterize this heretofore unreported exon 14-skipped splice variant of *FGFR3* and characterize the molecular ramifications of this variant on

PCa oncogenesis. Additionally, we propose that differential gene expression of RNA binding proteins, such as splicing factors, may be an upstream regulator of *FGFR3* dAS.

In this study, we successfully cloned and sequenced a previously unreported splice variant of *FGFR3*. This novel variant lacks exon 14, generating a short variant (*FGFR3-S*) that is predominantly expressed in AA PCa compared to the long variant (*FGFR3-L*) containing exon 14. We show that FGFR3-S promotes increased proliferation, migration, invasion, downstream oncogenic signaling, and decreased caspase activity compared to FGFR3-L. We also demonstrate that FGFR3-S has increased resistance to the pan-FGFR small molecule inhibitor dovitinib both *in vitro* and when examining tumor growth *in vivo*. We have identified seven splicing factors that are differentially expressed in AA versus EA PCa and shown that two, SRSF2 and hnRNPF, are directly involved in exon 14 skipping of *FGFR3*. Knockdown of *SRSF2* and *HNRNPF* leads to splice switching (i.e. preferential exon 14 inclusion over exon 14 skipping), a decrease in invasion and proliferation, and increase in caspase activity. Meanwhile, overexpression of FGFR3-S rescues this decreased oncogenic phenotype. This work identifies a novel *FGFR3* splice variant and supports the hypothesis that dAS plays a crucial role in PCa health disparities.

Table of Contents

Acknowledgements ..... **iv**

Abstract of Dissertation ..... **vii**

List of Figures ..... **x**

List of Tables ..... **xii**

List of Abbreviations ..... **xiii**

Chapter 1: Introduction 1

Chapter 2: Materials and Methods 64

Chapter 3: Verification of *FGFR3* splice variants 95

Chapter 4: Determination of oncogenicity of FGFR3-S compared to FGFR3–L 111

Chapter 5: Determination of differential expression of splicing factors and their contribution to *FGFR3* splicing patterns 130

Chapter 6: Discussion 149

References 165

Appendix 187

List of Figures

Figure 1 New cancer cases and deaths (2010-2014) 3

Figure 2 Prostate cancer trends in SEER incidence rates 2000-2015 by race/ethnicity ... 18

Figure 3 Prostate cancer trends in SEER mortality rates 2000-2015 by race/ethnicity 19

Figure 4 Schematic representations of different types of splicing events 24

Figure 5 Common *FGFR3* alterations by cancer type 52

Figure 6 Validation of *FGFR3* dAS in AA and EA specimens 61

Figure 7 Enrichment of FGFR3-S enhances proliferation in vitro 62

Figure 8 Representative chromatograms of *FGFR3-L* sequencing 97

Figure 9 Representative chromatogram of *FGFR3-S* sequencing 98

Figure 10 Consensus sequences of FGFR3 splice variants 100

Figure 11 Schematic of FGFR3 gene and generation of splice variants 101

Figure 12 PC-3+L, PC-3+S, LNCaP+L, LNCaP+S transfection screen 105

Figure 13 PC-3+vector, LNCaP+vector transfection screen 106

Figure 14 MDA PCa 2b+S, RC77 T/E+S transfection screen 107

Figure 15 MDA PCa 2b+vector, RC77 T/E+vector transfection screen 108

Figure 16 Expression of total FGFR3 was not significantly different in AA and EA PCa specimens 110

Figure 17 Prostate cancer patients with high FGFR3-S/-L ratios have decreased survival 113

Figure 18 FGFR3-S is resistant to dovitinib-mediated inhibition of proliferation 117

Figure 19 FGFR3-S is resistant to dovitinib-mediated inhibition of migration 118

Figure 20 FGFR3-S is resistant to dovitinib-mediated inhibition of invasion 119

Figure 21 FGFR3-S is resistant to docetaxel-mediated activation of caspase 3/7 activity 121

Figure 22 Dovitinib does not augment docetaxel-induced caspase activity 122

Figure 23 FGFR3-S exhibits increased downstream signaling via western blot analysis 125

Figure 24 Cell-free kinase assay protocol 126

Figure 25 FGFR3-S shows no activity in cell-free kinase assay 126

Figure 26 Outline of mouse model experiments 128

Figure 27 FGFR3-S is resistant to dovitinib-mediated inhibition of tumor growth 129

Figure 28 Gene expression of splicing factors in AA and EA PCa specimens 132

Figure 29 Differential expression of SF in AA vs EA PCa specimens 133

Figure 30 SFs are differentially expressed in AA versus EA PCa cell lines 134

Figure 31 SRSF1, SRSF2, and hnRNPF have predicted binding sites in exon 14 sequence space 136

Figure 32 SF knockdown causes splice switching from *FGFR3-S* to *FGFR3-L* variant 139

Figure 33 Splicing factor knockdown decreases oncogenicity of AA PCa 140

Figure 34 Western blot confirms knockdown of splicing factors 141

Figure 35 FGFR3-S overexpression rescues splicing factor knockdown-mediated inhibition of invasion 144

Figure 36 FGFR3-S overexpression rescues splicing factor knockdown-mediated inhibition of proliferation 145

Figure 37 FGFR3-S overexpression rescues splicing factor knockdown-mediated caspase 3/7 activation 146

Figure 38 Western blot confirms knockdown of splicing factors in MDA PCa 2b transfected cells 147

Figure 39 Western blot confirms knockdown of splicing factors in RC77 T/E transfected cells 148

Figure 40 Comparison of FGFR exon 14 sequences 158

Figure 41 FGFR3_GFP construct 160

Figure 42 Proposed mechanism for aberrant splicing of FGFR3 in PCa disparities 164

List of Tables

Table 1 Prostate cancer classification by ETS fusion status and associated mutations 9

Table 2 Prostate cancer treatments 13

Table 3 Summary of splicing events in prostate cancer 40

Table 4 Examples of differential alternative splicing events in PCa and normal specimens 44

Table 5 Summary of FGFR inhibitors 56

Table 6 Prostate cancer cell lines 66

Table 7 RT-PCR primers 67

Table 8 siRNAs 69

Table 9 Biochemical reagents 71

Table 10 Primary antibodies used for immunohistochemistry and immunocytochemistry 71

Table 11 Secondary antibodies used for immunohistochemistry and immunocytochemistry 72

Table 12 Primary antibodies used for western blots 72

Table 13 Secondary antibodies used western blots 73

Table 14 Patient information for IHC 92

Table 15 Vectors used for stable cell line transfection 104

Table 16 Primers used for stable cell line transfection confirmation 104

Table 17 Antibodies used for stable cell line transfection confirmation 104

Table 18 IC_{50} values calculated for PC-3+L, PC-3+S *in vitro* assays 120

Table 19 IC_{50} values calculated for LNCaP+L, LNCaP+S *in vitro* assays 120

Table 20 Differentially expressed genes in AA PCa versus AA normal prostate 162

Table 21 Differentially spliced genes in AA PCa versus EA PCa 162

List of Abbreviations

1. µg: Microgram
2. µl: Microliter
3. 17βHSD4: 17β-Hydroxysteroid dehydrogenase type 4
4. AA: African American
5. aa: Amino acid
6. ABL: Abelson murine leukemia viral oncogene homolog
7. ADP: Adenosine diphosphate
8. ADT: Androgen deprivation therapy
9. AKT: Protein kinase B
10. ALL: Acute lymphoblastic leukemia
11. AL: Activation loop
12. A-loop: Activation loop
13. ALS: Amyotrophic lateral sclerosis
14. ANOVA: Analysis of variance
15. AR: Androgen receptor
16. ARF: Animal Research Facility
17. ARv567es: Androgen receptor variant (exons) 5,6,7 exon skipping
18. ARv7: Androgen receptor splice variant 7
19. AS: Alternative splicing
20. ASO: Antisense oligonucleotide
21. ATCC: American Type Tissue Culture Collection
22. ATM: Ataxia telangiectasia mutated serine/threonine kinase

23. ATP: Adenosine triphosphate
24. AURKA: Aurora kinase A
25. BAK1: BCL2 antagonist/killer 1
26. BAX: BCL2 Associated X, Apoptosis Regulator
27. BCL2L1: B-cell lymphoma 2-like 1
28. BCR: Breakpoint cluster region protein
29. BCS: Body condition score
30. BIF: Bax-Interacting Factor 1
31. BLAST: Basic Local Alignment Search Tool
32. BRAC1,2: Breast cancer type 1,2 susceptibility protein
33. BrdU: 5-bromo-2'-deoxyuridine
34. BSA: Bovine serum albumin
35. BTNL2: Butyrophilin like 2
36. BUD31: BUD31 homolog (Functional spliceosome-associated protein 17)
37. C: Cystine
38. CAPG: Capping protein (actin filament), gelsolin-like
39. CBL: Cbl proto-oncogene
40. CCND1: Cyclin D1
41. CCR7: C-C motif chemokine receptor 7
42. CDH1: Chromodomain helicase DNA binding protein 1
43. CDK4: Cyclin-dependent kinase 4
44. cDNA: Complimentary deoxyribonucleic acid
45. CGI: Cytosine guanine dinucleotide island

46. CHD1: Chromodomain helicase DNA binding protein 1
47. CHGA: Chromogranin A
48. c-Kit: Mast/stem cell growth factor receptor
49. CLK1: CDC like kinase 1
50. cm: Centimeter
51. CML: Chronic meyloid leukemia
52. CMV: Cytomegalovirus
53. CNV: Copy number variation
54. CpG: Cytosine-phosphodiester bond-Guanine
55. CRC: Colorectal cancer
56. CRKL: Crk-like protein
57. CRPC: Castration-resistant prostate cancer
58. CSF1R: Colony stimulating factor 1 receptor
59. C-spine: Catalytic spine
60. D: Aspartic acid
61. DAB: 3,3'-Diaminobenzidine
62. DAG: Diacylglycerol
63. DAPI: 4'6-diamidino-2-phenylindole
64. dAS: Differential alternative splicing
65. DDX5,21,46: DEAD-box helicase 5,21,46
66. Del: Deletion
67. DFG motif: Aspartate-Phenylalanine-Glycine residue at N-terminus of A-loop
68. DHT: Dihydrotestosterone

69. DMD: Duchenne Muscular Dystrophy
70. DMEM: Dulbecco's modified eagle medium
71. DMSO: Dimethyl sulfoxide
72. DNA: Deoxyribonucleic acid
73. DNA-PK: DNA-dependent protein kinase
74. DRE: Digital rectal exam
75. DTT: Dithiothreitol
76. DUSP6: Dual specificity phosphatase 6
77. E: Glutamic acid
78. EA: European American
79. ECL: Enhanced chemiluminescence
80. EDTA: Ethylenediaminetetraacetic acid
81. EGFR: Epidermal growth factor receptor (e.g. ErbB-1)
82. EIF1AX: Eukaryotic Translation Initiation Factor 1A, X-Linked
83. EMT: Epithelial to mesenchyme transition
84. EP300: E1A binding protein P300
85. EPHA: Ephrin type-A receptor
86. ErbB: Erythroblastic oncogene B
87. ERG: Erythroblast transformation-specific-related gene
88. ERK: Extracellular signal-related kinase
89. ESE: Exonic splicing enhancer
90. ESS: Exonic splicing silencer
91. ETS: E26 transformation specific transcription factor

92. ETV: ETS variant
93. EZH2: Enhancer of zeste 2 polycomb repressive complex 2
94. FACS: Fluorescence-activated cell sorting
95. FBS: Fetal bovine serum
96. FFPE: Formalin-fixed paraffin-embedded
97. FGF: Fibroblast growth factor
98. FGFR: Fibroblast growth factor receptor
99. FOXA1: Forkhead box A1
100. FOXO1,O3: Forkhead box O1, O3
101. FOXP1: Forkhead box P1
102. FRET: Fluorescence resonance energy transfer
103. FRS2: FGFR substrate 2
104. G: Gauge
105. G: Glycine
106. GAB1: Grb2-associated-binding protein 1
107. GDP: Guanine diphosphate
108. GEO: Gene Expression Omnibus
109. GFP: Green fluorescent protein
110. GIST: Gastrointestinal stromal tumors
111. GOF: Gain of function
112. GRB2, 14: Growth factor receptor bound protein 2, 14
113. GST: Glutathione S-transferase
114. GTP: Guanine triphosphate

115. GWAS: Genome-wide association studies
116. HCC: Hepatocellular carcinoma
117. HER2: Human epidermal growth factor 2 (e.g. ErbB-2)
118. His: Polyhistidine tag
119. hnRNPF,H1,R,U: Heterogeneous nuclear ribonucleoprotein F,H1,R,U
120. hr: Hour
121. HRP: Horseradish peroxidase
122. HSD17B4: 17-β -Hydroxysteroid dehydrogenase 4
123. HSPG: Heparan sulfate proteoglycan
124. i.p.: Intraperitoneal
125. IACUC: Institutional Animal Care and Use Committee
126. IC_{50}: Concentration of an inhibitor where response/binding is reduced by 50%
127. ICC: Immunocytochemistry
128. IDR: Intrinsically disordered region
129. Ig: Immunoglobulin
130. IG20: Insulinoma glucagonoma clone 20 (e.g. MAP kinase activating death domain)
131. IGF1R: Insulin-like growth factor 1 receptor
132. IHC: Immunohistochemistry
133. IP3: Inositol triphosphate
134. IRB: Institutional Approval Board
135. ISE: Intronic splicing enhancer
136. ISS: Intronic splicing silencer
137. ITGA4: Integrin subunit alpha 4

138. ITGAL, M: Integrin subunit alpha L, M
139. K: Lysine
140. KIT: KIT proto-oncogene receptor tyrosine kinase
141. -L or +L: Long isoform
142. LADD: Lacrimo-auriculo-dento-digital
143. LB: Luria broth
144. LBD: Ligand binding domain
145. LHRH: Luteinizing hormone-releasing hormone
146. M: Methionine
147. M: Molar
148. MAPK: Mitogen-activated protein kinase
149. MB: Megabase
150. mCRPC: Metastatic castration-resistant prostate cancer
151. MDB2: Methyl-CpG-binding domain protein 2
152. MED1: Mediator complex subunit 1
153. MEK: Mitogen-activated protein kinase kinase
154. MET: MET proto-oncogene, receptor tyrosine kinase
155. MFA: Medical Faculty Associates
156. min: Minute
157. miRNA: microRNA
158. ml: Milliliter
159. mm: Millimeter
160. mPCa: Metastatic prostate cancer

161. mRNA: messenger RNA
162. MST1R: Macrophage stimulating 1 receptor
163. mTORC: Mammalian target of rapamycin complex
164. Mut: Mutation
165. MYC: MYC proto-oncogene (BHLH transcription factor)
166. N: Asparagine
167. NCAM1: Neural cell adhesion molecule 1
168. NCBI: National Center for Biological Information
169. NCOA2: Nuclear receptor coactivator 2
170. NCOR2: Nuclear receptor corepressor 2
171. NE: Neuroendocrine
172. NEPC: Neuroendocrine prostate cancer
173. NF1: Neurofibromin 1
174. NKX3.1: NK3 homeobox 1
175. nm: Nanometer
176. NOD/SCID: Non-obese diabetic /severe combined immune deficiency
177. NS: Nonsense
178. NSCLC: Non-small cell lung carcinoma
179. NSE: Neuron-specific enolase 2
180. NuRD: Nucleosome remodeling and deacetylase
181. Opti-MEM: Minimal essential medium, reduced serum medium
182. p.o.: *Per os* (oral administration)
183. -p: Phosphorylated

184. P: Proline

185. *p*: Test statistic (p-value)

186. P53: Tumor protein 53

187. PAGE: Polyacrylamide gel electrophoresis

188. PAK3,7: P21 (RAC1) activated kinase 3,7

189. PAK1IP1I : PAK1 interacting protein 1

190. PARP: Poly ADP-ribose polymerase

191. PBS: Phosphate buffered saline

192. PBST: Phosphate buffered saline Tween 20

193. PCa: Prostate cancer

194. PCR: Polymerase chain reaction

195. PCSK6: Proprotein convertase sutilisin/kexin type 6

196. PDGFR: Platelet-derived growth factor receptor

197. PDK1: Phospholipid dependent kinase 1

198. PD-L1: Programmed death-ligand 1

199. Ph+, Philadelphia chromosome positive

200. PHLPP1: PH domain and leucine rich repeat protein phosphatase 1

201. PI3K: Phosphoinositide 3-kinase

202. PIK3CA,D: Phosphatidylinositol-4,5-bisphosphate 3-kinase catalytic subunit alpha, delta

203. PIN: Prostatic intraepithelial neoplasia

204. PIP2: PtdIns(4,5)P2

205. PKC: Protein kinase c

206. PLCγ: Phospholipase-C gamma

207. P-loop: Nucleotide binding loop

208. PPA1: Pyrophosphatase (inorganic) 1

209. pre-mRNA: Precursor-mRNA

210. pro-GDF15: Pro-growth differentiation factor 15 (e.g. prostate differentiation factor)

211. PSA: Prostate specific antigen

212. PtdIns(3,4,5)P3: Phosphatidylinositol (3,4,5)-trisphosphate

213. PTEN: Phosphatase and tensin homolog

214. PVDF: Polyvinylidene fluoride

215. QI-FRET Quantitative imaging-fluorescence resonance energy transfer

216. qPCR: Quantitative polymerase chain reaction

217. R: Arginine

218. RACE: Rapid amplification of cDNA ends

219. RAF: RAF proto-oncogene serine/threonine kinase

220. RARRES2: Retinoic acid receptor responder 2

221. RASGRP2: RAS guanyl releasing protein 2

222. RB: Retinoblastoma

223. RBM39: RNA binding motif protein 39

224. RBP: Ribosomal binding proteins

225. RCC: Renal cell carcinoma

226. RNA: Ribonucleic acid

227. ROI: Regions of interest

228. ROX: Carboxy-x-rhodamine

229. RPMI: Rosewell Park Memorial Institute medium

230. R-spine: Regulatory (hydrophobic) spine
231. RT: Reverse transcription
232. RTK: Receptor tyrosine kinase
233. -S or +S: Short isoform
234. S: Serine
235. SAM68: Src-associated substrate in mitosis of 68 kDa
236. SCLC: Squamous cell lung carcinoma
237. SD: Standard deviation
238. SDS: Sodium dodecyl sulfate
239. SEF: Similar expression to *Fgf*
240. SEM: Standard error of the mean
241. SF: Splicing factor
242. SF3B1: Splicing factor 3b subunit 1
243. SH2,3: Src homology domain 2,3
244. SH3GLB1: SH3 domain-containing GRB2-like protein B1
245. SHP2: Src homology region 2-containing protein tyrosine phosphatase 2
246. siRNA: Short-interfering RNA
247. SMI: Small molecule inhibitor
248. SNAI1: Snail family transcriptional repressor 1
249. SNP: Single nucleotide polymorphism
250. snRNA: Small nuclear RNA
251. snRNP: Small nuclear ribonucleoprotein
252. SOC: Super optimal broth with catabolite repression

253. SOS: Son of sevenless
254. SPINK1: Serine peptidase inhibitor, kazal type 1
255. SPOP: Speckle type BTB/POZ protein
256. SPRY: Sprouty RTK signaling antagonist
257. SR: Serine/arginine protein
258. Src: SRC proto-oncogene, non-receptor tyrosine kinase
259. SRE: Splicing regulatory elements
260. SRRM4: Serine/arginine repetitive matrix 4
261. SRPK1,2: SRSF protein kinase 1,2
262. SRSF1,2,6,7: Serine/arginine splicing factor 1,2,6,7
263. ST6GalNac1: ST6 N-acetylgalactosaminide alpha-2,6-sialyltransferase 1
264. STAT: Signal transducer and activator of transcription
265. Sub-cu: Subcutaneous
266. SYP: Synaptophysin
267. TACC3: Transforming acidic coiled-coil containing protein 3
268. TBE: Tris borate ethylenediaminetetraacetic acid
269. TCGA: The Cancer Genome Atlas
270. TF: Transcription factor
271. TKI: Tyrosine kinase inhibitor
272. TM: Transmembrane
273. TMB: Tetra-methylbenzidine
274. TMPRSS2: Transmembrane protease
275. TP53: Tumor protein P53

276. Tris: Tris(hydroxymethyl)aminomethane
277. TSC2: Tuberous sclerosis complex subunit 2
278. Tyr: Tyrosine
279. U2AF1:U2 small nuclear RNA auxiliary factor 1
280. UBE2C: Ubiquitin Conjugating Enzyme E2 C
281. UCC: Urothelial cell carcinoma
282. UV: Ultraviolet
283. V5: SV5 PK epitope tag
284. VEGF: Vascular endothelial growth factor
285. VEGFR: Vascular endothelial growth factor receptor
286. WGA: Wheat germ agglutinin
287. wt: Wildtype

Chapter 1: Introduction

A. Prostate cancer

B. Prostate cancer health disparities

C. Molecular differences in African American prostate cancer

D. Alternative splicing

E. Alternative splicing and cancer

F. Alternative splicing and prostate cancer

G. Alternative splicing and prostate cancer health disparities

H. Fibroblast growth factor family

I. Fibroblast growth factor receptors and disease

J. Fibroblast growth factor receptor inhibitors

K. *FGFR3* has been identified as a possible candidate for dAS in PCa disparities

L. Statement of problem

A. Prostate cancer

Prostate cancer (PCa) is the most diagnosed cancer in men in the United States and accounts for over one-fifth of all newly diagnosed cancers in men (Siegel, Miller, and Jemal 2019) (**Figure 1**). More than 174,000 new cases are diagnosed each year. PCa is the second leading cause of male cancer-related deaths annually in the U.S with an estimated 31,620 deaths in 2019 (Siegel, Miller, and Jemal 2019). In 2015, over 1.6 million cases and 366,000 deaths were reported globally (Fitzmaurice et al. 2017). PCa has the highest heritability of any cancer at 10% (Lynch et al. 2016). First-degree relatives have 4-fold higher risk of developing PCa compared to the general population (Attard et al. 2016).

Figure 1 New cancer cases and deaths (2010-2014)

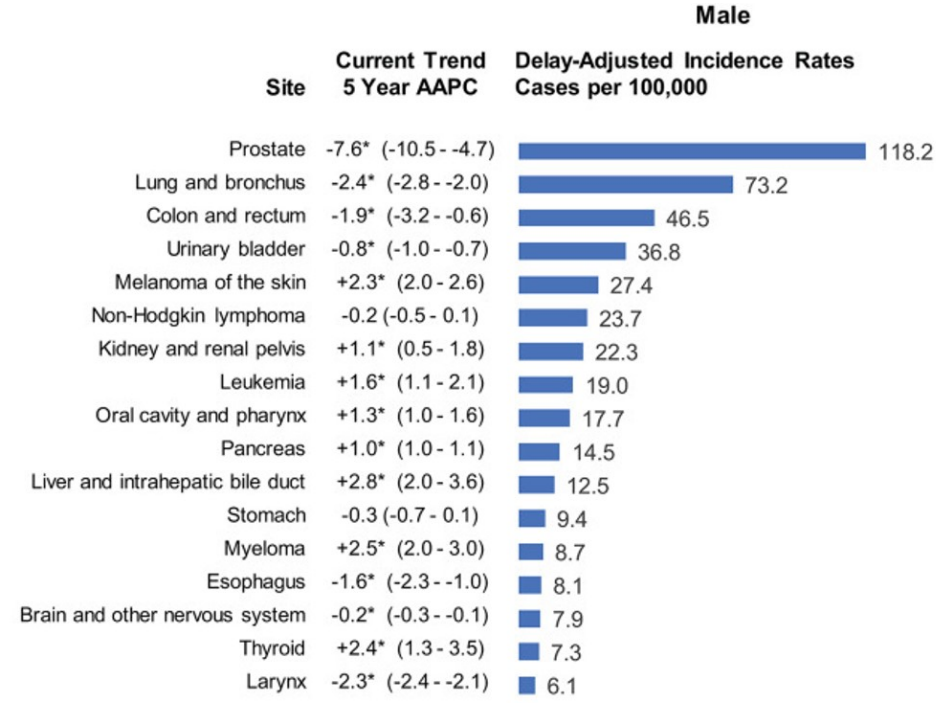

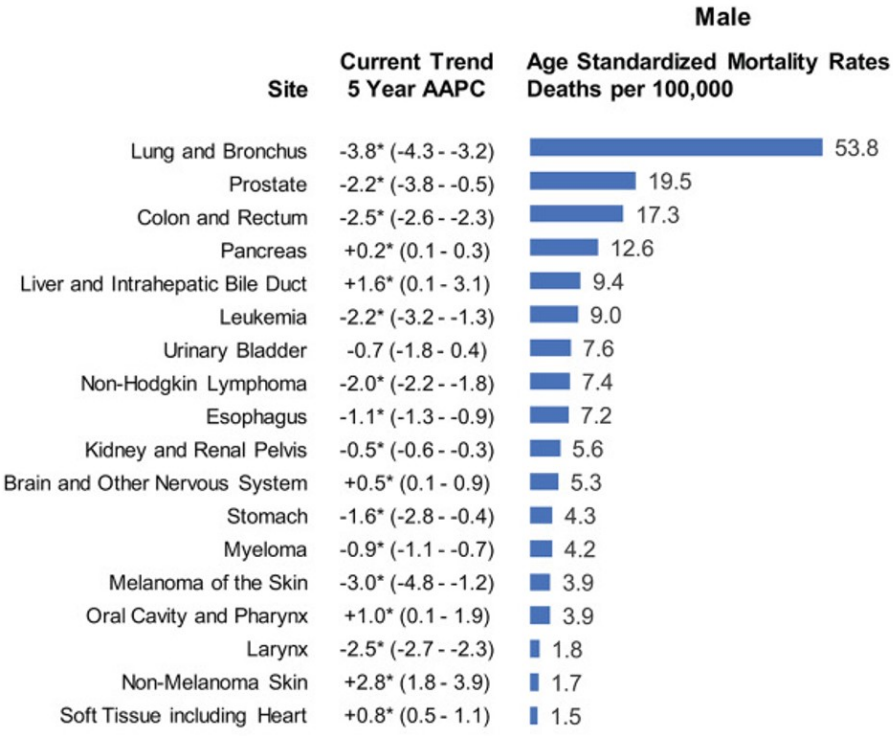

Age-standardized, delay-adjusted incidence rates and death rates (2010-2014) for common cancers in men. The 5-year average annual percent change (AAPC) is based on the joinpoint trend from 1999 to 2014. An asterisk indicates that the AAPC is statistically significantly different from zero (2-sided t test or Z test; $P < .05$). Modified from Cronin et al. 2018.

PCa is considered clinically and molecularly heterogeneous between patients and within tumors (Barbieri and Tomlins 2015). The majority of PCa cases are adenocarcinomas that originate in the luminal or basal gland epithelial of the prostate (Stoyanova et al. 2013; Wang et al. 2009). PCa develops from asymptomatic prostatic intraepithelial neoplasia (PIN). As PCa progresses, patients may experience problems urinating, blood in semen or urine, erectile dysfunction, pain in hips, spine, or ribs, weakness or numbness in legs or feet, and/or loss of bladder or bowel control ("Prostate Cancer" 2019). Main secondary sites for PCa metastasis are bone, lymph nodes, and lungs. Although PCa remains a disease of older men, increased use of detection methods and screening has led to increased diagnosis in younger men (Brawley 2012). Diagnosis is a combination of family history, measurement of prostate specific antigen (PSA) levels, digital rectal exam (DRE), and biopsies.

In order to determine pathological stage, predict disease progression, and design a treatment plan, clinicians classify PCa using three methods: Gleason score, TNM staging, and genetic characterization. PCa is graded by the assignment of a Gleason score based on histology patterns that take into account levels of gland architecture and cell differentiation (Lopez-Beltran et al. 2006). Tissue from needle core biopsies or radical prostatectomies are observed at low magnification and areas of gland architecture are divided into five patterns (or grades) based on decreasing differentiation. The most prevalent (primary) and second most prevalent (secondary) grades are summed to obtain the final Gleason score. Grades 2-4 (representing benign hyperplasia or very early PCa) are rarely seen. Grades 5-6 indicate low grade disease or low rates of progression post therapy. Grades 7-10 are associated with highly aggressive tumors with poor prognosis.

The American Joint Committee on Cancer has developed a staging system for solid tumors (Amin et al. 2017). The TNM staging system measures the extent of the tumor (T), the spread to lymph nodes (N), presence of metastases (M), and PSA level. Tumor extent is determined clinically (cT), based on DRE, biopsy, imaging, and physical exam results, or pathologically (pT), based on radical prostatectomy tissue. Each staging group is ranked from 0-4 and sectioned into final staging I-IV (A-D) categories.

Genetic alterations

At the genomic level, PCa is characterized by a low overall mutation rate (~1 mutation per MB) accompanied by large chromosomal rearrangements and gene amplifications (Attard et al. 2016; Lindberg et al. 2013; Liu et al. 2009; Taylor et al. 2010). In general, the most commonly altered genes in PCa are: *AR*; *ETS* family gene fusions; *SPOP, TP53, PTEN* (point mutations); *CHD1* (deletion); *SPINK1* (overexpression); and *FOXA1* (mutation and overexpression). (Barbieri and Tomlins 2015; Rubin and Demichelis 2018).The major alterations observed in PCa are summarized below.

Androgen signaling dysregulation: The androgen receptor (AR) is a steroid nuclear hormone that plays a major role in normal prostate homeostasis and PCa development. Genomic alterations in the AR increase ligand-independent signaling and decrease sensitivity to anti-androgen therapies. AR signaling is the most commonly modified/mutated signal transduction pathway in PCa (Robinson et al. 2015). Gain of function (GOF) point mutations (W741R, V757A, R846G, H874Y, and T877A) in the ligand and drug binding domains, as well as deletions in the zinc finger domain (deletion

of G589-A628 and associated regions of exon 3) have been identified (Jiang et al. 2010; Yadav et al. 2015). Many AS variants of the *AR* have been identified, including the clinically relevant ARv7 and ARv567es variants.

Whole genome sequencing (WGS) has identified alterations in downstream modulators such as *NCOA2, EP300, NCOR2, FOXA1, FOXP1, FOXO1,* and *FOXO3* (Barbieri et al. 2013; Lindberg, Mills, et al. 2013; Robinson et al. 2015). Metastases in patients who have been treated with androgen therapies and/or have castration resistant PCa (CRPC) almost always have amplifications, mutations, and/or splice alterations of *AR* (Barbieri and Tomlins 2015).

Pathway activation - Oncogenes: Upregulation of the receptor tyrosine kinase (RTK)/RAS/MAPK pathway occurs in the majority of PCa cases and is especially common in metastatic disease (Barbieri and Tomlins 2015). RTKs, *SPINK1* overexpression, and *KRAS* and *RAF* activation are some of the more frequent ways this pathway is activated (Ateeq et al. 2011; Barbieri and Tomlins 2015). HER2 overexpression is also a marker for poor PCa prognosis (Berger et al. 2006).

The PI3K/AKT/PTEN pathway is altered in 25-70% of PCa, through gain of function alterations in pathway members or loss of function alterations in pathway regulators (Barbieri and Tomlins 2015; Robinson et al. 2015). Almost 50% of metastatic CRPC (mCRPC) tumors have PI3K pathway somatic mutations (Barbieri and Tomlins 2015). PTEN deactivates PI3K signaling by dephosphorylating lipid-signaling molecules (Cairns et al. 1997). PTEN loss of function mutations or deletions are found in 20-60% metastatic PCa cases (Donovan and Cordon-Cardo 2013). Deletion of another PI3K pathway regulator, PHLPP1, is also deleted in PCa (Chen et al. 2011).

Co-amplification of AURKA, a serine-threonine kinase, and N-MYC, a transcription factor (TF), in PCa cases may be indicative of neuroendocrine prostate cancer (NEPC), a rare aggressive lethal resistant variant of PCa (Beltran et al. 2011; Otto et al. 2009). The promoter regions of *AR* and *FOXA1* contain *cis*-acting binding sites for N-MYC (Freedman et al. 2011). Additionally, a non-coding single nucleotide polymorphism (SNP) at 8q24 affects *MYC* expression and confers PCa risk (Ahmadiyeh et al. 2010).

Pathway inactivation - Tumor suppressors: The major tumor suppressors inactivated in PCa are P53 and RB. Over 40% of PCa have mutations in P53 at the primary and secondary site and P53 mutations are associated with decreased sensitivity to radiation treatment (Menon et al. 2013; Robbins et al. 2011). RB deletion occurs in 45% of CRPC and is associated with increased AR expression (Sharma et al. 2010).

Gene fusions: E26 transformation specific transcription factor (ETS) family gene fusions are the most common genetic mutation in PCa (Rubin and Demichelis 2018). These gene fusions are defined as the 5' UTR of an AR-regulated gene fused to the coding sequence of an ETS transcription factor (TF) family member (e.g. *TMPRSS2-ERG, TMPRSS2-ERG-ETV*) or coding sequences of other gene families (e.g. *SLC45A3-BRAF*) (Barbieri and Tomlins 2015; Robinson et al. 2015). Over 10 different non-ETS genes and over four ETS genes (*ETV1, ETV4, ETV5,* and *FLI1*) involved in gene fusions have been identified (Barbieri and Tomlins 2015; Robinson et al. 2015). Different combinations of gene fusions are mutually exclusive and absent from normal prostate tissue, benign prostate tissue and other tumors (Palanisamy et al. 2010; Tomlins et al. 2005). *TMPRSS-ERG* fusions are the most common and occur in 50-60% patients and is

>99% indicative of PCa (Rosen et al. 2012). Gene fusion status and associated mutation status is used to classify PCa tumor types (**Table 1**) (Attard et al. 2016).

Table 1 Prostate cancer classification by ETS fusion status and associated mutations

ETS fusion status	Associated mutations	Occurrence	Reference
ETS positive	*PTEN, TP53*	50-60%	(Attard et al. 2016)
ETS negative	*PTEN, TP53* loss	40%	(Barbieri et al. 2012; Lindberg, Mills, et al. 2013)
ETS negative	*RAS*, *RAF*, or *FGFR* family	1-2%	(Attard et al. 2016)
ETS negative	*CHD1* homozygous deletions	5-15%	(Barbieri et al. 2017; S Huang et al. 2012; Lindberg, Mills, et al. 2013; W Liu et al. 2012; Taylor et al. 2010)
ETS negative	*SPINK1* overexpression	5-10%	(Rubin, Maher, and Chinnaiyan 2011)
ETS negative	*SPOP*	5-15%	(Attard et al. 2016)

Abbreviations: ETS, E26 transformation specific transcription factor; PTEN, phosphatase and tensin homolog; TP53, tumor protein P53; RAF, RAF proto-oncogene serine/threonine kinase; FGFR, fibroblast growth factor receptor; CHD1, chromodomain helicase DNA binding protein 1; SPINK1, serine peptidase inhibitor, kazal type 1; SPOP, speckle type BTB/POZ protein.

Chromoplexy: Chromoplexy is the distinct breaking and rejoining of DNA. These breakpoints can cause copy number variants (CNVs) and chromosomal rearrangement (Baca et al. 2013). Chromoplexy events affecting the expression of *PTEN*, *CHD1*, and *TP53* are very common in early onset PCa cases (Barbieri and Tomlins 2015).

Epigenetics: PCa is characterized by an overall increase in CpG dinucleotide island (CGI)-specific methylation and generally correlates with gene inactivation and disease severity (Lin et al. 2013). Increased methylation is most common at chromosomal translocations and promoter regions of certain genes, such as retinoic acid receptor responder 2 (*RARRES2*) and that of capping protein *(*actin filament*),* gelsolin-like (*CAPG*) (Lin et al. 2013).

Chromatin regulation: Direct or indirect changes in the regulation of chromatin can have an impact on gene expression. Homozygous deletions of the chromodomain helicase DNA binding protein 1 (*CHD1*) gene, encoding a major chromatin remodeling enzyme, are found in 5-10% of PCa cases. This deletion is mutually exclusive with *TMPRSS2-ERG* fusions (Rubin, Maher, and Chinnaiyan 2011). Overexpression of *EZH2*, encoding a histone methyltransferase, causes activation of TF genes, specifically AR (Xu et al. 2012). Mutations in genes that alter H3 methylation are very common in PCa patients (Barbieri and Tomlins 2015).

DNA repair pathway dysregulation: Breast cancer type 1,2 susceptibility protein 1 and 2 (*BRAC1* and *BRAC2*) familial germline mutations confer increased risk and early onset of PCa (Attard et al. 2016). Deletions in *ATM* are also common in PCa (Taylor et al. 2010). Other genes that are silenced through loss, mutation, or hypermethalation include *SPOP*, which encodes the substrate recognition component of a CUL3-based E3

ubiquitin ligase, and *NKX3.1*, encoding an AR-regulated tumor suppressor that protects against oxidative damage via DNA repair (Asatiani et al. 2005; Barbieri et al. 2012).

Immune system regulation modulation: Missense mutations in *BTNL2*, which encodes a histocompatibility complex in a major family of immunoregulators, are associated with increased susceptibility for PCa (Fitzgerald et al. 2013). Butyrophilin-like receptors modulate T-cell function and negatively regulate interactions with epithelial cells and cytokine production (Abeler-Dörner et al. 2012; Rhodes, Reith, and Trowsdale 2016).

Treatments and therapies

Due to the long natural history accompanied by long term follow ups and complexity of disease classification, selection of the ideal management strategy for PCa is difficult (Fitzmaurice et al. 2017). Treatment plans for PCa are devised based on risk assessment, taking into account the patient's age, tumor stage, PSA serum levels, Gleason score, and biopsy results (**Table 2**) (Attard et al. 2016). Clinical disease varies widely between patients, from indolent disease that requires no immediate treatment and is often over treated, to aggressive disease. In addition, the clinical response to therapy also has wide variability, from patients who are disease-free for years before a recurrence to patients who experience immediate relapse. It is oftentimes difficult for clinicians to determine specifics in tumor characteristics and progression rate before treatment due to the heterogeneous nature of PCa (Cheng et al. 1998; Lindberg, Klevebring, et al. 2013; Yadav et al. 2015).

When a patient's disease progresses from PIN to localized PCa, the patient either enters an active surveillance period (monitoring PSA levels and occasional biopsies without treatments) or goes into remission after localized therapy. Local treatments include radical prostatectomy, external-beam radiotherapy, brachytherapy, cryotherapy, high-intensity focal ultrasound, and photodynamic therapy, with or without chemotherapies (e.g. docetaxel, carboplatin) (Attard et al. 2016). Low grade, localized PCa (Gleason score < 6) has a 99% five-year survival rate (Brawley 2012; Siegel, Miller, and Jemal 2015). Patients with high-risk, localized PCa undergo a more aggressive treatment course of AR-deprivation therapy and radical radiotherapy. If the genetic makeup of the tumor indicates a good match for a targeted therapy, small molecule inhibitors (SMIs) against PI3K/AKT/mTOR pathway, IGF, or VEGF can be used. Most often, AR-deprivation therapies that block androgen signaling are used for more aggressive disease (Attard et al. 2016).

Disease recurrence is accompanied by increasing PSA levels and is no longer responsive to androgen deprivation therapies. Many patients develop CRPC and mCRPC that spreads to the bones (causing bone pain, fractures, and spinal cord compression), lungs, and lymph nodes. Less than 30% of patients with metastatic PCa survive past five years (Brawley 2012; Lapuk et al. 2014; Noone et al. 2018; Siegel, Miller, and Jemal 2015). PCa metastasizes to bone more frequently and consistently than any other malignancy, with over 70% of PCa patients developing bone metastases (Hensel and Thalmann 2016). Treatments for mCRPC include CYP17 inhibitors, anti-androgens with steroids, taxane chemotherapies, osteoclast inhibitors, radiopharmaceuticals, and anti-PSA vaccines.

Table 2 Prostate cancer treatments

Treatment/ Target	Generic Name	Trade Name	Company	Stage
Active surveillance				Early/localized
Radiation therapy				Early/localized
ADT (Surgical castration)				Early/localized
Corticosteroids	Dexa-methasone	Ozurdex	Allergan Inc.	
	Prednisone	Deltasone, Rayos, Prednisone Intensol	Pharmacia & Upjohn Inc., Horizon Pharma USA Inc., Roxane Laboratories Inc.	
LHRH agonist	Goserelin	Zoladex	TerSera Pharmaceuticals	High-risk/advanced
	Histrelin	Vantas	Endo Pharmaceuticals Solutions Inc.	High-risk/advanced
	Leuprolide	Lupron Depot, Eligard	Abbvie, Tolmar Pharmaceuticals	High-risk/advanced
	Triptorelin	Trelstar	Allergan Inc.	High-risk/advanced
LHRH antagonist	Degarelix	Firmagon	Ferring Pharmaceuticals	Advanced
CYP17 inhibitor	Abiraterone	Zytiga	Janssen Biotech Inc.	Advanced (high risk/CRPC)
Anti-androgen	Apalutamide	Erleada	Janssen Biotech Inc.	mCRPC
	Bicalutamide	Casodex	AstraZeneca Pharmaceuticals	mCRPC
	Darolutamide	BAY1841788	Bayer (Orion)	mCRPC
	Enzalutamide	Xtandi	Astellas Pharma US Inc., Pfizer Inc.	mCRPC
	Flutamide	Eulexin	Schering Corporation	mCRPC
	Ketoconazole	Nizoral	Janssen Biotech Inc.	mCRPC
	Nilutamide	Nilandron	Concordia Pharmaceuticals Inc.	mCRPC
Cytotoxic chemotherapies	Cabazitaxel	Jevtana	Sanofi-Aventis (Genzyme)	mCRPC
	Carboplatin	Paraplatin	Pfizer Inc.	mCRPC
	Docetaxel	Taxotere	Sanofi-Aventis	mCRPC
	Estramustine	Emcyt	Pfizer Inc.	mCRPC

	Mitoxantrone	Novantrone	Amgen Inc. (Immunex)	mCRPC
	Temozolo-mide	Temodar	Merck	CRPC
Vaccine	Sipuleucel-T	Provenge	Dendreon Pharmaceuticals	Advanced with few symptoms
Osteoclast inhibitor	Denosumab	Xgeva, Prolia	Amgen Inc.	Bone metastasis
	Zoledronic acid	Zometa	Novartis Pharmaceuticals	Bone metastasis
Radiopharmaceuticals	Radium-223	Xofigo	Bayer	mCRPC
	Samarium-153	Quadramet	Lantheus Medical Imaging Inc.	mCRPC
	Strontium-89	Metastron	GE Healthcare (Medi-Physics Inc.)	mCRPC
PI3K/AKT/mTORC	AZD2014	Vistuserib	AstraZeneca	High-risk
	AZD5363	Capivasertib	AstraZeneca	CRPC
	AZD8186		AstraZeneca	CRPC
	BKM120	Buparlisib	Novartis Pharmaceuticals	High-risk
	Everolimus	Afinitor	Novartis Pharmaceuticals	CRPC
	GDC-0980	Apitolisib	Genentech	CRPC
	GSK2636771		GlaxoSmithKline plc	CRPC
	LY3023414		Lilly	CRPC
	MK2206		Merck	recurrent
	MK8669	Ridaforolimus	Merck	Taxane-resistant, AR independent
	MLN0128/TAK-228	Sapanisertib	Millenium Pharmaceuticals	CRPC
	RG7440	Ipatasertib	Roche	CRPC
	Ridaforolimus	MK-8669	ARIAD Pharaceuticals	AR independent
	Sirolimus	Rapamune	Pfizer Inc.	CRPC
	Temsirolimus	Torisel	Pfizer Inc.	High-risk
IGF1R	IMC-A12	Cixutumumab	Eli Lilly	CRPC
VEGF	Bevacizumab	Avastin	Genentech	Advanced
VEGFR	Cediranib	AZD2171	AstraZeneca	CRPC
DNA-PK/mTORC	CC-115		Celgene	CRPC
PARP	ABT-888	Veliparib	AbbVIe	CRPC

	Niraparib	Zejula	TESARO Inc.	CRPC
	Olaparib	Lynparza	KuDOS Pharmaceuticals	High-risk
	Rucaparib	Rubraca	Clovis Oncology	CRPC
PD-L1	Atezolizumab	Tecentriq	Genentech	CRPC
	Avelumab	Bavencio	Pfizer Inc., EMD Serono	mPCa
	Durvalumab	Imfinzi	Medimmune, AstraZeneca	mPCa
	Pembrolizu-mab	Keytruda	Merck	CRPC

Treatments for PCa, generic and trade names of drugs, company, and stage of PCa approved for treatment. Abbreviations: ADT, androgen deprivation therapy; LHRH, luteinizing hormone-releasing hormone; PI3K, phosphoinositide 3-kinase; AKT, protein kinase B; mTORC, mammalian target of rapamycin complex; IGF1R, insulin-like growth factor 1 receptor; VEGF, vascular endothelial growth factor; VEGFR, vascular endothelial growth factor receptor; DNA-PK, DNA-dependent protein kinase; PARP, poly ADP-ribose polymerase; PD-L1, Programmed death-ligand 1; CRPC, castration resistant prostate cancer; mCRPC, metastatic castration resistant prostate cancer; mPCa, metastatic prostate cancer; AR, androgen receptor.

Controversies in the field

Even with the increased knowledge of PCa causation and progression, no improvement in patient survival has been seen in 20 years (Wu et al. 2014). Controversies in the field center on patient screening, treatment of localized disease, classification of tumor subtypes, identification of high risk patients and patients at risk for advanced disease, and treatment schedules (Attard et al. 2016). PSA testing is also contentious as its low specificity often leads to over diagnosis and over treatment. A recent alternative testing method that adjusts PSA values for prostate size is a more sensitive and specific measure of PCa risk and may be more valuable for diagnosis once it is incorporated into clinics (Jue et al. 2017). Finally, identification of risk alleles that are clinically meaningful (e.g. can be translated to new treatment recommendations) are rare in contrast to other cancer sites (Rebbeck 2017b).

B. Prostate cancer health disparities

In addition to family history, well established risk factors of PCa include Lynch syndrome, age, and race/ethnicity (Brawley 2012; Powell 2007). Due to increased access to health care and screening, higher incidence rates of PCa are reported in developed countries. Despite increased screening and overall decreasing mortality rates of PCa, African American (AA) men have significantly higher rates of PCa incidence, high-risk cancer, and mortality (Cooperberg 2013).

AA men are 1.7 times more likely to be diagnosed with PCa at any age and five times more likely to be diagnosed under 50 years of age (**Figure 2**) (DeSantis et al. 2016; Kelly et al. 2017). AA men also have a 2.4 times greater mortality rate compared to

European American (EA) men (**Figure 3**). This mortality ratio is the largest of any other malignancy in the United States (Rebbeck 2017a). In 2015, AA men were diagnosed at a rate of 157.6 per 10,000 compared to EA men at 93.9 per 10,000 and the mortality rate of AA men with PCa was 37.5 per 10,000 versus EA men at 17.7 per 10,000 (Noone et al. 2018). Additionally, PCa appears to develop at an earlier age in AA men who present with significantly higher PSA plasma levels, more clinically advanced disease, and develop higher grade metastatic disease at a 3- to 4-fold greater rate (Chornokur, Dalton, Borysova, and Kumar 2011; Martin, Starks, and Ambs 2013; Oltean et al. 2006; Powell and Bollig-Fischer 2013). This health disparity has been attributed to epidemiological differences in socioeconomic status, health seeking behavior, access to healthcare, and biased treatment plans (Chornokur et al. 2011; Martin, Starks, and Ambs 2013). Even after adjusting for clinical and epidemiological factors, however, AA men still have significantly higher occurrence and mortality rates (Evans et al. 2008; Robbins, Whittemore, and Thom 2000; Tyson and Castle 2014). This disease disparity suggests that genetic ancestry plays an important role in PCa incidence, progression, and aggressiveness.

Figure 2 Prostate cancer trends in SEER incidence rates 2000-2015 by race/ethnicity

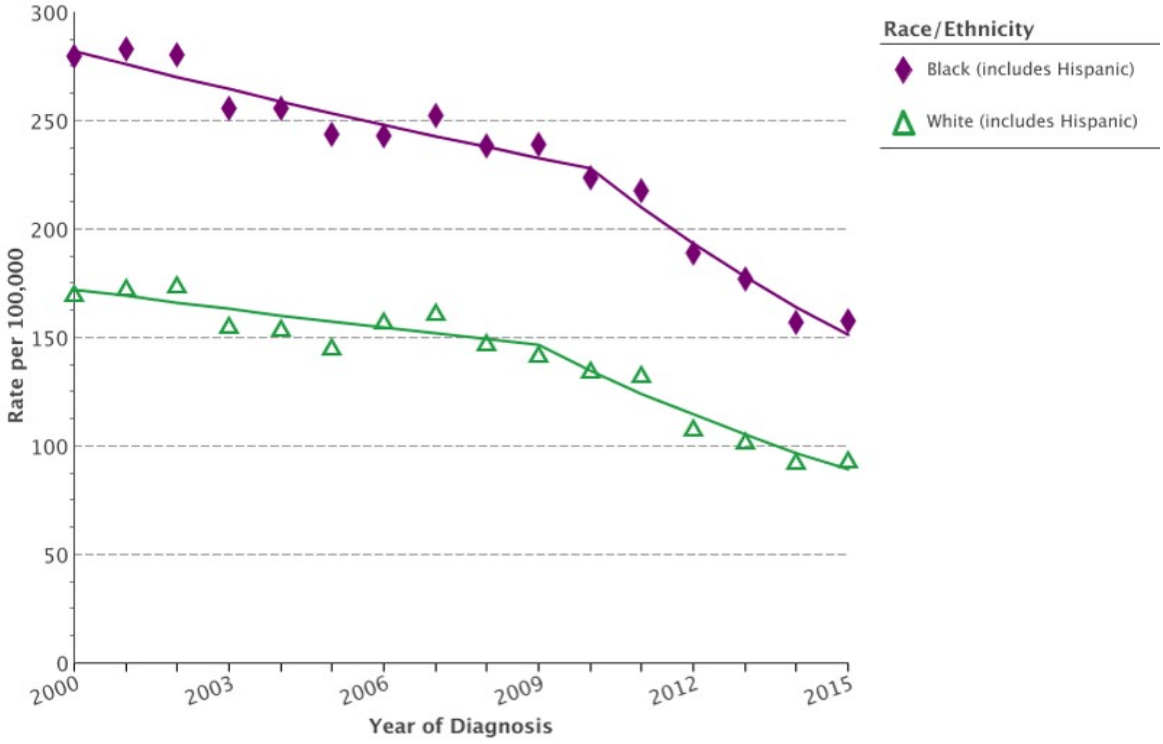

Prostate cancer incidence trends of black (AA) and white (EA) men in the United States. Rates are per 100,000 and are age-adjusted to the 2000 US Std Population. Cancer incidence rates adjusted for reporting delay. The Annual Percent Change (APC) estimates were calculated from the underlying rates using the Joinpoint Trend Analysis Software, Version 4.6, February 2018, National Cancer Institute. Modified from seer.cancer.gov (Noone et al. 2018).

Figure 3 Prostate cancer trends in SEER mortality rates 2000-2015 by race/ethnicity

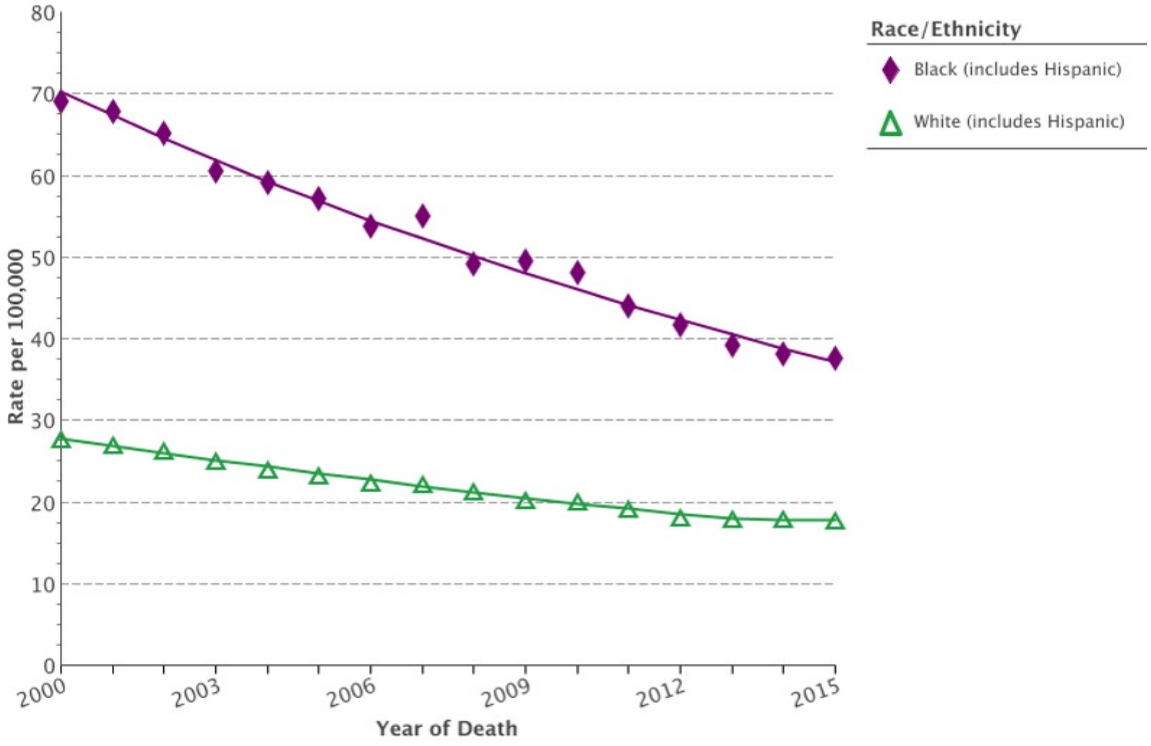

Prostate cancer mortality trends of black (AA) and white (EA) men in the United States. Rates are per 100,000 and are age-adjusted to the 2000 US Std Population. Cancer mortality rates provided by US Mortality Files, National Center for Health Statistics, CDC. Modified from seer.cancer.gov (Noone et al. 2018).

C. Molecular differences in African American prostate cancer

Multiple studies have shown genetic and biological differences in prostate tumors in AA and EA patient populations. *TMPRSS2-ERG* gene fusions and *PTEN* deletions were once thought to be characteristic of all prostate tumors. However, recent reports have shown these genetic alterations occur at a much lower frequency in AA PCa. Only 20-30% of AA PCa tumors contain *TMPRSS2-ERG* gene fusions compared to 40-50% in EA patients (Magi-Galluzzi et al. 2011) and loss of *PTEN* was observed in 34% of EA men and only 18% of AAs (Tosoian et al. 2017).

Due to differences in inherited risk alleles, as well as the limited number of samples and studies in AA men, many of the PCa risk loci identified in EA and Asian populations are not replicated in populations of African descent or the magnitude was less significant (Rebbeck 2017b). Genome-wide association studies (GWAS) have identified multiple loci that confer a greater risk for PCa in AA men compared to EA men. The rs1447295 variant at the 8q24 locus has been associated with earlier diagnosis and increased risk in AA patients (Schumacher et al. 2007). Six other variants (rs16901979, rs7000448, rs6983267, rs111906932, rs114798100, and rs111906923) have also been linked to increased PCa risk in AA men (Haiman et al. 2007; Han et al. 2016). African ancestry-specific PCa risk alleles have been identified at chromosomes 13q34 and 22q12 (Conti et al. 2017). Additionally, a risk variant at the 17q21 locus has been found more frequently in men of African descent compared to other populations (Haiman et al. 2011). Many of these alleles reside within long coding RNA sequences.

SNPs in genes that regulate androgen and testosterone metabolism have also been linked to PCa disparity in AAs. Polymorphisms in the cytochrome P450 enzyme *CYP17*

increases the risk of PCa in AA men by 60% (Taioli et al. 2013). A homozygous 'CC' genotype in the 5' promoter region (rs743572) in AA men is clinically associated with advanced PCa disease (Kittles et al. 2001).

In terms of the cancer transcriptome, our laboratory and others have demonstrated that AA PCa has increased expression of genes that promote growth and proliferation (e.g. *EGFR* and *AKT1*) and metastasis (e.g. *CXCR4* and *BMP2*) compared to EA PCa (Powell et al. 2013; Shuch et al. 2004; Wallace et al. 2008; Wang et al. 2013). For the *IL-6* gene, a race-specific and inversely correlated expression pattern is observed during PCa progression. Namely, EA PCa has increased expression of *IL-6* compared to EA normal prostate, while *IL-6* is downregulated in AA PCa compared to AA normal prostate (Teslow et al. 2018). Exogenous treatment with IL-6 downregulated TP53 in AA PCa cell lines and upregulated expression of a splice variant of methyl-CpG-binding domain protein 2 (*MBD2)* through expression of alternative exon 3 leading to a truncated protein that lacks the transcriptional repression domain. The MBD2_v2 isoform has been shown to promote a cancer stem-like cell phenotype in AA PCa (Teslow et al. 2018). Additionally, AA PCa exhibits an increased inflammatory signature, including increased expression of inflammatory genes (e.g. *CCR7*) and more frequent copy number variations of genes related to the immune response (e.g. *IL-27*, *ITGAL*, *ITGAM*) (Hardiman et al. 2016; Powell et al. 2013; Rose et al. 2010; Wallace et al. 2008).

AA PCa cell lines and patient specimens have distinct miRNA profiles compared to EA PCa. AA PCa cell lines have increased expression of hsa-miR-26a compared to EA cell lines derived from tumors of similar stage and grade (Theodore et al. 2010). Theodore et al. (2014) showed decreased expression of five miRNAs due to

hypermethylation of CpG islands within promoter regions in AA PCa. Of particular interest, miR-152 had significantly lower expression in AA patients versus EA patients in both non- and malignant tissue. Ectopic over-expression of miR-152 in PCa cell lines downregulated expression of *DNMT1* by binding to the 3'UTR of the mRNA, leading to decreased proliferation, migration, and invasion.

Work from our laboratory has identified that 10 miRNAs exhibit enriched or depleted expression in AA versus EA PCa (Wang et al. 2015). These miRNAs, including miR-133a (AA depleted), miR-513c (AA depleted), and miR-96 (AA enriched), were computationally predicted and experimentally shown to target key genes known to promote cancer, such as *MCL1, STAT1*, and *FOXO3A*. Ectopic treatment of PCa cell lines with mimics of AA-depleted miRNA (for miR-133a and -513c) or antagomirs of AA-enriched miRNA (for miR-96) resulted in decreased proliferation, invasion, and caspase activity. In agreement with these *in vitro* findings, AA PCa specimens showed significantly increased expression of MCL-1 and STAT1 and decreased expression of FOXO3A compared to EA PCa samples.

The role of epigenetics in PCa disparities is also being explored. Using quantitative pyrosequencing, our group working in conjunction with the lead laboratory of Dr. Kwabi-Addo revealed increased gene promoter methylation in AA PCa specimens compared to EA PCa (Kwabi-Addo et al. 2010; Devaney et al. 2015). *RARβ2*, *SPARC, TIMP3, NKXX2-5*, *ABCG5*, and *SNRPN* genes were all found to be highly methylated in AA PCa samples and cell lines. Tang et al. (2013) identified an association between increased *RARB* and *APC* methylation and increased PCa risk in AA men.

D. Alternative splicing

An area of research that has recently garnered considerable attention with the advent of genome-wide approaches (e.g. exon arrays, RNA-Seq) is the role of alternative splicing (AS) in cancer and cancer disparities. AS is the major mechanism for post-transcriptional regulation of gene expression, mRNA diversity, and protein modification. During AS, introns are typically excised from the precursor mRNA (pre-mRNA) and the remaining exons can be joined together in different combinations to produce multiple unique mature mRNA transcripts from a single gene. It is estimated that over 90% of human genes transcribe pre-mRNAs that undergo AS with an average of five unique mRNA variants per coding gene. This generates a proteomic complexity of ~100,000 distinct protein isoforms from ~20,000 protein-coding genes. Types of splicing events include exon skipping (removal of specific exons), cryptic exon expression, selection between two mutually exclusive exons, exon scrambling, intron retention, alternative 5' or 3' splice sites (altering boundaries between introns and exons), alternative promoters (which can alter reading frames), and alternative polyadenylation sites (**Figure 4**). This is a highly complex and flexible system that responds to cell type, tissue type, developmental stage, physiological system, and disease state.

Figure 4 Schematic representations of different types of splicing events

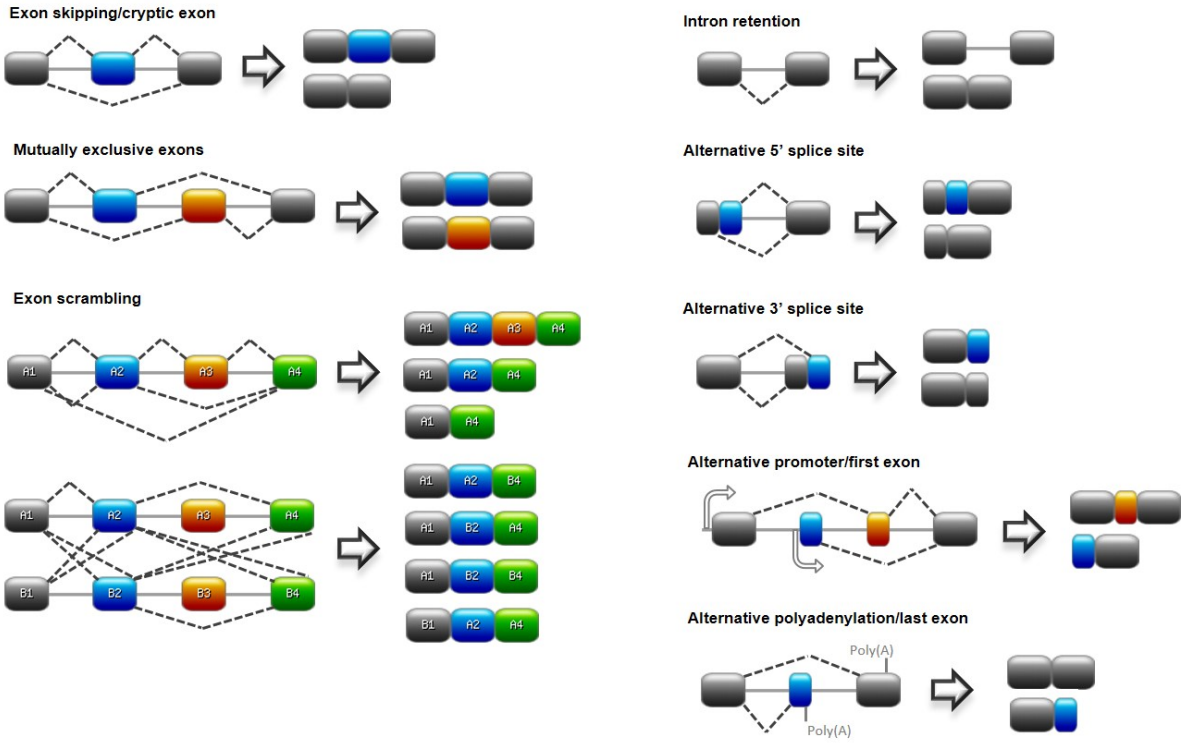

Exons are depicted as rectangles and introns as solid lines. Broken lines represent splicing events. Abbreviations: Poly(A), polyadenylation site. Designed on https://prosite.expasy.org.

AS generates a variety of protein isoforms with different sequences and altered functions from the same gene, promoting diversification of the transcriptome and proteome at both the species and interspecies levels. Although not all AS variants are functional, many can have similar or different functions, different stability kinetics, alternative subcellular localizations, or encode isoforms that are susceptible to different post-translational modifications (e.g. phosphorylation, ubiquitination). By altering the repertoire of splice variants within a cell in a time- and/or spatial-dependent manner, AS can lead to protein isoforms with different interactome networks by promoting or inhibiting different DNA-protein, protein-protein, protein-ligand, and protein-drug interactions.

Splicing events are regulated by *cis*-acting sequences (splice sites, splicing enhancers or silencers, and branch points) located within the pre-mRNA and 30-500 *trans*-acting factors including small nuclear RNAs (snRNAs), small nuclear ribonucleoproteins (snRNPs) complexes, and RNA-binding proteins (RBPs). AS is also strongly influenced by RNA polymerase kinetics, chromatin modifications, chromatin structure, epigenetic modifications (e.g. DNA and/or RNA methylation), nucleosome occupancy, location of *cis*-elements, secondary structure of pre-mRNA, and sequence editing (Baralle and Giudice 2017; Gallego-Paez et al. 2017).

Cis-regulatory sequences are divided into two groups: splice sites that are required for spliceosome binding and binding sites for other RBPs. Sequences within exons (5' and 3' splice sites) and within introns (branch point and polypyrimidine sequences) designate exon-intron boundaries for the spliceosome. These splice sites can be constitutive (always recognized as splice sites) or alternative. The strength of a splice

site is important for splicing accuracy and frequency. Strong splice sites contain consensus sequences that are well recognized by the spliceosome, thereby undergo splicing at a high rate. Weak splice sites rely on *cis*-acting sequences and cell context for splicing to occur. Splicing regulatory elements (SREs) include intronic or exonic splicing enhancers (ISE, ESE) or silencers (ISS, ESS). These provide binding sites for *trans*-acting factors, such as splicing factors (SF).

The spliceosome is composed of five snRNPs and over 200 SFs and auxiliary proteins. SnRPs (U1, U2, U4, U5, and U6) are the core components of the spliceosome ribozyme and are responsible for recognizing splice sites. The spliceosome also contains DEAD/H-box RNA-dependent ATPases that allows for changes in RNA-RNA base pairing (Will and Lührmann 2011). A splicing event begins with U1 binding the 5' splice site, the SF3b complex within U2 binding the branch point site, and U2AF1 and U2AF2 auxiliary proteins binding the 3' splice site. U1 and U2 interact to form the pre-spliceosome. Next, U4, 5, and 6 are recruited, the spliceosome rearranges, U1 and U4 are released, and the spliceosome becomes activated. In the first splicing reaction, the phosphodiester bond at the 5' splice site is cleaved via nucleophilic attack from the adenosine in the branch point site. The intron then forms an intermediate lariat structure and the phosphodiester bond at the 3' splice site is cleaved via nucleophilic attack by the free 3' hydroxyl group on the phosphate of the 5' splice site. Finally, the two exons are ligated together and the intron lariat is released (Wongpalee and Sharma 2014).

Trans-acting RBPs, such as SFs and auxiliary proteins (e.g. SF1, U2AF), complex with the spliceosome to add additional flexibility and complexity to the splicing process. RBPs bind *cis*-regulatory sites to promote or inhibit splice site recognition which is

dependent on location of binding (e.g. within intronic or exonic sequences, upstream of an alternative exon, within a downstream intron), cellular context, regulation by other RBPs, and expression level of the RBP (Fu and Ares 2014; Rossbach et al. 2014). The most well studied *trans*-acting factors are the serine/arginine-rich SF (SRSF) and heterogeneous nuclear ribonucleoprotein (hnRNP) families. SRSFs are composed of two RNA recognition motifs at the N-terminus and a serine-rich domain at the C-terminus that is involved in protein-protein interactions. SRSFs are generally considered positive splicing regulators. They promote exon inclusion by preferentially binding to purine-rich ESE or ISE sequences and recruiting U1 to 5' splice sites and U2AF to 3' splice sites (Zhou and Fu 2013). SRSF protein kinases (SRPKs) and CDC-like kinases (CLKs) activate SRSFs by phosphorylation in the cytoplasm or nucleus, respectively. The hnRNP family is largely classified as negative splicing regulators. Like SRSFs, they have two RNA recognition motifs, however their protein-protein interaction domains are unstructured. HnRNPs promote exon skipping by binding ESS and ISS sequences and inhibiting recognition of splice sites. They may also prevent spliceosome assembly after 3' splice site recognition via steric hindrance of snRNPs.

SRSFs and hnRNPs have more nuanced roles than exclusively positive or negative splicing regulators (Huelga et al. 2012; Pandit et al. 2013). Their effect on splicing can depend on several factors, such as the location of the binding site. For example, SRSFs enhance splicing when binding to sequences within exons and repress splicing when bound to introns (Zhou and Fu 2013). The functional consequences of SF binding can also be influenced by cell differentiation, cell fate, tissue-identity, organ development, and disease state (Wang et al. 2008).

E. Alternative splicing and cancer

All components of the splicing process are tightly regulated and any alteration can lead to disease causation and progression. The involvement of splicing dysregulation in oncogenic processes is known to activate oncogenes and inactivate tumor suppressors. Gene expression program changes via aberrant splicing in cancer cells can select for functional changes that promote the malignant progression of the tumor (Gonçalves, Pereira, and Jordan 2017). Modifications in splice sites or splicing machinery can lead to DNA damage, genomic instability, epigenetic changes, alterations in transcriptional elongation, and changes in gene expression thus helping to promote any of the "hallmarks of cancer" (Dvinge et al. 2016; Ryan et al. 2016; Sebestyén et al. 2016). Splice variants are being used to characterize tumor subtypes and are targets of interest for cancer biomarkers and therapeutics (Oltean and Bates 2014). Due to the potential for functional differences, individual AS variants need to be studied separately to better understand each variant's role in disease progression. In addition, an understanding of the overall splicing changes, as a change in one *trans*-acting factor can affect the splicing of hundreds of transcripts, will be instrumental in identifying the role of AS in cancer.

The Cancer Genome Atlas (TCGA) data has been used to identify genome-wide AS events in cancer versus normal tissues and between different tumor subtypes and stages. Globally, AS events occur more frequently than somatic mutations in driver genes. AS also occurs more often in cancer related pathways and in genes that are frequently mutated in cancers (Climente-González et al. 2017; Wang et al. 2017). Analysis of TCGA data has also identified key somatic mutations in splice sites that affect exon-intron boundaries, resulting in changes in expression of oncogenes and tumor

suppressors in cancer (Supek et al. 2014). In general, splicing of proto-oncogenes generates constitutively active or gain of function (GOF) variants that confer an increased oncogenic advantage. Synonymous mutations, which can alter splice sites, are also more highly enriched in oncogenes. Conversely, AS of tumor suppressors can introduce premature stop codons and altered reading frames, resulting in decreased protein levels via nonsense mediated decay or proteins with decreased function. Cancer cells have increased levels of intron retention in tumor suppressor transcripts which promote premature termination, nonsense-mediated decay, and tumor suppressor inactivation (Dvinge and Bradley 2015; Hu, Yau, and Ahmed 2017; Jung et al. 2015). Mutations in splice sites or splice site choice can result in isoform switching or generation of novel splice variants (Alsafadi et al. 2016). Thus, somatic mutations in key genes or splice sites involved in AS may be a major driver in many cancers.

Differential splicing can generate variants with opposing functions or shift the balance between two isoforms. For example, while the full-length isoform of caspase-9 is pro-apoptotic, a shorter isoform missing exons 3-6 is anti-apoptotic and has been identified in cancers, including non-small cell lung carcinoma (NSCLC) (Seol and Billiar 1999). SRSF1, which is overexpressed in many cancers, binds within intron 6 to promote inclusion of exons 3-6 to generate the long variant (Shultz et al. 2011). Conversely, hnRNPL binds an ESS in exon 3 and induces splicing exclusion of exons 3-6 to generate the short variant (Goehe et al. 2010). Kinases such as AKT are predicted to phosphorylate and activate both SRSF1 and hnRNPL (Vu et al. 2013). The known tumor suppressor gene *TP53* has over seven different splice variants that have been detected in a variety of cancers (Chen and Weiss 2015). Splicing events are concentrated in the 5’ and 3’ ends

and result in alternative promoter selection, exon skipping, intron retention, alternative 5' and 3' splice sites, or alternative reading frames. These P53 isoforms can inhibit full-length P53, impair growth or senescence suppression, and are associated with decreased patient survival.

Frequently, tumors display alterations in *trans*-acting factors. Perturbations in the expression level, localization, activity, or degradation of RBPs, SFs, or their upstream regulators can vary dramatically among different cancers. While hnRNPA2/B1 is an oncogenic driver in glioblastoma via splicing of tumor suppressors genes *IG20* and *MST1R* (Golan-Gerstl et al. 2011), RBM4 controls apoptosis, proliferation, and migration as a tumor suppressor in a variety of other solid tumors (Wang et al. 2014). The most common SF mutations in hematological and solid tumors are heterozygous missense gain or alteration of function mutations in *SF3B1*, *U2AF1*, and *SRSF2* and homozygous loss of function mutations in *ZRSR2* (Agrawal et al. 2018; Dvinge et al. 2016). SF3B1 is a member of the SF3B complex within the U2 snRNP of the spliceosome. Mutations have been observed in the 3' splice site of the *SF3B1* pre-mRNA resulting in nonsense mediated decay, which commonly occurs in breast cancer (Maguire et al. 2015). Mutations in the zinc finger domains of U2AF1, a U2 small nuclear RNA auxiliary factor, are frequently identified in NSCLC (Imielinski et al. 2012). Missense mutations are often observed in SRSF2 that change its binding affinity to ESE sequences and are common in chronic myelomonocytic leukemia (Yoshida et al. 2011). ZRSR2 is a zinc finger RBP in the U12 minor spliceosome complex. Mutations that introduce in-frame stop codons or disrupt the reading frame are common in myelodysplastic syndrome (Madan et al. 2015).

Due to the pivotal role of AS in cancer, many researchers are focusing their efforts on identifying or developing molecules that target aberrant AS in cancers (Bates et al. 2017; Dvinge et al. 2016; Gallego-Paez et al. 2017). Potential targets for these therapies include mutations in splice sites, *cis*-regulatory elements, and promoter or coding regions of *trans*-acting factors. Due to the high mutation rates observed in cancers, SF3B1 is a major target for splicing-modulating drugs. In addition, upstream factors such as SF kinases and specific splice isoforms of oncogenes or tumor suppressors are also attractive targets. Cancers that rely on splicing activity are ideal candidates for AS-targeted therapy. For example, MYC-driven cancers rely on the spliceosome, through BUD31, for promoting oncogenesis (Hsu et al. 2015). BUD31 associates with SF3B1, U2AF1, and other core spliceosome factors. Inhibition of the spliceosome via spliceosome inhibitors or *BUD31* depletion downregulates survival, tumor growth, and metastatic potential of breast cancers driven by MYC.

There are a variety of types of therapeutic compounds used to target AS. The most well-known are antisense oligonucleotides (ASOs) which are composed of nucleotides or analogs that hybridize with a complimentary nucleic acid sequence. By coding for the complimentary sequence of the target, ASOs can potentially block splice sites via steric hindrance, target mRNAs for degradation, redirect splicing, or prevent *trans*-factors from binding. ASOs have gained traction in treating Duchenne Muscular Dystrophy (DMD), spinal muscular atrophy (SMA), and amyotrophic lateral sclerosis (ALS) (Gallego-Paez et al. 2017)**.** In oncology, two ASOs, AZD9150 targeting *STAT3* and AZD4785 targeting *KRAS*, are in clinical trials for solid advanced and metastatic diseases (Hong et al. 2015; Ross et al. 2017).

Small molecule inhibitors (SMIs) have been designed to target SF kinases and spliceosome components. SRPIN340 which targets SRPKs and TG-003 which targets CLKs cause decreased activity of SFs and subsequent decreased expression of "splice-correct" signaling proteins, such as VEGF and P70-S6K (Araki et al. 2015; Siqueira et al. 2015). ML315, a chemically modified quinazoline probe, selectively inhibits the CLK family as well (Coombs et al. 2010). Cp028 has been shown to inhibit intermediate stage spliceosome assembly by causing the early release of U4/U6 (Sidarovich et al. 2017).

Natural products and their derivatives have also shown promise in targeting different stages of AS. Leucettine L_{41}, derived from the marine sponge product leucettamine B, is an ATP-competitive inhibitor targeting CLK1 and CLK3 and has been shown to inhibit phosphorylation of SRSF4 and SRSF6 (Debdab et al. 2011). Another natural product, N-palmitoyl-l-leucine targets late stage spliceosome assembly (Effenberger et al. 2015).

Indole derivatives, such as benzopyridoindoles and pyridocarbazoles, alter SF-ESE-dependent splicing in key oncogenic genes such as *MST1R* (Ghigna et al. 2010; Soret et al. 2005). The RBP RBM39 is a target of sulfonamides derived from para-aminobenzoic acid. Mutations in *RBM39* and resistance to indisulam are common in leukemia and lymphomas. These mutations block the complex formation of RBM39 with the CUL4-DCAF15 ubiquitin ligase complex, halting the normal proteasomal degradation of RBM39 and resulting in aberrant pre-mRNA splicing (Han et al. 2017). SRPIN340 is an isonicotinamide compound shown to inhibit expression of SRPK1 and a pro-angiogenic *VEGF* variant (Gammons et al. 2014). Derivatives of the natural compound FR901464 have shown promising ability to inhibit SF3B. These analogs

include spliceostatin A, meayamycin, and sudemycin (Albert et al. 2009; Convertini et al. 2014; Kaida et al. 2007).

Pladienolide-scaffold derivatives have had the most success in clinical trials. E7107, derived from pladienolide B, inhibits SAP130 of the SF3B complex (Kotake et al. 2007). This weakens the binding interaction between U2 and the pre-mRNA by locking SF3B1 in an inactive conformation and sterically preventing binding to the branch point adenosine (Finci et al. 2018). E7107 was one of the first splicing modulator drugs to enter clinical trials in solid tumors, such as colorectal and pancreatic carcinomas, in 2007 (Eskens et al. 2013; Hong et al. 2014), however further studies in humans were suspended due to unexpected visual toxicity. H3B-8800, another pladienolide-derivative, selectively inhibits wildtype and mutated SF3B1 isoforms and enriches for intron retention in SF-coding mRNAs (Seiler et al. 2018). Trials using H3B-8800 in hematological cancers have been ongoing since 2016.

Our current limited understanding of overall "splicing sickness", restoration of normal splicing, and downstream effects of spliceosomal mutations need to be addressed in order to develop new AS drugs. Overcoming issues of systemic delivery, toxicity, off-target effects, efficacy, and targeting the desired cell type will be key in splice-modulating therapies becoming a safe and efficacious therapeutic option for cancer patients.

F. Alternative splicing in prostate cancer

A number of genes undergoing AS have been associated with PCa development and progression. The AR is a primary pharmacological target for early PCa treatment.

PCa tumors, however, develop AR-targeted treatment resistance (e.g. castrate-resistant) as the disease progresses. One mechanism in which PCa tumors develop drug resistance is through AS of the *AR* (see review by Olender and Lee 2019). Among the 20 different *AR* splice variants identified, *ARv7* is the most clinically frequent and relevant variant. The *ARv7* variant is generated by inclusion of a cryptic exon within exon 3 that encodes a protein isoform with a truncation of the entire C-terminal ligand binding domain (LBD). The LBD is important for AR activation by androgens and subsequent translocation of the AR into the nucleus for transcriptional regulation of androgen-dependent genes. The ARv7 isoform acts independently of androgen binding and is constitutively present in the nucleus of prostate cells, regardless of androgen stimulation (Cao et al. 2014). Levels of *ARv7* mRNA in PCa patients can help predict responsiveness to anti-androgen therapies, such as abiraterone and enzalutamide (Antonarakis et al. 2014). The SF hnRNPA1 and RBP SAM68 are believed to contribute to regulation of the *ARv7* variant. Relocalization of hnRNPA1 from the nucleus to the cytoplasm decreases expression of *ARv7* in PCa cells and resensitizes them to enzalutamide (Antonarakis et al. 2014; Ko et al. 2014; Nadiminty et al. 2015; Tummala et al. 2017). SAM68 preferentially increases expression of ARv7 in PCa cells, via SAM68 stabilization of the *ARv7* mRNA via direct RNA-protein binding and indirect mediation by SRSF1 (Stockley et al. 2015).

A second clinically relevant *AR* splice variant, *ARv567es*, has been identified in PCa cells where exons 5-7 (of 8 total) are skipped, truncating the majority of the LBD. Similar to the ARv7 isoform, ARv567es is constitutively active and androgen independent (Sun et al. 2010). This variant is highly expressed in metastatic and malignant prostate tissue (Hörnberg et al. 2011). ARv567es regulates oncogenes involved

in cell cycle progression including *UBE2C*, which codes for a ubiquitin-conjugating protein involved in the machinery that inactivates the mitotic checkpoint and promotes proliferation (Liu et al. 2015).

The *fibroblast growth factor receptor* (*FGFR*) *2* undergoes AS of the third Ig-like extracellular domain, generating two isoforms: FGFR2IIIb and FGFR2IIIc. FGFR2IIIb is expressed highly in normal prostate epithelial cells and is a known tumor suppressor. FGFR2IIIc is involved in autocrine signaling and expressed more highly in mesenchymal cells. While no change in overall FGFR2 protein expression is observed as PCa progresses (Sahadevan et al. 2007), a switch in FGFR2 isoforms occurs due to AS. Decreased expression of the IIIb isoform and exclusive expression of the IIIc isoform is associated with epithelial to mesenchyme transition (EMT) and loss of AR sensitivity (Carstens et al. 1997). This increase in FGFR2IIIc expression correlates with an increase in fibroblast growth factor (FGF) 8b, a ligand associated with PCa (Gnanapragasam et al. 2003).

The vascular endothelial growth factor (VEGF) is largely responsible for cellular growth and survival via angiogenesis in both normal and cancerous conditions. "Canonical" splicing of *VEGF* produces a VEGF isoform that is pro-angiogenic, while an alternative 3' splice site event generates an anti-angiogenic isoform $VEGF_{165}b$, which is the main isoform. $VEGF_{165}b$ differs from pro-angiogenic VEGF in the last six amino acids and acts as an antagonist of the VEGF receptor (Woolard et al. 2004). Expression of pro-angiogenic VEGF is an early driver of PCa and increased expression corresponds with later stage PCa and increased expression of SRSF1 (Rennel et al. 2008). Inhibition of the SF kinase SRPK1, a known activator of SRSF1, causes splice switching to the

VEGF$_{165}$b variant in PCa cells, resulting in decreased tumor formation in PCa mouse models (Mavrou et al. 2015).

BCL-x plays a pivotal role in regulating apoptosis. Alternative 5' splice site usage within exon 2 of the *BCL2L1* pre-mRNA generates two variants that have opposing functions. The long anti-apoptotic isoform, BCL-x(L), is associated with cell survival, while the shorter isoform (BCL-x(S) promotes apoptosis, cell death, and sensitivity to chemotherapeutics in PCa (Mercatante, Mohler, and Kole 2002). High BCL-x(L) to BCL-x(S) ratios have been observed in PCa and overexpression of the short isoform induces apoptosis-mediated cell death in cancer cells (David and Manley 2010; Rajan et al. 2009). SAM68 selectively favors the upstream 5' splice site, thus favoring production of the *BCL2L1* long variant and preventing apoptosis. Increased expression of BCL-x(L) has been identified in PCa patients and cell lines, resulting in decreased apoptotic-induced cell death and decreased sensitivity to cytotoxic therapeutics (Busà et al. 2007).

Splice variants of another apoptotic-related gene *SH3GLB1*, which codes for the BAX binding protein BIF-1, has recently been implicated in the transition of adenocarcinoma to aggressive treatment-induced neuroendocrine (t-NE) PCa. BIF-1a, the pro-apoptotic protein isoform encoded by a variant lacking exon 6, is the predominant isoform expressed in adenocarcinoma specimens (Gan et al. 2018). BIF-1b (encoded by a variant containing a short version of exon 6) and BIF-1c (encoded by a variant containing a long version of exon 6), however, become highly expressed in t-NE PCa. This switch in dominant variant expression is regulated by the SF SRRM4.

Cyclin D1 associates with cyclin-dependent kinase 4 (CDK4) to promote cell cycle progression through the G1 phase. Two alternative splice variants of *CCDN1* have

been identified: the cyclin D1a mRNA, which is the full-length and more common variant, and the cyclin D1b variant, in which intron 4 is retained leading to early termination. The cyclin D1b protein isoform plays a distinct role as an AR co-regulator to promote expression of AR-dependent genes associated with tumor growth and metastasis in PCa, specifically *SNAI1* (Augello et al. 2013). Additionally, increased expression of SRSF1 in PCa cells correlates with enhanced expression of cyclin D1b, but not D1a (Olshavsky et al. 2010; Paronetto et al. 2010).

ST6GalNac1 is an enzyme that synthesizes the sialyl-T (sTn) antigen and modifies the glycosylation pattern of cell surface glycoproteins that play a role in cell adhesion and metastasis. ST6GalNac1 is androgen-sensitive, thus indicating a role for this enzyme in PCa. Recently, RNA-seq data have identified a shorter splice variant of *ST6GalNac1* that has only been reported in PCa (Munkley et al. 2015). The short protein isoform results from the inclusion of an additional exon (exon 2) within the 5' UTR that generates a new start codon within a longer mRNA variant but encoding a shorter, fully functional protein isoform that has increased expression compared to the full-length protein isoform missing exon 2. *In vitro* studies suggest a role for the short isoform in promoting EMT through decreased cell adhesion and increased cell motility.

A new splice variant of *PCSK6* has been identified in PCa. *PCSK6* codes for the proprotein convertase PACE4 that modifies proprotein substrates in secretory and known oncogenic pathways. Couture et al. (2017) identified a variant of *PCSK6* with a shorter 3'UTR via AS of exon 25 (variant known as *PACE4-altCT*). While both the full-length PACE4 and the shorter PACE4-altCT are expressed in PCa specimens, PACE4-altCT showed increased expression in higher grade tumors. Additionally, PACE4-altCT appears

less susceptible to degradation and secretion, is more stable, more rapidly activated, and increases growth and proliferation when compared to the full-length protein. PACE4-altCT directly increases the processing of pro-GDF15 (e.g. prostate differentiation factor), a TGFβ ligand with a known role in immunosuppression, protection against radiation-induced cell death, and neovascularization.

Three splice variants of *CLK1* have been identified: full-length *CLK1*, $CLK1^{T1}$ (skipping of exon 4), and $CLK1^{T2}$ (retention of intron 4). CLK1 is responsible for phosphorylating and activating SRSFs and other SFs. Both T1 and T2 isoforms lack the catalytic domain and are inactive. The $CLK1^{T2}$ has been found to be the more prominent isoform in PCa. Treating PCa cells with a CLK1 inhibitor shifts the *CLK1* variant expression ratio to favor both the expression of full-length active CLK1, as well as expression of the pro-apoptotic variants of *CASP9, MCL-1, BCL2L1*, and *survivin* (Uzor et al. 2018).

The *HSD17B4* gene encodes 17β-hydroxysteroid dehydrogenase type 4 (17βHSD4), an enzyme involved in testosterone and dihydrotestosterone metabolism. Recently, five splice variants of *HSD17B4* were identified, four of which encode enzyme isoforms that do not inactivate testosterone and dihydrotestosterone via conversion to inert steroid products (Ko et al. 2018). The remaining isoform, isoform 2, is the major enzyme expressed in prostate tissue and is able to inactivate androgens. The splice variant encoding isoform 2 of 17βHSD4 is missing part of exon 2 and all of exon 3, which code for sections of the short-chain alcohol dehydrogenase domain. This isoform was found to be functionally suppressed in metastatic castration-resistant PCa.

As outlined above, AS plays an important role in PCa development, progression and drug resistance. While it is fairly well accepted that AA PCa is genetically different from EA PCa, the role of AS in PCa disparities is less clear. Over 60% of the studies cited above used only cell lines derived from EA patients (**Table 3**). Of the remaining studies, two cell lines (22Rv1 and M12) of mixed or self-reported AA ancestry were utilized. The 22Rv1 cell line was derived from the CWR22 line, a primary prostatic carcinoma serially transplanted in nude mice (Sramkoski et al. 1999; Wainstein et al. 1994.). A recent study determined 22Rv1 was only 41% AA ancestry (Woods-Burnham et al. 2017). The M12 line was immortalized from the P69SV40T cell line via transfection with SV40 T antigen and passaged in nude mice (Bae et al. 1994, 1998). While the ancestry of the M12 line has not been confirmed by genotyping, the parental cell line was reported to be derived from prostate epithelial cells from 63 year old AA man. Only one of these studies use an AA PCa cell line with over 50% AA genetic ancestry, such as MDA PCa 2b or RC77 T/E (74% and 73%, respectively) (Woods-Burnham et al. 2017). Forty-one percent of the studies cited analyzed primary prostatic samples, but none specified the ancestry (genotyped or self-reported) of the patients.

The lack of AA cell lines and patient samples used in AS PCa studies reflects the lack of minority subjects across all cancer, and specifically PCa, research (Spratt et al. 2016). In order to better understand PCa disparities, eliminate the disproportionate disease burden, provide novel biomarkers, and improve survival and quality of life in AA PCa patients, increased awareness, use, and availability of AA PCa cell lines and specimens is required.

Table 3 Summary of splicing events in prostate cancer

Reference	Spliced gene (Splicing factor)	Alternative splicing event	Cell lines and/or patient samples
Cao et al. 2014	*ARV7*	Cryptic exon	LNCaP, **22Rv1**, PC-3
Antonarakis et al. 2014	*ARV7* (hnRNPA1)	Cryptic exon	Patients (ethnicity N/A)
Ko et al. 2014	*ARV7* (hnRNPA1)	Cryptic exon	PC-3
Nadiminty et al. 2015	*ARV7* (hnRNPA1)	Cryptic exon	LNCaP, **22Rv1**, VCaP, C4-2B
Tummala et al. 2017	*ARV7* (hnRNPA1)	Cryptic exon	**22Rv1**, C4-2B
Stockley et al. 2015	*ARV7* (SAM68, SRSF1)	Cryptic exon	**22Rv1**, VCaP, CWR22, PC3-M
Sun et al. 2010	*ARv567es*	Exon skipping	**M12**, LNCaP, LuCaP
Hörnberg et al. 2011	*ARv567es*	Exon skipping	Patients (ethnicity N/A)
Liu et al. 2015	*ARv567es* (MED1)	Exon skipping	LNCaP, **M12**
Sahadevan et al. 2007	*FGFR2*	Mutually exclusive exons	PC-3, DU145, patients (ethnicity N/A)
Carstens et al. 1997	*FGFR2*	Mutually exclusive exons	LNCaP, PC-3, DU145, DUP9479, DUKAP-1, DUPKAP-2
Gnanapragasam et al. 2003	*FGFR2*	Mutually exclusive exons	Patients (ethnicity N/A)
Woolard et al. 2004	*VEGF*	Alternative 3' splice site	Patients (ethnicity N/A)
Rennel et al. 2008	*VEGF*	Alternative 3' splice site	PC-3, patients (ethnicity N/A)
Mavrou et al. 2015	*VEGF*	Alternative 3' splice site	PC3, LNCaP, DU145
Mercatante, Mohler, & Kole 2002	*BCL2L1*	Alternative 5' splice site	PC-3
Busà et al. 2007	*BCL2L1* (SAM68)	Alternative 5' splice site	LNCaP, patients (ethnicity N/A)
Gan et al. 2018	*SH3GLB1* (SRRM4)	Alternative 5' splice site, exon skipping	LNCaP, **22Rv1**, PC-3, DU145, NCI-

			H660, LNCaP95, patients (ethnicity N/A)
Augello et al. 2013	*CCND1*	Intron retention	LNCaP, VCaP, LAPC4, PC-3, C4-2
Olshavsky et al. 2010	*CCND1* (SRSF1)	Intron retention	LNCaP, LAPC4
Paronetto et al. 2010	*CCND1*	Intron retention	PC3, LNCaP
Munkley et al. 2015	*ST6GalNAc1*	Exon skipping	LNCaP, VCaP, PC-3, 22Rv1, DU145, LNCaP-AI, and LNCaP-cdxR, BPH-1
Couture et al. 2017	*PCSK6*	Exon skipping	DU145, LNCaP, patients (ethnicity N/A)
Uzor et al. 2018	*CLK1*	Exon skipping, intron retention	PC-3, DU145, VCaP
Ko et al. 2018	*17βHSD4*	Alternative 5' splice site, exon skipping	LNCaP, LAPC4, VCaP, PC-3, DU145, RWPE-1, **22Rv1**, patients (ethnicity N/A)
Teslow et al. 2018	*MBD2*	Alternative exon	MDA PCa 2b, RC77T, DU145, PC-3, LNCaP, Patients (AA, EA)
Wang et al. 2017	*PIK3CD*	Exon skipping	**MDA PCa 2b**, VCaP, LNCaP, PC-3, Patients (AA, EA)

Cell lines and patient samples with known AA ancestry are in bold and underlined. Abbreviations: *ARV7*, androgen receptor splice variant 7; hnRNPA1, heterogeneous nuclear ribonucleoprotein A1; SRSF1, serine/arginine splicing factor 1; *ARv567es*, androgen receptor variant (exons) 5,6,7 exon skipping; MED1, mediator complex subunit 1; *FGFR2*, fibroblast growth factor receptor 2; *VEGF*, vascular endothelial growth factor; *BCL2L1*, B-cell lymphoma 2-like 1; SAM68, Src-associated substrate in mitosis of 68 kDa; *SH3GLB1*, SH3 domain-containing GRB2-like protein B1; SRRM4, serine/arginine repetitive matrix 4; *CCND1*, cyclin D1; SRSF1, serine/arginine splicing factor 1; *ST6GalNAc1*, ST6 N-acetylgalactosaminide alpha-2,6-sialyltransferase 1; *PCSK6*, proprotein convertase sutilisin/kexin type 6; *CLK1*, CDC like kinase 1; *17βHSD4*, 17β-

Hydroxysteroid dehydrogenase type 4; *PIK3CD*; phosphatidylinositol-4,5-bisphosphate 3-kinase catalytic subunit delta.

G. Alternative splicing and prostate cancer health disparities

In order to further our understanding of AS in PCa health disparities, our laboratory recently applied a functional genomics approach to investigate differential AS (dAS) events in AA and EA PCa patients (Wang et al. 2017). Twenty AA and 15 EA PCa tumor and matched normal specimens (treatment naïve, Gleason score 6-8, age 49-81) were collected and samples were analyzed using the Affymetrix Human GeneChip exon array to identify genes undergoing AS (**Table 4**). We identified 158 unique genes that underwent AS in both AA and EA PCa. It can be concluded that these genes, which included *TMPRSS2* and *AR*, are important for PCa development regardless of race. In comparing AA versus EA PCa, 1,876 unique genes undergoing dAS were identified, including *RASGRP2, NF1,* and *BAK1*. Over 2,200 unique genes underwent AS in AA versus EA normal prostate tissue, suggesting a role for these genes in normal prostate homeostasis. We identified 644 unique genes, including *PIK3CD, ITGA4,* and *MET*, that underwent dAS in both AA PCa and AA normal tissue compared to EA specimens (both normal and cancer). We also identified 1,575 unique genes undergoing dAS in AA PCa versus AA normal, such as *FGFR3* and *TSC2*. These two comparisons identify two important groups of dAS genes: dAS gene variants that are inherited based on African ancestry and dAS variants that occur *de novo* during PCa progression solely in AA men.

Table 4 Examples of differential alternative splicing events in PCa and normal specimens

Patient groups	# of AS genes	Examples
AA PCa and EA PCa vs. normal prostate	158	*TMPRSS2, AR*
AA PCa vs. EA PCa	1,876	*RASGRP2, NF1, BAK1*
AA normal vs. EA normal	2,205	*MTOR, EGFR, BCL2L1*
AA PCa and AA normal vs. EA PCa and EA normal	644	*PIK3CD, ITGA4, MET*
AA PCa vs. AA normal	1,575	*FGFR3, TSC2*

Abbreviations: AA, African American; EA, European American; PCa, prostate cancer; *TMPRSS2*, transmembrane protease serine 2; *AR*, androgen receptor; *RASGRP2*, RAS guanyl releasing protein 2; *NF1*, neurofibromin 1; *BAK1*, BCL2 antagonist/killer 1; *MTOR*, mammalian target of rapamycin kinase; *EGFR*, endothelial growth factor receptor; *BCL2L1*, B-cell lymphoma 2-like 1; *PIK3CD*, phosphatidylinositol-4,5-bisphosphate 3-kinase catalytic subunit delta; *ITGA4*, integrin subunit alpha 4; *MET*, MET proto-oncogene, receptor tyrosine kinase; *FGFR3*, fibroblast growth factor receptor 3; *TSC2*, tuberous sclerosis complex subunit 2.

Over 70% of dAS events identified in AA PCa versus EA PCa occur in pathways known to contribute to oncogenesis (e.g. cell growth, proliferation, cell survival, cell adhesion, DNA repair) and the majority were in-frame exon skipping events. Further validation of a subset of genes identified as potential targets for dAS was performed in an additional cohort of 22-25 AA and 21-24 EA specimens. Ninety one percent of genes chosen for validation via RT-PCR were confirmed. The exon array results also identified 886 differentially expressed genes in AA versus EA PCa (compared to 1,876 dAS genes). These data suggest dAS is playing a much greater role in AA PCa disparities than differential gene expression. I have selected the *fibroblast growth factor receptor 3* (*FGFR3*) gene for further characterization.

H. Fibroblast growth factor family

FGFR signaling plays an important role in growth, development, and homeostasis. The pattern and timing of ligand and receptor expression varies between tissues and between stages of development. FGFR signaling can trigger proliferation, growth, differentiation, migration, EMT, and survival and thus plays a role in embryonic development, organogenesis, tissue repair, angiogenesis, and inflammation (Porta et al. 2017).

The FGF/FGFR family is comprised of over 22 ligands and 5 receptors. The FGF ligands are grouped based on their phylogeny: FGF1 (FGF1 (acidic), FGF2 (basic)); FGF4 (FGF4,5,6); FGF7 (FGF3,7,10,22); FGF8 (FGF8,17,18); FGF9 (FGF9,16,20); FGF15/19 (FGF15/19,21,23); and FGF11 (FGF11,12,13,14). The first five groups are canonical, secreted ligands that are involved in paracrine signaling, the FGF15/19

subfamily are involved in endocrine signaling, and the FGF11 subfamily are intracellular ligands (Katoh 2016a).

FGFRs are members of the receptor tyrosine kinase (RTK) family and are comprised of three extracellular immunoglobulin (Ig)-like domains, an acid box residue between Ig-I and Ig-II, a single pass transmembrane domain, and an intracellular split kinase domain. FGFR5 lacks the intracellular kinase domain and FGFR1-3 can undergo AS of exons 8-9 to generate IIIb and IIIc isoforms (Porta et al. 2017).

The intracellular split kinase domain is composed of an N-terminal lobe and a C-terminal lobe, which coordinate ATP and substrate binding, respectively (Bunney et al. 2015). The N lobe contains the P-loop, which binds the γ-phosphate of ATP, and the catalytic loop (e.g. the active site/ATP binding pocket where most SMIs bind). The C lobe contains the activation loop (A-loop) that covers the substrate binding pocket when the kinase is inactivated. The two lobes are connected by the hinge region (or regulatory (R)-spine), a highly conserved region that creates a network of hydrogen bonds that serve as an autoinhibitory molecular break that restricts transition between the active and inactive states. The kinase domains also contain conserved tyrosine residues that are phosphorylated in a sequential and ordered manner when the kinase is activated and play a critical role in increased enzymatic activity and activating signaling pathways (Furdui et al. 2006; Ornitz and Itoh 2015).

FGFR3 signaling begins with an FGF ligand binding to an FGF receptor. Adaptor proteins stabilize the ligand-receptor complex, as well as aid in presenting ligands to receptors (Ornitz and Itoh 2015). Paracrine FGFs bind heparin-sulfate cofactor molecules and endocrine FGFs are stabilized with Klotho family proteins (Porta et al. 2017). Ligand

binding causes dimerization of the receptors, bringing the intracellular domains into close proximity and generating structural changes in stages that lead to activation of downstream signaling pathways. The close proximity of the kinase domains allows for trans-autophosphorylation of key tyrosine residues in three ordered stages (Furdui et al. 2006). The first stage of autophosphorylation of Tyr647 on the A-loop leads to a 50- to 100-fold increase in kinase activity. The second stage results in phosphorylation of Tyr577, 760, and 724. Finally, the second tyrosine residue in the A-loop, Tyr648, is phosphorylated and increases kinase activity by another 10-fold. Phosphorylation of these tyrosine residues creates docking sites for adaptor molecules and causes a conformational shift of the A-loop, exposing the substrate binding pocket.

FGFR3 signals through four major pathways: RAS/MAPK, PI3K/AKT, PLCγ, and STAT. Signaling through RAS/MAPK begins with activation and autophosphorylation of FGFR3. Phosphorylated tyrosine residues on the FGFR kinase domain act as docking sites for FGFR substrate 2 (FRS2α) and Crk-like protein (CRKL). FGFR phosphorylates FRS2α which then recruits the membrane bound and Src homology domain 2 (SH2)-containing growth factor receptor bound protein 2 (GRB2). GRB2 then recruits the guanine nucleotide exchange factor (GEF) son of sevenless (SOS) which facilitates the guanine nucleotide binding and GTPase protein Ras to release GDP, bind GTP, and become activated. RAS-GTP binds and activates RAF kinase which phosphorylates the serine/threonine kinase mitogen-activated protein kinase kinase (MEK). MEK phosphorylates mitogen-activated protein kinase (MAPK), resulting in MAPK translocating to the nucleus and activating expression of genes that positively (e.g. *ETS*) or negatively (e.g. Sprouty RTK signaling antagonist (*Spry*), similar

expression to *Fgf* (*Sef*), dual specificity phosphatase 6 (*Dusp6)*) regulate gene expression. SPRY inhibits GRB2 recruitment to phosphorylated FGFR (p-FGFR), while SEF is a transmembrane protein that inhibits the dissociation of MEK and MAPK. DUSP6 dephosphorylates and deactivates MAPK. A fourth negative regulator, Cbl proto-oncogene (CBL), is an E3 ubiquitin ligase that targets FGFR and FRS2α for degradation.

To activate the PI3K/AKT signaling pathway, FRS2α-bound GRB2 recruits GRB2-associated-binding protein 1 (GAB1). The inhibitory subunit of PI3K, p85, contains two SH2 domains and binds to GAB1. This allows activation of the catalytic subunit, p110, which phosphorylates phosphatidylinositol (3,4,5)-trisphosphate (PtdIns(3,4,5)P3) and activates phospholipid dependent kinase 1 (PDK1). PDK1, a serine/threonine kinase, and mTORC2 phosphorylate protein kinase B (AKT). AKT in turn phosphorylates and inhibits the TF Forkhead box A1 (FOXO1) and induces this TF to translocate out of the nucleus. Moreover, AKT phosphorylates and inactivates TSC complex subunit 2 (TSC2), which leads to activation of mTORC1. Inactivation of FOXO1 and TSC2 result in increased expression of genes for cell survival, cell growth, and proliferation (e.g. ribosomal protein S6). Phosphatase and tensin homolog (PTEN) inhibits this pathway via PtdIns(3,4,5)P3. Src homology region 2-containing protein tyrosine phosphatase 2 (SHP2) also inhibits this pathway by dephosphorylating FRS2α and GRB2 (which also inhibits SHP2).

Phosphorylated FGFR3 also binds and phosphorylates phospholipase-c γ (PLCγ) which hydrolyzes PtdIns(4,5)P2 (PIP2) into two lipid second messengers: inositol trisphosphate (IP3) and diacylglycerol (DAG). IP3 initiates the release of calcium from the endoplasmic reticulum, activating calcium-dependent intracellular signaling. DAG

activates protein kinase c (PKC), which phosphorylates RAF, feeding into the RAS/MAPK pathway. GRB14 inhibits this pathway by binding pTyr760 on FGFR3 and blocking binding of PLCγ.

Signal transducer and activator of transcription (STAT) 1, 3, and 5 bind pTyr760 of FGFR3 via their SH2 domains. After phosphorylation by mTORC and MAPK, STATs bind DNA and activate gene transcription.

I. Fibroblast growth factor receptor 3 and disease

GOF missense mutations in *FGFR3* are the main cause of skeletal dysplasias (Katoh 2016b; Ornitz and Itoh 2015). Achondroplasia, the most common form of short limbed dwarfism is caused by a G380R ligand-dependent activating mutation in the transmembrane domain of *FGFR3* (Foldynova-Trantirkova, Wilcox, and Krejci 2012). Lethal skeletal dysplasias, such as Thanatophoric dwarfism types I and II, are caused by R248C (extracellular domain) or K650E (A-loop) mutations, resulting in ligand-independent FGFR3 signaling (Bonaventure et al. 1996). Meunke nonsyndromic coronal cryiosynostosis, an autosomal dominant disorder due to a GOF missense mutation in *FGFR3* (P250R), causes skull, hand, and feet malformations, as well as hearing loss (Muenke et al. 1997). Lacrimo-auriculo-dento-digital (LADD) syndrome is caused by mutations (D513N, R621H) in the tyrosine kinase domains of *FGFR3* (Rohmann et al. 2006).

GOF alterations in FGFRs, including FGFR3, are common in many cancers (**Figure 5**). *FGFR3* is frequently mutated, overexpressed, or translocated in prostate,

lung, NSCLC, bladder, urothelial cell carcinoma (UCC), cervical, glioblastoma, oral and oropharyngeal squamous cell cancers (Hallinan et al. 2016).

FGFR mutations occur in about 7% of all solid tumors and can occur in the ligand-binding, transmembrane, or kinase domain (Babina and Turner 2017; Patani et al. 2016). *FGFR3* mutations have been identified in multiple myeloma, gastric, colorectal, breast, endometrial, urothelial, bladder, skin, cervical, and lung cancers (Katoh 2016b; Ornitz and Itoh 2015). The most common *FGFR3* mutation is S249C which is also the most frequent alteration in bladder cancer (Porta et al. 2017). Somatic GOF *FGFR3* mutations occur in non-muscle invasive urothelial cancer (75%), high-grade invasive urothelial cancers (15%), muscle invasive bladder tumors (50%), and cervical cancer (5%) (Cappellen et al. 1999; Gust et al. 2013; Helsten et al. 2016; Rosty et al. 2005). G370C, K650E, R248C, and S249C missense mutations have been identified in NSCLC (Helsten et al. 2016). *FGFR3* mutations have been linked to low-grade PCa. Exons 7, 10, and 15 of *FGFR3* have revealed polymorphisms (F386L), missense mutations (S249C, F384L, F386L, A393E), and frameshift mutations in low-risk or low-grade PCa (Hernández et al. 2009; Lo Iacono et al. 2016; Pilié et al. 2017). Other studies, however, have found no *FGFR3* mutations in PCa specimens when analyzing these hotspot mutation sites (Koufou et al. 2010; Zuiverloon et al. 2011).

Gene fusions account for 8% of all FGFR alterations (Porta et al. 2017). *FGFR3* most frequently fuses to transforming acidic coiled-coil containing protein 3 (*TACC3*), leading to constitutive activity via ligand-independent signaling (Helsten et al. 2016). *FGFR3-TACC3* fusions have been identified in multiple myeloma (15-20% cases),

squamous cell lung, bladder, glioblastoma, lymphoma, NSCLC, and prostate cancers (Babina and Turner 2017; Ornitz and Itoh 2015; Wu et al. 2013).

Overexpression of *FGFR1* and *FGFR2* has been reported in prostate cancer, although neither have been shown to be clinically relevant (Hernández et al. 2009). *FGFR3* overexpression is clinically relevant for bladder and breast cancers (Agarwal et al. 2014; Fischbach et al. 2015; Kuroso et al. 2010; Tomlinson et al. 2007). *FGFR3* overexpression is observed in 50% of breast cancer tumors and is a marker for high risk patients and poor prognosis (André et al. 2013; Gust et al. 2013).

Over 60% of all cancers with FGFR alterations contain gene amplifications of *FGFRs*, with *FGFR1* amplification being the most common (Porta et al. 2017). 3% of bladder and urothelial tumors contain *FGFR3* amplifications (Katoh 2016b; Ornitz and Itoh 2015; Porta et al. 2017).

Figure 5 Common *FGFR3* alterations by cancer type

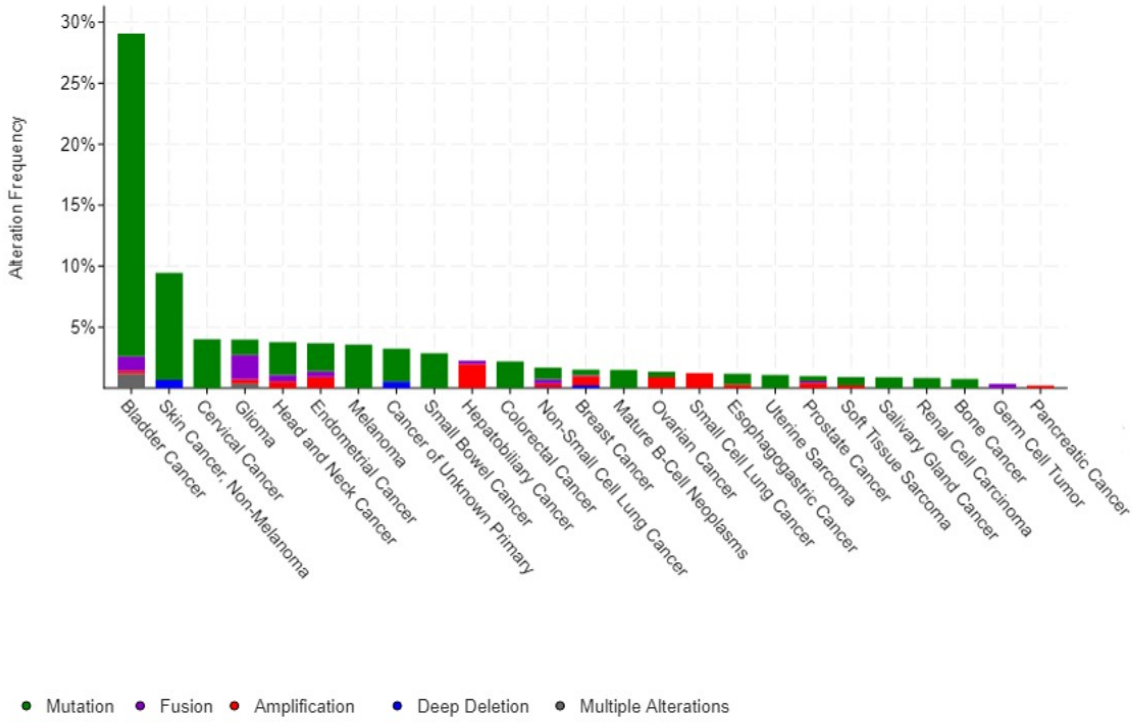

MSK-IMPACT Clinical Sequencing Cohort (MSKCC, Nat Med 2017) data set from cBioPortal (cbioportal.org) (Cerami et al. 2012; Gao et al. 2013).

J. Fibroblast growth factor receptor inhibitors

As a result of the prevalence of FGFR3 aberrations in cancer specimens, a variety of anti-FGFR therapies have been developed. These therapies include multi-target TKI inhibitors, selective FGFR inhibitors, and monoclonal antibodies against FGFRs (**Table 5**). Multi-target TKI inhibitors are ATP-competitive binding small molecules that bind in the intracellular kinase domain to inhibit catalytic activity or phosphorylation of tyrosine residues. These SMIs bind to a conserved ATP-binding domain and thus lack kinase selectivity. In addition to binding FGFRs, non-selective TKI inhibitors also target VEGFRs and PDGFRs (Chae et al. 2017). Dosing of multi-target TKIs, especially for FGFR-related aberrant cancers, is limited due to hypertension as a result of VEGFR inhibition and toxicity. Pan-FGFR "selective" TKIs include dovitinib, a second-generation SMI that targets FGFR1-3, VEGFR1-3, and PDGFRβ. Dovitinib has shown efficacy in preclinical studies of breast cancer (FGFR-amplified) and multiple myeloma (FGFR3 translocation) (André et al. 2013; Trudel et al. 2005; Xin et al. 2006). It has advanced to clinical trials of advanced renal cell carcinoma (Phase I and II) (Angevin et al. 2013; Escudier et al. 2014).

Wan et al. (2014) showed PCa cell lines, patient samples, and patient derived xenografts induced expression of *FGF2* and *FGFR1-IIIc* in bone. Additionally, their study showed dovitinib treatment significantly reduced tumor volume, induced apoptosis, reduced tumor angiogenesis, and blocked FGFR signaling in mouse models of mPCa. 83% of patients treated with dovitinib had stable disease or partial response to disease progression (Wan et al. 2014). Responding patients also experienced reduction in skeletal pain. A 3D co-culture model for PCa bone metastases replicated the reduction in tumor

volume with dovitinib treatment and highlighted the importance of the microenvironment in regulating and promoting bone metastases (Fong et al. 2016). A recent Phase II clinical trial of dovitinib in patients with mCRPC showed modest anti-tumor activity accompanied by tolerated toxicities in chemo-naïve patients (Choi et al. 2018). Dovitinib has also been shown to reduce genomic instability observed in PCa cells exposed to FGF2 (Pecqueux et al. 2018).

Selective FGFR inhibitors, including AZD4547 and BGJ398, specifically target FGFR1-3, thus limiting off-target toxicity. These inhibitors appear to have a higher response rate in tumors with *FGFR* gene fusions (Babina and Turner 2017). Preclinical and clinical studies with FGFR-selective SMIs have commenced in NSCLC, breast cancer, bladder cancer, gastric cancer, and other solid tumors (Babina and Turner 2017).

Anti-FGFR antibodies bind to the extracellular domain of FGFR to inhibit FGF binding and FGFR dimerization. Their specificity comes from their binding to the FGF-FGFR interface. The efficacy of antibodies to FGFR2IIIb (GP369, FPA144) and FGFR3 (MGFR1877S) are being assessed in gastric cancer, breast cancer, bladder cancer, multiple myeloma, urothelial carcinoma, and other solid tumors (Babina and Turner 2017; Chae et al. 2017).

A challenge of targeting FGFR signaling in the clinic is the acquired and intrinsic drug resistance to targeted FGFR therapies. Cancer cells inhibit the effect of these therapies via introducing mutations in the ATP binding pocket, known as gatekeeper mutations, and through activation of other RTKs.

The gatekeeper residue of FGFR3, V555, is located in the hinge region between the N and C kinase lobes. It is positioned deep in the active site and helps anchor SMIs

(Yoza et al. 2016). Many cancers mutate this site to bulky hydrophobic residues, such as methionine or isoleucine, to decrease binding affinity of TKIs. In FGFR3, V555 is commonly mutated to methionine (Byron et al. 2013; Chell et al. 2013). The resistance of a myeloma cell line to SMIs AZD4547 and PD173074 are a result of the V555M mutation (Chell et al. 2013). As a result, the development of irreversible covalent inhibitors to overcome resistance has begun. Inhibitors FIIN-2 and FIIN-3 have shown potency against wildtype and gatekeeper mutation-containing FGFR1-3 (Tan et al. 2014).

A second escape mechanism used by FGFR-driven tumors are to activate alternative RTKs, especially ERBB family members. FGFR3-dependent bladder cancer cell lines rapidly switch to HER2 or ERBB3 signaling when treated with BGJ398 (J. Wang et al. 2015). Additionally, NSCLC cell lines with *FGFR1* amplification and resistance to BGJ398 showed activation of PDGFRα and HER2 (Kotani et al. 2016). Inhibition of FGFR3 via PD173074 in bladder cancer cell lines increased EGFR intracellular signaling, suppressed *FGFR3* expression, and increased cell death (Herrera-Abreu et al. 2013).

Table 5 Summary of FGFR inhibitors

Therapeutic Classification	Generic Name	Trade Name	Company	Target	Cancer type in preclinical or clinical trials
Multi-target TKI inhibitors	BMS-582664	Brivanib	Bristol-Myers Squibb	FGFR1-3, VEGFR1-3	HCC
	AZD2171	Cediranib	AstraZeneca Pharmaceuticals	FGFR1,2, VEGFR	PCa, melanoma, NSCLC, head and neck cancer, liver cancer, breast cancer, GIST, solid tumors
	TKI258	Dovitinib	Novartis Pharmaceuticals	FGFR1-3, VEGFR1,3, PDGFRB, c-Kit	Gastric cancer, UCC, metastatic RCC, breast cancer, bladder cancer, PCa
	E3810	Lucitanib	Servier (Clovis Oncology, Inc.)	FGFR1,2, VEGFR1-3	Advanced solid tumors, metastatic breast cancer, advanced/metastatic lung cancer
	HMPL-012	Sulfatinib	Hutchison Medipharma	FGFR1, VEGFR1-3	Solid tumors
	Lenvatinib	Lenvima	Eisai Co., Ltd.	FGFR, VEGFR	NSCLC, solid tumors
	Nintedanib	Ofev	Boehringer Ingelheim	FGFR1-3, VEGFR1-3, PDGFR	Solid tumors
	Pazopanib	Votrient	GlaxoSmithKline	FGFR1-3, FGFR2_N549H, VEGFR1,3,4, KIT, PDGFRA,B	Approved for advanced soft tissue sarcoma, advanced RCC

	PD173074		Pfizer, Inc.	FGFR1-3, VEGFR2	
	Ponatinib	Iclusig	Takeda Pharmaceuticals (Ariad)	FGFR1-4, VEGFR2, BCR-ABL, VEGFR3, KIT, PDGFRA	Biliary cancer, advanced stage, approved for CML and Ph+ ALL
	Regorafenib	Stivarga	Bayer	FGFR1,2, KIT, PDGFRA,B, VEGFR1,3, ABL	Approved for GIST and previously treated metastatic CRC
	Sorafenib	Nexavar	Bayer (Onyx Pharmaceuticals)	FGFR1,2, FGFR2_N549H ABL1, KIT, PDGFRA,B, VEGFR1,3,4	Approved for liver, thyroid, and kidney cancers
	Stivarga	Regorafenib	Bayer	FGFR1,2, KIT, PDGFRA,B, VEGFR,3, ABL	Approved for advanced GIST and previously treated metastatic CRC
	Sunitinib	Sutent	Pfizer, Inc.	FGFR1,2, VEGFR1,3,4, PDGFRA,B, KIT	Approved for pancreatic neuroendocrine tumors, kidney cancer, and GIST
Selective FGFR family inhibitors	ASP5878		Astellas Pharma	FGFR 1-4, VEGFR2	Solid tumors
	AZD4547		AstraZeneca Pharmaceuticals	FGFR1-3	NSCLC, SCLC, breast cancer
	BGJ398	Infigratinib	Novartis Pharmaceuticals	FGFR1-4	NSCLC, SCLC, bladder cancer, glioma, cholangiocarcinoma, solid tumors and

					haematological cancers with FGFR abberation
	BLU9931		Blueprint Medicines	FGFR4	
	Debio 1347-101		Debiopharm International SA	FGFR1-3	Solid tumors
	E7090		Eisai Co., Ltd.	FGFR1	Advanced solid tumors
	FIIN-2			FGFR1-4	
	FIIN-3			FGFR1-4, EGFR	
	INCB054828		Incyte Corporation	FGFR1-3	Advanced malignancies
	JNJ-42756493	Erdafitinib	Janssen Biotech Inc.	FGFR 1-4	HCC, NSCLC, gastric cancer, UCC, oesophageal cancer, cholangiocarcinoma
	LY2874455		Eli Lilly and Co.	FGFR1-4, VEGF2	Advanced solid tumors
	TAS-120		Taiho Pharma Co. Ltd.	FGFR 1-4	Multiple myeloma, advanced solid tumors
Monoclonal antibodies	BAY1179470		Bayer	FGFR2	Solid tumors
	FPA144	Bemarituzumab	Five Prime Therapeutics	FGFR2IIIb	Bladder cancer, gastric cancer, advanced solid tumors
	GP369		AVEO Pharmaceuticals, Inc.	FGFR2IIIb	

	MFGR1877S		Genentech Inc.	FGFR3	Multiple myeloma, UCC, advanced solid tumors,

Therapeutic classification, generic and trade names of inhibitor, manufacturer, target, and types of cancer with FGFR aberration approved for or studying in preclinical or clinical trials. Abbreviations: TKI, Tyrosine kinase inhibitor; FGFR, fibroblast growth factor receptor; VEGFR, vascular endothelial growth factor; PDGFR, platelet-derived growth factor receptor; Src, SRC proto-oncogene; KIT, KIT proto-oncogene receptor tyrosine kinase; BCR, Breakpoint cluster region protein; ABL, Abelson murine leukemia viral oncogene homolog; HCC, Hepatocellular carcinoma; PCa, prostate cancer; NSCLC, Non-small cell lung carcinoma; GIST, Gastrointestinal stromal tumors; UCC: Urothelial carcinoma; RCC, Renal cell carcinoma; CML, Chronic meyloid leukemia; ALL, Acute lymphoblastic leukemia; Ph+, Philadelphia chromosome positive; CRC, Colorectal cancer; SCLC, Squamous cell lung carcinoma. Modified from Babina and Turner 2017, Hallinan et al. 2016.

K. *FGFR3* has been identified as a possible candidate for dAS in PCa disparities

Recently, evidence of a novel exon skipping event of *FGFR3* was identified in PCa by our lab (Wang et al. 2017). Affymetrix exon array data and Alternative Splice ANOVA modeling suggested decreased expression of exon 14 of *FGFR3* in AA PCa specimens (**Figure 6B**). RT-PCR showed predominant expression of *FGFR3-S* (missing exon 14) in AA PCa patients and predominant expression of *FGFR3-L* (containing exon 14) in EA patients (**Figure 6A,C**). Validation of *FGFR3* splice variants in a separate cohort confirmed increased *FGFR3-S/-L* expression ratios in AA versus EA PCa.

Wang et al. hypothesized that increasing, or enriching, the *-S/-L* expression ratio may contribute to a more aggressive phenotype. To test this, an siRNA was designed to specifically target exon 14 of *FGFR3* (e.g. siFGFR3-ex14), thus decreasing expression of only *FGFR3-L*. Treatment with siFGFR3-ex14 in an EA PCa cell line, VCaP, significantly decreased expression of *FGFR3-L*, which is the only splice variant expressed in this cell line, compared to control cells (**Figure 7**). Knockdown of *FGFR3-L* in VCaP cells had no significant difference compared to siRNA-nonsense treated control cells on invasion or proliferation. Next, AA cell line MDA PCa 2b, which expresses both *FGFR3-L* and *FGFR3-S*, were treated with siFGFR3-ex14. Knockdown of *FGFR3-L* also enriched expression of *FGFR3-S* by over 20-fold (**Figure 7**). While no significant difference in invasion was observed between control and siFGFR3-ex14-treated MDA PCa 2b cells, knockdown of *FGFR3-L* and enrichment of *FGFR3-S* significantly increased the proliferative capacity of these cells.

Figure 6 Validation of *FGFR3* dAS in AA and EA specimens

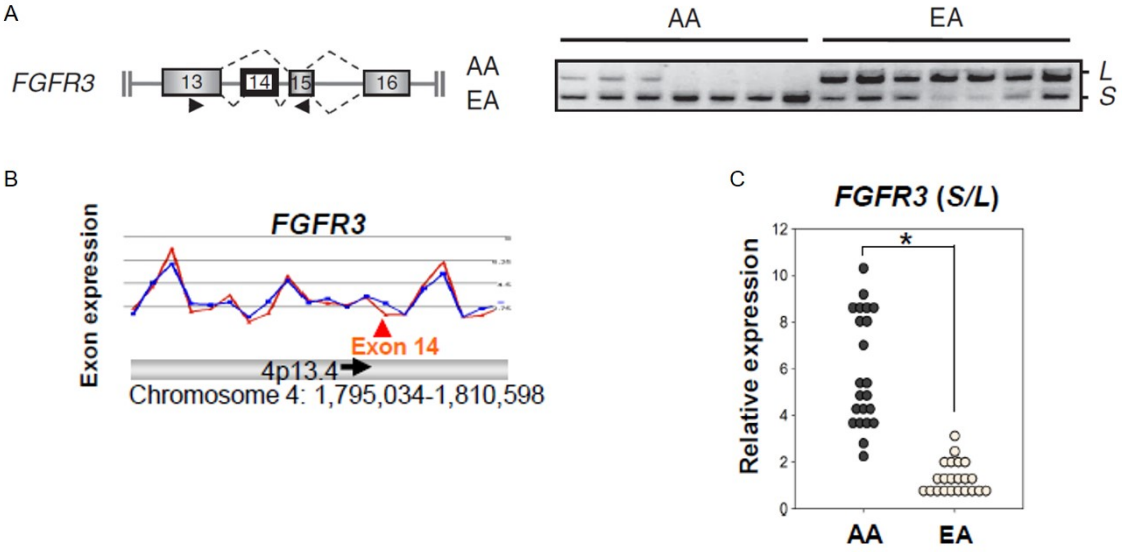

A) Schematic representation and representative RT-PCR validation of *FGFR3* splicing event. Broken lines represent splicing events, arrow heads represent primer location. B) Log2 regression plots of Alternative Splice ANOVA modeling of *FGFR3* in AA (red) and EA (blue) PCa specimens. Genomic location of each gene is represented below the plot, the black arrow below the x-axis indicates the coding direction of gene, and each point on the plot indicates the expression of a single exon. Red arrow indicates the skipped exon. C) Quantification of ratio of *FGFR3-S/L* expression in validation cohort. n=22 AA and 30 EA, two-sided t-test,*p<0.05. Modified from Wang et al. 2017.

Figure 7 Enrichment of FGFR3-S enhances proliferation in vitro

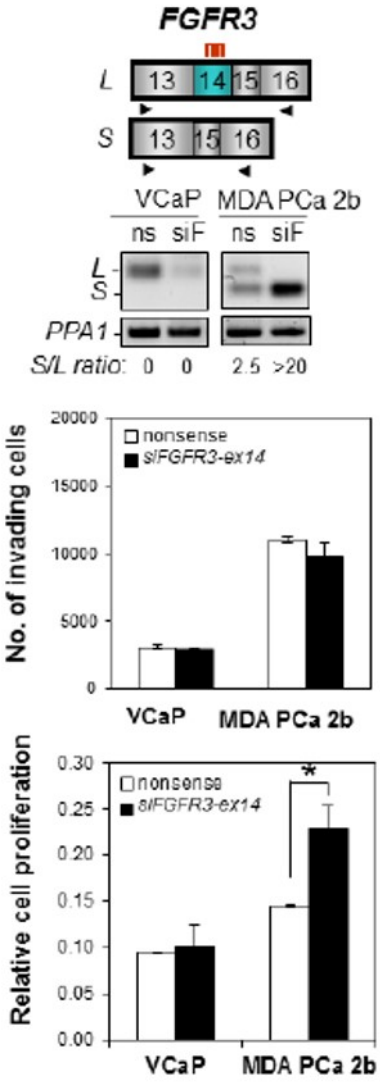

Exon 14-specific siRNA (siF, red mark) was designed to target *FGFR3-L*. Knockdown efficiency in EA cell line VCaP and AA cell line MDA PCa 2b was determined via RT-PCR. Ratio of -S/-L expression is shown beneath gel (upper panel). *PPA1* is used as a loading control. Invasion and proliferation after knockdown is nonsense control siRNA (nonsense) or siF (siFGFR3-ex14) in both cell lines is shown in the bottom panels. Data are represented as mean±SEM, n=3-5 independent experiments, one-way ANOVA with Tukey post-hoc, *p<0.05. Modified from Wang et al. 2017.

L. Statement of problem

The functional consequences of dAS in PCa disparities are just beginning to be investigated. There is currently no research linking *FGFR3* or the splicing of this gene to PCa nor PCa health disparities. The results from Wang et al. (2017) suggest a role for dAS of *FGFR3* in PCa health disparities. The *FGFR3-S* variant has never before been reported and remains to be confirmed. Excluding splicing of the Ig-like domains, no other splice variants of *FGFR3* have been reported thus far. The *in vitro* and *in vivo* effect of FGFR3-S in PCa requires further assessment as well. Determining the molecular characteristics of novel *FGFR3* splice variants *in vitro* and *in vivo* at baseline, as well as in response to treatment with SMIs or cytotoxic therapeutics, will have important implications for treating PCa patients and identifying new biomarkers and high-risk patients. Additionally, the role of aberrant expression of SFs in PCa disparities is not well understood. Upstream factors, such as SFs, involved in the skipping of exon 14 of *FGFR3* have not been identified.

We hypothesize that aberrant expression of splicing factors mediates differential alternative splicing of *FGFR3* which may be contributing to prostate cancer health disparities in African American patients. The following aims were addressed in this study:

Aim 1: Verification of *FGFR3* splice variants

Aim 2: Determination of oncogenicity of FGFR3-S compared to FGFR3–L

Aim 3: Determination of differential expression of splicing factors and their contribution to *FGFR3* splicing patterns

Chapter 2: Materials and Methods

A. Cell culture

B. Reagents

C. RNA isolation

D. Reverse transcription-polymerase chain reaction

E. Molecular cloning and sequencing of *FGFR3* variants

F. Transfections and derivation of stable cell lines

G. Kaplan-Meier survival curve analysis

H. Proliferation assay

I. Migration assay

J. Invasion assay

K. Caspase assay

L. Cell-free kinase assay

M. Western blots

N. Animal studies

O. Microarray gene expression analysis

P. Immunohistochemistry

Q. Immunocytochemistry

R. siRNA-mediated gene knockdowns

S. Statistical Analysis

A. Cell culture

European American (EA) prostate cancer (PCa) cell lines PC-3 (CRL-1425), LNCaP (CRL-1740), and VCaP (CRL-2876) and African American (AA) PCa cell line MDA PCa 2b (CRL-2422) were purchased from the American Type Tissue Collection (ATCC, Manassas, VA) (**Table 6**). AA PCa cell line RC77 T/E was a gift from Dr. Johng Rhim (**Table 6**). PC-3 cells were maintained in Dulbecco's Modified Eagle Medium (DMEM) supplemented with 10% fetal bovine serum (FBS) and 1% penicillin-streptomycin and 1% L-glutamine (Thermo Fisher Scientific, Waltham, MA). LNCaP cells were grown in Rosewell Park Memorial Institute (RPMI) medium with 10% FBS and 1% L-glutamine (Thermo Fisher Scientific). MDA PCa 2b cells were grown in BRFF-HPC1 medium (Athena Enzyme Systems, Baltimore, MD) supplemented with 20% FBS and 1% penicillin-streptomycin. RC77 T/E cells were grown on plates coated with FNC coating mix (Athena Enzyme Systems) in Keratinocyte-SFM medium supplemented with 1% L-glutamine, 0.15ng/ml epidermal growth factor 1-53, and 25µg/ml bovine pituitary extract (Thermo Fisher Scientific). All cells were maintained in $10cm^3$ culture dishes at 37ºC and 5% CO_2. Cells were passaged 2-3 times per week at a 1:4 dilution. Cells were detached with 2ml of 0.05% trypsin-EDTA (Thermo Fisher Scientific). Cell aliquots were stored at -80ºC in medium supplemented with 20% FBS and 10% dimethyl sulfoxide (DMSO, Sigma Aldrich, St. Louis MO). Cells were thawed in a 37ºC water bath immediately after removal from long term storage and resuspended in pre-warmed medium. All cells used were ≤ 20 passages.

Table 6 Prostate cancer cell lines

Cell line	Race	Derivation	Tumor-igenic	AR	PSA	ETS	PTEN	SPOP	TP53	Other	Citation
PC-3	EA	Metastasis (bone)	+	-	-	*ETV1* +	del/ mut	wt	wt	unresponsive to AR, glucocorticoids; more neoplastic; *ETV1* fusion and overexpression	Kaighn et al. 1979
LNCaP	EA	Metastasis (lymph node)	+	+	+	*ETV4* +	del/ mut	wt	del/ mut	resistant to fibroblast interferon; *ETV4* overexpression	Horoszewicz et al. 1983
MDA PCa 2b	AA	Metastasis (bone)	+	+	+	*ETV1* + *ETV4* +			wt	AR mutations, androgen responsive (but not required), *ETV1* translocation, *ETV4* overexpression	Navone et al. 1997
RC77 T/E	AA	Metastasis (malignant)	+	+	+						Theodore et al. 2010

Molecular characteristics of prostate cancer cell lines. Abbreviations: EA, European American; AA, African American; AR, androgen receptor; PSA, prostate specific antigen; ETS, E26 transformation specific transcription factor; ETV, ETS variant; PTEN, phosphatase and tensin homolog; SPOP, speckle type BTB/POZ protein; TP53, tumor protein P53; del, deletion, mut, mutation; wt, wildtype. Modified from Barbieri et al. 2013; van Bokhoven et al. 2003; Mesquita et al. 2015; Tomlins et al. 2007.

B. Reagents

The following primers (**Table 7**), siRNAs (**Table 8**), biochemical reagents (**Table 9**), and antibodies (**Table 10, 11, 12, 13**) were used in this study.

Table 7 RT-PCR primers

Gene Name	Gene Symbol	RefSeq	Forward Primer	Reverse Primer
DExD-box helicase 21	*DDX21*	NM_001256910.1	GCTACGGGAAGTGACGAG	CAGCGTCACTACGGAGTTTT
DEAD-box helicase 5	*DDX5*	NM_001320595.1	CGACCAAAACCCGTCAAAGGA	CCGATGACACCAGCCGAAG
Eukaryotic Translation Initiation Factor 1A, X-Linked	*EIF1AX*	NM_001412	GTACTGGAGAGGGGAGAGCA	TGAAGCTGAAACAAGCAGGA
Fibroblast Growth Factor Receptor 3	*FGFR3* (5' end)	NM_001163213.1	GCAGCATGCCCGCGCGCGCTG	
Fibroblast Growth Factor Receptor 3	*FGFR3* (3' end)	NM_001163213.1		GCTGTCTCTCCATCTGCACTG
Fibroblast Growth Factor Receptor 3	*FGFR3* (exon 3)	NM_001163213.1	ACTGTCTGGGTCAAGGATGG	GCACACTGAAGTGGCACAGT
Fibroblast Growth Factor Receptor 3	*FGFR3* (exon 6)	NM_001163213.1	ATCAGCAGTGGAGCCTGGT	CAGCACGTCCAGCGTGTA
Fibroblast Growth Factor Receptor 3	*FGFR3* (exon 9)	NM_001163213.1	ATGCAGGCATCCTCAGCTAC	GGAAGCGGGAGATCTTGTG

Fibroblast Growth Factor Receptor 3	*FGFR3* (exon 11)	NM_001163213.1	GTCACCGTAGCCGTGAAGAT	
Fibroblast Growth Factor Receptor 3	*FGFR3* (exon 12)	NM_001163213.1		CCCAGCAGGTTGATGATGTT
Fibroblast Growth Factor Receptor 3	*FGFR3* (exon 16)	NM_001163213.1	CTGGTCCTTTGGGGTCCT	AGGTCGTGTGTGCAGTTGG
Heterogeneous Nuclear Ribonucleo-protein F	*HNRNPF*	NM_001098204.1	GCGGTCCTTGCGTCCTTC	TTCCACCGAAGCTCAACCAC
Heterogeneous Nuclear Ribonucleo-protein R	*HNRNPR*	NM_001102397.2	GGTTCCCAACCCATCGCT	TGTCTACTTCCACTGTTGCCC
Serine and Arginine Rich Splicing Factor 1	*SRSF1 (ASF/SF2)*	NM_001078166.1	ACCTCCAGACATCCGAACCA	TCGAACTCAACGAAGGCGAA
Serine and Arginine Rich Splicing Factor 2	*SRSF2 (SC35)*	NM_001195427.1	CGCCCAGTTGTTACTCAGGT	CGCGCCTCTCAGGCAGTT
Serine and Arginine Rich Splicing Factor 7	*SRSF7 (9G8)*	NM_001031684.2	AAGCAGCCGATCAAAGTCCA	ACTTGAGAGCTTCAGTCCATTCT

Gene names, symbols, accession numbers, forward and reverse primer sequences used in RT-PCR reactions.

Table 8 siRNAs

Gene Name	Gene Symbol	RefSeq	siRNA Name	siRNA Sequence (5'-3')	Catalog No.
DExD-box helicase 21	*DDX21*	NM_001256910.1	siDDX21_1	CAGGAGAAAUGGCAUGAUU	J-011919-05
DExD-box helicase 21	*DDX21*	NM_001256910.1	siDDX21_2	UCACCAAACUUAAGCAUGU	J-011919-06
DEAD-box helicase 5	*DDX5*	NM_001320595.1	siDDX5_1	GCAAAUGUCAUGGAUGUUA	J-003774-05
DEAD-box helicase 5	*DDX5*	NM_001320595.1	siDDX5_2	CAACCUACCUUGUCCUUGA	J-003774-06
Heterogeneous Nuclear Ribonucleoprotein F	*HNRNPF*	NM_001098204.1	siHNRNPF_1	CGUACCAAGCGACCGAGAA	J-013449-09
Heterogeneous Nuclear Ribonucleoprotein F	*HNRNPF*	NM_001098204.1	siHNRNPF_2	AUGGAAGAGUGACGGGUGA	J-013449-11
Heterogeneous Nuclear Ribonucleoprotein R	*HNRNPR*	NM_001102397.2	siHNRNPR_1	GGUGAAUGGUAAUGCGGUA	J-010905-09
Heterogeneous Nuclear Ribonucleoprotein R	*HNRNPR*	NM_001102397.2	siHNRNPR_2	CGGUCAGAAUAGAGGGUAU	J-010905-10
Serine and Arginine Rich Splicing Factor 1	*SRSF1 (ASF/SF2)*	NM_001078166.1	siSRSF1_1	CGUGGAGUUUGUACGGAAA	J-018672-09
Serine and Arginine Rich Splicing Factor 1	*SRSF1 (ASF/SF2)*	NM_001078166.1	siSRSF1_2	UGACCUAUGCAGUUCGAAA	J-018672-10

Serine and Arginine Rich Splicing Factor 2	*SRSF2 (SC35)*	NM_001195427.1	siSRSF2_1	GCGGUGUCCUCUUAAGAAA	J-019711-05
Serine and Arginine Rich Splicing Factor 2	*SRSF2 (SC35)*	NM_001195427.1	siSRSF2_2	GCACGAAGGUCCAAGUCCA	J-019711-06
Serine and Arginine Rich Splicing Factor 7	*SRSF7 (9G8)*	NM_001031684.2	siSRSF7_1	GAGGAGAAACCAAGGUGUA	J-015909-05
Serine and Arginine Rich Splicing Factor 7	*SRSF7 (9G8)*	NM_001031684.2	siSRSF7_2	GAGAAUUCGAAGAUCCUAGA	J-015909-06
Scrambeled Nonsense (negative control)			siNS	CCAAAUUAUACCUACAUUGCUdTdT	

Gene names, symbols, accession numbers, siRNA name, siRNA sequence, and GE Dharmacon catalog number for siRNAs used for gene knockdowns.

Table 9 Biochemical reagents

Reagent Name	Company	Catalog Number	Solvent
Dovitinib (TKI258)	Selleckchem	S7765	100% DMSO, 1X PBS, 0.9% saline
Docetaxel	Selleckchem	S1148	100% DMSO, 1X PBS

Reagent name, supplier, catalog number, and solvent of reagents used.

Table 10 Primary antibodies used for immunohistochemistry and immunocytochemistry

Primary Antibody Abbreviation	Protein Name	Host	Company	Catalog No.	Dilution
DDX21	DExD-box helicase 21	Mouse	Santa Cruz	sc-376953	1:1000 IHC/ 1:50 ICC
DDX5	DEAD-box helicase 5	Rabbit	Abcam	ab21696	1:50
FGFR3 (B-9)	Fibroblast Growth Factor Receptor 3	Mouse	Santa Cruz	sc-13121	1:50
His tag	6X Polyhistidine tag	Rabbit	Abcam	ab14923	1:50
hnRNPF	Heterogeneous Nuclear Ribonucleoprotein F	Mouse	Santa Cruz	sc-32310	1:50
hnRNPR	Heterogeneous Nuclear Ribonucleoprotein R	Rabbit	Abcam	ab30930	1:50
SRSF1 (ASF/SF2)	Serine and Arginine Rich Splicing Factor 1	Mouse	Santa Cruz	sc-33652	1:50
SRSF2 (SC35)	Serine and Arginine Rich Splicing Factor 2	Rabbit	LS Bio	LS-C97287	1:50
SRSF7 (9G8)	Serine and Arginine Rich Splicing Factor 7	Rabbit	LS Bio	LS-C169029	1:25 IHC/ 1:50 ICC
WGA	Wheat Germ Agglutinin (Alexa 488 conjugate)		Molecular Probes	W11261	1:200

Protein abbreviation, name, antibody host, supplier, catalog number, and dilution of primary antibodies used for IHC and ICC.

Table 11 Secondary antibodies used for immunohistochemistry and immunocytochemistry

Secondary Antibody	Host	Company	Catalog No.	Dilution
Alexa Fluor 594 Anti-Mouse	Goat	Life Technologies	A11005	1:200
Alexa Fluor 594 Anti-Rabbit	Donkey	Life Technologies	R37119	1:200
Biotinylated IgG	Mouse + Rabbit	Dako	K0675	
Streptavidin HRP		Dako	K0675	

Antibody name, host, supplier, catalog number, and dilution of secondary antibodies used for IHC and ICC.

Table 12 Primary antibodies used for western blots

Primary Antibody Abbreviation	Protein Name	Host	Company	Catalog No.	Dilution
AKT	Protein Kinase B	Rabbit	Cell Signaling	9272S	1:1000
AKT (pSer473)	Protein Kinase B	Rabbit	Cell Signaling	9271S	1:1000
AKT (pThr308)	Protein Kinase B	Rabbit	Cell Signaling	2965S	1:1000
β-actin	β-actin	Mouse	Abcam	ab8226	1:500
β-actin	β-actin	Mouse	Santa Cruz	sc-47778	1:200
FGFR3 (pTyr577)	Fibroblast growth factor receptor 3	Rabbit	Invitrogen	PA5-64797	1:1000
His tag	6X Polyhistidine tag	Rabbit	Abcam	ab14923	0.5ug/ml
S6	Ribosomal Protein S6 (5G10)	Rabbit	Cell Signaling	2217S	1:1000
S6 (pSer235/236)	Ribosomal Protein S6 (5G10)	Rabbit	Cell Signaling	4857S	1:1000
STAT3	Signal transducer and activator of transcription 3	Mouse	Cell Signaling	9139S	1:1000
STAT3 (pTyr705)	Signal transducer and activator of transcription 3	Rabbit	Cell Signaling	9131S	1:1000
V5 tag	SV5 PK Epitope tag	Mouse	Santa Cruz	sc-81594	1:1000

Protein abbreviation, name, antibody host, supplier, catalog number, and dilution of primary antibodies used for western blots.

Table 13 Secondary antibodies used western blots

Secondary Antibody	Host	Company	Catalog No.	Dilution
Anti-Mouse IgG (H+L) HRP	Donkey	Southern Biotechnology	6410-05	1:3000
Anti-Rabbit IgG (H+L) HRP	Donkey	Southern Biotechnology	6440-05	1:10000

Antibody name, host, supplier, catalog number, and dilution of secondary antibodies used for western blots.

C. RNA isolation

Total RNA was isolated from cells and patient prostate biopsy specimens via the Trizol method or the QIAgen miRNeasy kit (Valencia, CA) per manufacturer's protocol. Cells were trypsonized, centrifuged at 1,200xg for 5min at 4 ºC, and resuspended in ice cold 1X PBS. The cell suspension was transferred to a 1.7ml eppendorf tube and centrifuged at 10,000xg for 5min at 4 ºC to pellet the cells.

Trizol protocol: Cell pellets were resuspended and sheared in 1ml Trizol using a 25G needle. After incubation in Trizol for 5min at room temperature, 200µl of chloroform was added and the suspension was vortexed vigorously for 15sec. The suspension was incubated for 3min at room temperature and then centrifuged at 10,000xg for 15min at 4ºC. The clear upper aqueous phase was carefully transferred to a fresh 1.7ml eppendorf tube. 500µl of isopropanol was added and the sample was stored in -80ºC overnight. After thawing, the sample was centrifuged at 10,000xg for 15min at 4ºC. The isopropanol was carefully removed and 1ml 70% ethanol was added to wash the pellet. The sample was centrifuged at 10,000xg for 5min at 4ºC. The ethanol was gently decanted and the eppendorf tube was left open on the bench top for 5min to allow any remaining ethanol to evaporate. The RNA pellet was resuspended in 30-40µl of RNase-free water.

QIAgen miRNeasy protocol: Cell pellets were resuspended and sheared in 700µl QIAzol using a 25G needle. After incubation in QIAzol for 5min at room temperature, 200µl of chloroform was added and the suspension was vortexed vigorously for 15sec. The suspension was incubated for 3min at room temperature and then centrifuged at 12,000xg for 15min at 4ºC. The clear upper aqueous phase was transferred to a fresh

1.7ml eppendorf tube and mixed with 525µl 100% ethanol. The supernatant was added to the RNeasy column, centrifuged at 8,000xg for 30sec, and washed once with 500µl RWT buffer. DNase I (10µl in 70µl RDD Buffer) was added to the column and incubated for 15min at room temperature, followed by one wash each with 500µl RWT and 700µl RPE buffers, with a 30sec 8,000xg spin between each wash. The spin column was placed in a new 2ml elution tube and centrifuged at max speed for 1min. RNA was eluted in 40µl of RNase-free water in a new 1.7ml eppendorf tube.

RNA integrity was measured via 1% agarose gel and RNA concentration was determined using a Nanodrop ND-1000 Spectrophotometer (Thermo Fisher Scientific). Purified RNA was stored at -80ºC.

D. Reverse transcription-polymerase chain reaction

Reverse transcription (RT) of 1µg purified RNA to cDNA was performed using the Taq Man Reverse Transcription kit (Applied Biosystems, Foster City, CA) using random hexamer primers according to manufacturers' instructions, using the following reaction mix and incubation protocol:

10X Reaction buffer	5µl
$MgCl_2$ solution	11µl
dNTP mixture (2.5M each)	10µl
Random hexamers (50µM)	2.5µl
RNase inhibitor (20U/µl)	1µl
Reverse Transcriptase II (50U/µl)	1.25µl
1µg RNA	
Nuclease/RNase free water	up to 50µl

25ºC	10min
42 ºC	30min
95 ºC	5min
4 ºC	∞

Primers for RT-polymerase chain reaction (PCR) were designed using PrimerBlast (National Center for Biotechnology Information (NCBI), Bethesda, MD**).** Primer pairs were selected for a length of 15-21 base pairs, PCR product length of 100-150bp, melting temperature 58-62ºC, G/C content 20-70%, and zero 3' self-complementarity. Human specificity for each sequence was verified using BLAST (NCBI). Primers were produced by Genscript (Piscataway, NJ)**.**

PCR was performed using the 2X GoTaq Green Master Mix (Promega, Madison, WI) using 1µl of cDNA with the following reaction mix and cycling conditions:

2X Go Green Taq Master Mix	12.5µl
Primer_Forward (10µM)	1µl
Primer_Reverse (10µM)	1µl
cDNA template	1µl
Nuclease/RNase free water	9.5µl

95ºC	3min	
95 ºC	30sec	
55 ºC	30sec	30-35X
72 ºC	30sec	
72 ºC	6min	
4 ºC	∞	

PCR products were analyzed via 1% agarose gel run at 120V for 20-30min. Housekeeping gene Eukaryotic Translation Initiation Factor 1A, X-Linked 1A (*EIF1AX*) was used as a loading control.

E. Molecular cloning and sequencing of *FGFR3* variants

RNA isolation, cDNA generation, and PCR amplification was performed as described previously. *FGFR3-L* and *FGFR3-S* were amplified using 5' and 3' rapid amplification of cDNA ends (RACE) in the following sections: exons 2-3 (primers FGFR3_F, exon 3_R), exons 3-6 (primers exon 3_F, exon 6_R), exons 6-12 (primers exon 6_F, exon 12_R), exon 11-16 (primers exon 11_F, exon 16_R), exons 16-18 (primers exon 16_F, FGFR3 3'_R). Exons 11-16 were also sequenced from RC77 T/E. After PCR products were separated on 1% agarose cells for 30-40min, bands were excised using a razor blade. DNA was purified from the agarose using the QIAgen Gel Extraction kit. Briefly, the gel slice was weighed and three volumes of Buffer QG was added and the gel slice was incubated at 50 ºC for 10min or until the gel was fully dissolved. One volume of isopropanol was added and the sample was mixed well before being transferred to a spin column. The column was centrifuged at 13,000rpm for 1min. Two wash steps, 1X 500µl Buffer QG and 1X 750µl Buffer PE, were performed with a 1min centrifugation step between each wash. After the flow through from the last wash was discarded, the column was centrifuged for an additional minute. The column was then transferred to a new 1.7ml eppendorf tube and 50µl of water was added to elute the DNA.

Next, DNA was cloned into the pCR2.1 TOPO vector (Life Technologies, Grand Island, NY) by incubating 1µl DNA with 1µl salt solution, 3µl water, and 1µl of vector on ice for 5min. Two microliters of the cloning reaction were added to a vial of One-Shot TOP10 Chemically Competent *E. coli* cells (Thermo Fisher Scientific) and incubated on ice for 5-30min. Cells were then heat shocked in a 42ºC water bath for 30sec and

immediately placed on ice for 2min. 250µl of room temperature super optimal broth with catabolite repression (SOC) medium was added and the vials were placed horizontally to shake at 220rpm at 37ºC for 1hr. Then, 5-10µl were spread on a pre-warmed luria broth (LB) agar plate (with 50µg/ml carbenicillin) using sterilized glass beads. The plate was incubated at 37ºC overnight. The next day, approximately 12 individual colonies were picked, seeded on a new LB plate, and added to a PCR reaction to verify the colony contained the sequence of interest. PCRs were performed using nested primers using the cycling conditions listed previously (exception: initial denaturing step was performed for 5min). Two to three positive colonies were inoculated into 2ml of LB+carbenicillin (50µg/ml) and placed in a 37ºC shaker at 220rpm overnight.

The following day, 1ml of bacteria was added to a cryovial with 160µl glycerol. This glycerol stock was stored in -80 ºC. The remaining bacteria was transferred to a 1.7ml eppendorf tube to use in Qiagen's Miniprep kit to isolate the inserted vector. The following protocol steps were conducted at room temperature and all centrifuge steps were carried out at 13,000rpm unless otherwise noted. Bacteria were centrifuged at 8,000rpm for 3 minutes at room temperature. Bacterial pellets were resuspended in 250µl Buffer P1 and 250µl Buffer P2 was added. Tubes were inverted four to six times and 250µl Buffer N3 was added. Tubes were inverted four to six times before centrifuging for 10min. The supernatant was transferred to a spin column and centrifuged for 1min. The spin column was washed 1X with 500µl Buffer PB and 1X 750µl Buffer PE with one 30sec centrifuge step between each wash and following the PE wash. The column was transferred to a new eppendorf tube and 40ul water was added to elute the DNA. The column was allowed to stand for 1min before centrifuging for 1min. DNA concentration

was determined by Nanodrop ND-1000 Spectrophotometer**.** The insert of interest was confirmed by running PCR using primers that anneal within the PCR product of interest (e.g. nested primers).

Purified plasmids were submitted to Sequetech (Mountain View, CA) for Sanger sequencing (3µg per run, forward and reverse reads using vector M13 primer pair). Sequences were analyzed for 1) clean chromatograms via Chromas Lite (Technelysium Pty Ltd, South Brisbane, Australia), 2) sequence similarity to *FGFR3* via BLAST (NCBI), and 3) 100% alignment to the reference sequence. Two to three colonies with forward and reverse reads were generated for each sequence of interest and used to generate a final consensus sequence. The sequence of the short variant was deposited into Genbank (accession number MK542707).

F. Transfections and derivation of stable cell lines

Genes of interest were subcloned into vectors by Genscript. PC-3, LNCaP, and MDA PCa 2b cells were transfected in 10cm^3 culture plates with Lipofectamine 3000 (Thermo Fisher Scientific). The day before transfection, cells were plated at 70-90% confluency. Immediately before transfection cell culture medium was replaced with antibiotic free medium. In two separate tubes, 500µl Opti-MEM medium, 20µg DNA, and 40µl P3000 reagent, and 33µl Lipofectamine 3000 reagent in 500µl Opti-MEM medium were mixed separately. The mixtures were combined and incubated together at room temperature for 15min. The transfection mix was then added dropwise to the cell culture dish and cells were incubated for 24-48hrs. Medium was replaced with fresh medium containing maintenance antibiotics and cells were allowed to grow until normal

morphology was achieved. Cells were then split 1:10 in 15cm^3 dishes in medium containing G418S (Thermo Fisher Scientific) (PC-3: 150µg/ml, LNCaP: 200µg/ml) or hygromycin (Gold Biotechnology, St. Louis, MO) (MDA PCa 2b: 200µg/ml) and allowed to grow for 3-5 weeks until individual colonies had formed. Single colonies were picked using cloning rings and seeded into 24 well plates. Once cells reached confluency, they were seeded into 6 well plates, and then 10cm^3 plates successively. Colonies were screened for expression of correct *FGFR3* variant, V5 tag and/or His tag, and pcDNA3.1 vector via RT-PCR and western blot.

RC77 T/E cells were transfected using the Amaxa Cell Line Nucleofector Kit C (Lonza Cologne AG, Cologne, Germany). Cells were trypsinized and 1 x 10^6 cells were resuspsended in 100µl of Nucleofector Solution C with supplement. Five micrograms of vector was added to the cells and the cell/DNA suspension was added to a certified cuvette. The cuvette was capped and inserted into the holder on the Nucleofector instrument and protocol T-30 was performed. The cuvette was immediately removed from the holder, 500µl of prewarmed Keratinocyte medium was added to the cells, and the cell/medium suspension was transferred into a prepared 6 well plate containing 1.5ml Keratinocyte medium using a sterilized plastic pipette. After 24hrs, the medium was changed. Once cells exhibited normal morphology, cells were split 1:10 in 10 cm^3 dishes in medium containing 100µg/ml of hygromycin (Gold Biotechnology). Isolation, expansion, and analysis of individual colonies were performed as described above.

G. Kaplan-Meier survival curve analysis

Variant expression of *FGFR3-S* and *FGRF3-L* were determined using the method of Kim et al. (2011) on prostate (PRAD), colon (COAD) and breast (BRCA) RNA-seq data from The Cancer Genome Atlas (TCGA). Briefly, variants were calculated through minimizing a weighted non-negative least squares problem based on exon expression. The expression values of *FGFR3-S* and *FGRF3-L* in these patients were then used as predictors to fit the Cox-Proportional Hazards (Cox-PH) regression model for relapse free survival. A prognosis index (PI) score was generated for each patient using the Cox proportional hazards model, as reported earlier (Chaudhary et al. 2018; Ching et al. 2016; Ching, Zhu, and Garmire 2018; Sijia Huang et al. 2014; Wang et al. 2017; Wei et al. 2016). Patients were dichotomized into high- versus low- *FGFR3-S*/*FGRF3-L* ratio groups. The log-rank *p* value was calculated to assess statistical significance between Kaplan-Meier curves of high- versus low- *FGFR3-S*/*FGRF3-L* ratio groups.

H. Proliferation assay

Proliferation was assessed using the BrdU Cell Proliferation Assay from Millipore Sigma (Burlington, MA) per manufacturer's instructions. Each experiment was performed in duplicate with blank (medium only) and background (cells with no BrdU label) control wells. Cells were seeded in 96-well plates at a density of 2 x 10^4 cells in 100µl of medium. Cells were allowed to adhere overnight. When treating cells with a drug of interest, 2µl pharmacological reagent (varying concentrations) or 2µl vehicle were added to each well for 12hr at 37 ^{o}C**.** Cells were then incubated with 20µl 1:2,000 BrdU label for 4hr. The medium was removed and the cells were fixed and denatured,

incubated with 100µl anti-BrdU antibody for 1hr, washed 3X with 1X wash buffer, and incubated with 100µl peroxidase goat anti-mouse IgG HRP for 1hr. Cells were washed 3X with 1X wash buffer and 1X with deionized water. 100µl of Substrate Solution was added for 2-5min to convert the chromogenic substrate tetra-methylbenzidine (TMB) from a colorless solution to a blue solution. The reaction was halted with the addition of 100µl Stop Solution, turning the solution yellow. Absorbance at 450-540nm was measured via Nanodrop ND-1000 Spectrophotometer (Thermo Fisher Scientific) or the SpectraMax MiniMax 300 Imaging Cytometer (Molecular Devices) using a 6-point well scan.

I. Migration assay

The Boyden chamber method was used to measure cell migration using the QCM Fluorimetric Chemotaxis 96-well Cell Migration Assay (Millipore Sigma). All reagents were allowed to equilibrate to room temperature before use. Cells were serum-starved 24hrs prior to the experiment. Cells were seeded into the migration chamber tray at 5 x 10^4 cells/ml in 100µl of 0.1% FBS medium. 150µl of 10% FBS medium was added to the lower feeder tray. Equivalent concentrations of vehicle or drug were added to the insert and lower tray. Cells were incubated for 12hrs at 37ºC. Cells and media in the insert were removed by gently decanting the cell suspension. The migration chamber tray was placed in a fresh feeder tray that contained 150µl Cell Detachment Solution in each well and incubated for 30min at 37ºC. During the incubation, the plate was gently tilted back and forth several times to dislodge cells completely. Next, the migration chamber tray was removed and 50µl of Lysis Buffer/Dye Solution (1:75) was added to each well and

incubated for 15min at room temperature. 150µl of the mixture was then added to a white with clear bottom 96-well plate. Fluorescence was measured via the SpectraMax MiniMax 300 Imaging Cytometer using a 480/520nm filter set and 6-point well scan. All experiments were performed in duplicate.

J. Invasion assay

Matrigel invasion chambers (VWR, Radnor, PA) were hydrated with 200µl DMEM in the top well and 750µl DMEM in the bottom chamber for 2hrs at 37ºC. The medium was removed and the top well was seeded with 5 x 10^2 cells resuspended in 200µl 0.1% FBS medium with or without pharmacological reagent. The bottom chamber contained 750µl 10% FBS medium with or without pharmacological reagent. Cells were incubated in invasion chamber for 48hrs at 37ºC. Following the incubation period, medium from the top well was removed via aspirator and the chamber was stained in IMEB DIF-Quik Stain (Thermo Fisher Scientific) according to manufacturer's instructions. Each chamber was incubated for 2min in 750µl fixative (methanol), 750µl cytoplasmic (hematoxylin), and 750µl nuclear (eosin) stains. Inserts were rinsed in distilled water, removed from the chamber with a razor blade, mounted on a glass slide, and covered with a coverslip. The total number of invading cells was manually counted using a light microscope. All experiments were performed in duplicate.

K. Caspase assay

Apoptotic activity was measured by caspase 3/7 luminescence using the Caspase-Glo 3/7 Assay (Promega). Each experiment was performed with blank (medium only)

control wells. PC-3, MDA 2b PCa, and RC77 T/E cells were seeded at 2 x 10^4 in 100µl and LNCaP cells were seeded at 1 x 10^4 in 100µl. Cells were allowed to adhere overnight and treated with 2µl pharmacological reagent (varying concentrations) or 2µl vehicle for 24hrs. Cells were equilibrated to room temperature for 1.5hrs and then incubated with 100**µl** Caspase-Glo reagent for 1hr at room temperature. Luminescence was measured via the SpectraMax MiniMax 300 Imaging Cytometer using a 6-point well scan. All experiments were performed in duplicate.

L. Cell-free kinase assay

The cell-free kinase assay for FGFR3wt and FGFR3-S was modified from FGFR1 Kinase Enzyme System (Promega). The recombinant intracellular domains of FGFR3wt (aa 397-end) and FGFR3-S (d613-653) were generated by SignalChem (Richmond, British Columbia, Canada) via baculovirus expression in Sf9 insect cells using an N- terminal GST tag. The following reagents (Promega, SignalChem) were used in the assay:

5X Reaction Buffer A: 40mM Tris, 7.5, 20mM $MgCl_2$, 0.1mg/ml BSA, 50µM DTT

Substrate: Poly (Glu_4,Tyr_1), 1mg/ml stock, 0.4mg/ml final

ATP: 10mM stock, 25µM final

In a 96-well plate, 20ul of recombinant enzyme (diluted in 2.5X Kinase Reaction Buffer) and 5ul substrate/ATP mix (diluted in 2.5X Kinase Reaction Buffer) were mixed and incubated for 60min at room temperature. Next, 25ul ADP-Glo reagent was added and incubated for 40min. 50ul of the Kinase Detection reagent was then added and incubated for 30min. Luminescence was measured via the SpectraMax MiniMax 300

Imaging Cytometer using a 6-point well scan. All experiments were performed in duplicate.

M. Western blots

Cells were grown to 70% confluency in a $10cm^3$ plate and washed with 1X PBS. On ice, 1.5ml ice cold PBS was added to the culture dish and cells were scraped off the plate and transferred to a 1.7ml eppendorf tube. Cells were centrifuged at 10,000xg for 5min at 4ºC. Cell pellets were resuspended in 400µl 1X Cell Lysis Buffer (Cell Signaling, Danvers, MA) with 1% Halt Protease and Phosphatase Inhibitor Cocktail (Thermo Fisher Scientific) and lysed via sonication. Lysate was centrifuged at 14,000xg for 15min at 4ºC to pellet cell debris. Lysate was transferred to a new 1.7ml eppendorf tube and protein concentrations were determined by A280 measurement on a Nanodrop ND-1000 Spectrophotometer. 150µg of lysate mixed 1:1 with loading buffer (19:1 Laemmeli BioRad, Hercules, CA) and β-mercaptoethanol (Sigma Aldrich)) was separated using 4-20% precast sodium dodecyl sulfate-polyacrylamide gel electrophoresis (SDS-PAGE) (BioRad) at 160V for 40-45min. Samples were transferred to polyvinylidene fluoride (PVDF) membranes at 100V for 1hr at 4ºC(wet transfer) or at 25V for 7min at room temperature (semi-dry transfer). Membranes were washed with 3X 5min 1X phosphate buffered saline (PBS) containing Tween 20 (PBST) and blocked for at least 1hr with 5% BSA in 1X PBST at room temperature with an ice pack on a rocker. Primary antibodies diluted in 2.5% BSA in 1X PBST were incubated overnight at 4ºC or 2hrs at room temperature on a rocking platform and washed 3X 5min with 1X PBST. Blots were incubated with secondary antibody diluted in 1X PBST for at least 1.5hr at

room temperature on a rocker. After 3X 5min 1X PBST washes, membranes were incubated with Pierce Enhanced chemiluminescence (ECL) Western Blotting Substrate (Thermo Fisher Scientific) and exposed to radiography film. Blots were stripped using the *OneMinute* Advance Western Blot Stripping Buffer from GM Biosciences (Frederick, MD). After developing, blots were rinsed 1X with 1XPBST. Buffer A was diluted in Buffer B (1:24) and incubated with the blot on a rocker for 5min at room temperature. Buffer A/B was poured off and the *OneMinute* Western Blot Stripping Buffer was incubated with the blot for 1min at room temperature on a rocker. The Stripping Buffer was poured off and the blot was washed 3X 10min with 1X PBST at room temperature.

Bands were quantified using ImageJ (NIH, Bethesda, MD) and normalized to control, β-actin, and/or total protein. Western blot films were scanned and saved as .png files. In the ImageJ program, the western blot image was converted to 8-bit (Image > Type > 8-bit). Measurement criteria was selected (Analyze > Set Measurements > only check "Grey Mean Values") and the first ROI was selected (Select "rectangle tool" and draw a frame around the first band). The band intensity of the ROI was then measured (Ctrl + M or Analyze > Measure (this will open up the measurement window)). The ROI box was selected and dragged to the next band and band intensity was measured as above. This was repeated for all bands of interest. The background for each band was then measured by dragging the ROI rectangle to an area above or below each band and measuring the grey mean intensity as detailed above. The measurement values were then exported into Microsoft Excel to calculate the intensity of each band (taking into account inverted pixel density and background subtraction), the ratio of sample/treated band to β-actin control, and the normalized ratio value:

1) Intensity of each band:
    a. Inverted pixel density = 225-ROI measurement
    b. Final ROI density = inverted pixel density of ROI - inverted pixel density of background
2) Normalize intensity of sample band to β-actin or total protein band:
    a. Ratio = final ROI density of sample / final ROI density of β-actin
    b. Normalize to NS or vehicle treated band = ratio of treatment / ratio of NS or vehicle treatment

N. Animal studies

All experiments were conducted under protocol A272 and approved by The George Washington University Institutional Animal Care and Use Committee (IACUC). Male non-obese diabetic /severe combined immune deficiency (NOD/SCID) (homozygous for *Prkdc*^{scid} mutation) (Cat #001303) mice at three weeks of age were purchased from Jackson Laboratory (Bar Harbor, ME). All mice were housed in room 665F of The George Washington University Animal Research Facility (ARF). Mice were monitored for proper wound healing and weighed every day for seven days post-injection and once a week for the remainder of the study. Carprofen (5mg/kg) via subcutaneous injection (Henry Schein Animal Health, Dublin, OH) was available for pain management if needed. Animals were sacrificed using isoflurane (Henry Schein Animal Health) and cervical dislocation at the completion of the study or if they were assessed to have a body condition score (BCS) score of ≤ 2 defined by prominent skeletal structure, 10% body

weight loss, labored breathing, impaired ambulation, non-responsive when touched, or distended abdomen.

Tumor xenograft (subcutaneous injection): PC-3+L or PC-3+S cells were washed in 1X PBS and trypsinized (Thermo Fisher Scientific). Cells were centrifuged at 1,200xg at 4^{o}C for 5min to pellet the cells. The supernatant was removed and cells were resuspended in ice cold 1X PBS at 2 x 10^{6} cells per 200µl. One hour was the maximum time allowed from trypsinization to injection to avoid lysis and cell death. Animals were anaesthetized using isoflurane in the E-Z Anesthesia system (E-Z Systems Inc., Palmer, PA) in surgery room 665E. Mice were placed on a heated surface and fur was removed from the right hind flank using clippers. The skin was lifted to create a "tent" and a 25Gx1 needle attached to a 1ml syringe was inserted at the base of the "tent". 200µl of cells in 1X PBS was inserted gently and the needle was removed. When visible tumors measuring 3mm^{3} had formed (approximately two weeks after injection), animals began daily treatment *p.o.* of 100µl 0.9% saline (Henry Schein Animal Health) or 100µl 30mg/kg dovitinib (TKI258) (Selleckchem, Houston, TX) dissolved in 0.9% saline delivered via a curved 20G, 3.8cm length, 2.4mm tip stainless steel gavage needle (Kent Scientific, Torrington, CT). Animals were sacrificed after four weeks of treatment and tumors were dissected and stored in 37% formaldehyde (Thermo Fisher Scientific). Tissue samples from *in vivo* mouse studies were processed, embedded, sectioned, stained with hematoxylin and eosin (H&E), and mounted by Histoserv (Germantown, MD).

O. Microarray gene expression analysis

Gene microarray data from prostate biopsy cores were previously generated using the Affymetrix Human Exon 1.0 ST GeneChip (Santa Clara, CA) and can be accessed at

Gene Expression Omnibus (GEO) using accession number GSE64331 (Wang et al. 2017). Raw array data underwent quantile normalization, GC-content adjustment, background correction, and $\log_2$ transformation using Partek Genomics Suite 6.6 (Partek Incorporated, St. Louis, MO). Gene-wise analysis of splicing factors was performed in Partek using One-Step Tukey's Biweight algorithm for detection of outlier probe-sets.

P. Immunohistochemistry

AA and EA formalin-fixed paraffin-embedded (FFPE) prostate tissue were provided by the Pathology Core and GW Biorepository at The George Washington University (**Table 14**). All PCa specimens were treatment naïve and had Gleason scores 6-9. There was no significant difference in age or Gleason score between the ethnic groups.

The following reagents were obtained from Dako (Carpinteria, CA): Dual Endogenous Enzyme Block, LSAB2 System-HRP (Streptavidin-HRP and Biotin link), Liquid DAB+ Substrate Chromagen System, and Glycerol Mounting Media. Slides were incubated at 65ºC for 30min to remove paraffin. The following washes were then performed in a slide rack: 100% xylene 2X 3min, 1:1 100% xylene:100% ethanol 1X 3min, 100% ethanol 2X 3min, 95% ethanol 1X 3min, 70% ethanol 1X 3min, 50% ethanol 1X 3min, cold running tap water 3min. Slides were then immersed in sodium citrate buffer (10mM sodium citrate, 0.05% tween 20, pH6.0) and microwaved for 17min. The buffer was allowed to cool to room temperature and the slides were rinsed under cold tap water for 10min. Slides were placed in a humidified chamber and blocked with Dual Enzyme Peroxidase for 30-45min at room temperature. Slides were rinsed with distilled water, washed with 1X PBS for 5min, and blocked with 2.5% BSA in 1XPBS for 30min

at room temperature and incubated with primary antibody in 2.5% BSA for 30min at room temperature or overnight at 4ºC. Two washes in 1X PBS (5min) were followed by incubation with secondary anti-rabbit and anti-mouse biotinylated IgG for 30min at room temperature, 2X 1X PBS washes (5min), incubation with streptavidin conjugated to horseradish peroxidase for 30min at room temperature, and 2X 1X PBS washes (5min). Slides were then stained with 3,3'-Diaminobenzidine (DAB+) chromagen (30sec – 2min), rinsed with distilled water, stained with hematoxylin (Sigma Aldrich) (1.5min), incubated with 0.037mM ammonia (5min), washed once with distilled water, and a coverslip was placed using glycerol mounting media.

All slides were imaged on the Carl Zeiss Cell Observer Spinning Disk Confocal (Thornwood, NY) with a 63X oil immersion objective. Digital slides were constructed using the scanning tiling feature on the Zen Blue software (Carl Zeiss). All images were analyzed by a board-certified pathologist.

After acquisition of the image, individual tiles were stitched and fused into a single image via edge detection using the ZEN software. DAB+ chromagen staining was quantified using ImagePro (Media Cybernetics, Rockville, MD). Only staining in epithelial regions of tissue were quantified as regions of interest (ROI). Once ROIs were selected, a standardized color cube was generated as a mask to identify DAB+ staining. All images were analyzed using the same mask for consistency. From these selections, the total area, the mean density of staining/area, total density, and total relative density values were determined. The relative intensity of staining/area was then calculated.

These calculations were then binned into Scores 1-4, with Score 1 being low/no DAB+ chromagen staining and Score 4 being high/very positive DAB+ chromagen staining (Varghese et al. 2014). All DAB+ chromagen relative intensity of staining/are

numbers were arranged in increasing order and duplicates were removed. This list was divided into four equal sections (Scores 1-4). Each number was then binned into its respective score.

Table 14 Patient information for IHC

	Average age	Average Gleason score
AA	59.8	6.8
EA	55.3	6.7
n	19	21
t-test	$p > 0.05$	$p > 0.05$

Average age, average Gleason score, and number of patient specimens used for IHC. There was no significant difference in age nor Gleason score between AA (n=19) and EA (n=19-21) groups.

Q. Immunocytochemistry

Cells were plated at 50-70% confluency on UV sterilized coverslips in 6 well plates and allowed to adhere overnight. Cells were fixed in 1ml ice cold methanol (Sigma Aldrich) on ice for 20min and blocked with 1% BSA in 1X PBS on ice for 30min before incubation with wheat germ agglutinin (WGA) Alexa 488 for 10min at room temperature in the dark. Due to light sensitivity of the WGA reagent, all subsequent incubations were done in the dark. Coverslips were washed 2X 1ml 1X PBS, incubated with 500µl primary antibody diluted in 1% BSA for 1hr at room temperature, washed 2X 1ml 1X PBS, incubated with 500µl Alexa Fluor-conjugated secondary antibody diluted in 1% BSA, and washed 2X 1ml 1X PBS. Coverslips were mounted on microscope slides with ProLong Gold Antifade Mountant with DAPI (Thermo Fisher Scientific). All slides were imaged on the Carl Zeiss 710 Spectral Confocal with 20X oil immersion objective.

R. siRNA-mediated gene knockdowns

Cells were plated at 20-30% confluency in 6 well or 10cm plates in the appropriate medium. Immediately prior to transfection, medium was replaced with antibiotic free medium. Two short interfering RNA (siRNA) sequences per gene of interest (to account for off target effects) and the scrambled nonsense control (siNS) siRNA were purchased from G.E. Life Sciences Dharmacon (Lafayette, CO). Transfections were conducted in Opti-MEM medium (Thermo Fisher Scientific) with 100µM final siRNA concentration and Dharmafect4 transfection reagent (Dharmacon). Cells were incubated with the transfection reagents for 24hrs prior to collection and use for *in vitro* assays or western blots. Knockdown efficiency was measured by western blot.

S. Statistical analysis

All data are represented as mean and standard error of the mean (SEM, = SD/√n). At least three replicates were performed per experiment. Unpaired t-test analysis was used to compare two groups (one categorical and one continuous). When three or more categorical groups were being compared, a one-way analysis of variance (ANOVA) was conducted followed by Dunnett (to compare groups back to control) or Tukey (to examine all pairwise comparisons) post-hoc tests. A χ^2 test was used to calculate an approximate p-value for two categorical variables. A p value ≤ 0.05 was considered statistically significant.

IC_{50} values for proliferation, migration, and invasion assays were calculated using GraphPad Prism (San Diego, CA). The data from each individual experiment was entered into an XY data table. The X values were transformed into log form (x=log(x)) and the Y values were normalized on a common scale (0%=smallest value in data set, 100%=largest value in data set, results presented as percentages). Data were then curve fitted to a nonlinear regression (Nonlinear regression (curve fit) > log(agonist) vs. normalized response – Variable slope) and the IC_{50} was generated. IC_{50} values were determined for each run, after which the mean and SEM were calculated.

Chapter 3: Verification of *FGFR3* splice variants

A. Cloning of *FGFR3* splice variants

B. Generation of stable cells lines

C. FGFR3 expression in AA and EA specimens

A. Cloning of *FGFR3* variants

Affymetrix exon array results from a previous study implied evidence of a previously undiscovered exon 14 skipping event in FGFR3 that may be involved in PCa disparities (Wang et al. 2017). PCa specimens from EA patients predominantly expressed the full-length, or long variant, containing exons 1-18. AA PCa specimens, however, showed predominant expression of a short variant in which exon 14 was predicted to be missing.

To confirm the existence of this novel FGFR3 splice variant, we cloned both long (FGFR3-L) and short (FGFR3-S) variants from PCa cell lines using the 5'- and 3'-RACE method. Sequencing of the FGFR3-L variant from MDA PCa 2b confirmed the presence of exon 14 (**Figure 8, 10**), while sequencing of FGFR3-S from MDA PCa 2b and RC77 T/E AA cell lines confirmed the in-frame loss of exon 14 (**Figure 9, 10**). There were no other differences in sequence between FGFR3-L and FGFR3-S.

Exon 14 (123bp) codes for the 41 amino acid activation loop (A-loop) located within the C-terminal intracellular kinase domain of FGFR3 (**Figure 11**). This loop covers the substrate binding pocket and is involved in shifting the kinase from an inactive to active conformation when stimulated by ligand binding. Thus, we hypothesized that loss of this critical molecular break may increase FGFR3 signaling and promote a more oncogenic phenotype in AA PCa.

Figure 8 Representative chromatograms of *FGFR3-L* sequencing

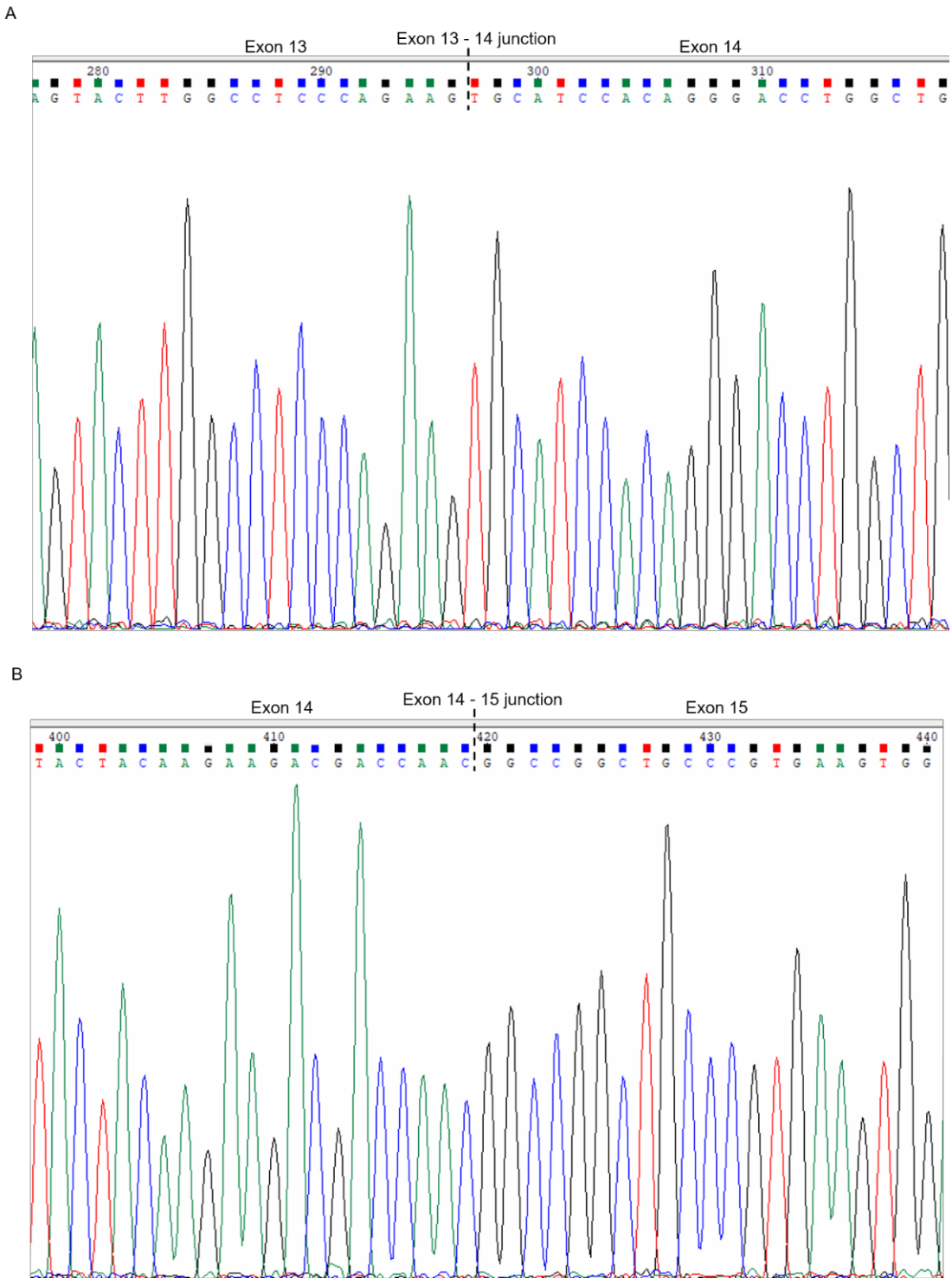

Chromatogram showing junction of exons 13-14 (A) and exons 14-15 (B) from Sanger sequencing of *FGFR3-L*.

Figure 9 Representative chromatogram of *FGFR3-S* sequencing

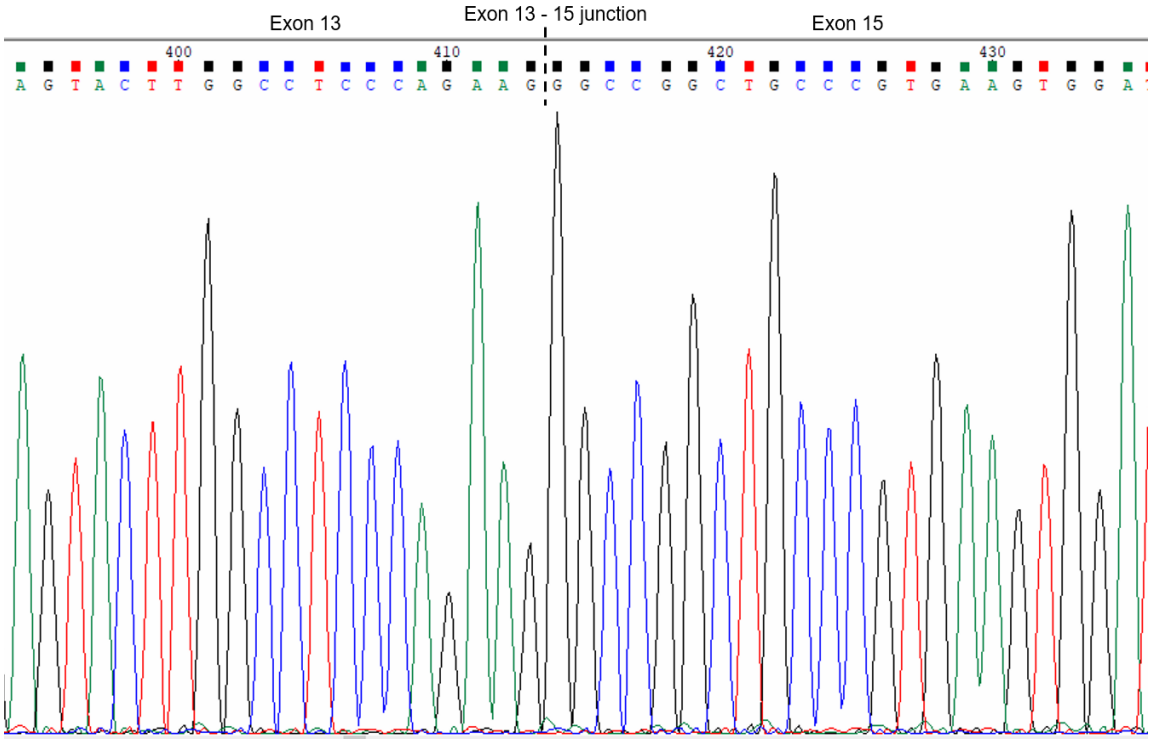

Chromatogram showing junction of exons 13-15 and in-frame deletion of exon 14 from Sanger sequencing of *FGFR3-S*.

Figure 10 Consensus sequences of FGFR3 splice variants

Consensus sequence of *FGFR3-L* containing exon 14 and *FGFR3-S* with in-frame deletion of exon 14 (123bp). Amino acid sequence is shown above, with exon 14 (41aa) shown in red.

Figure 11 Schematic of FGFR3 gene and generation of splice variants

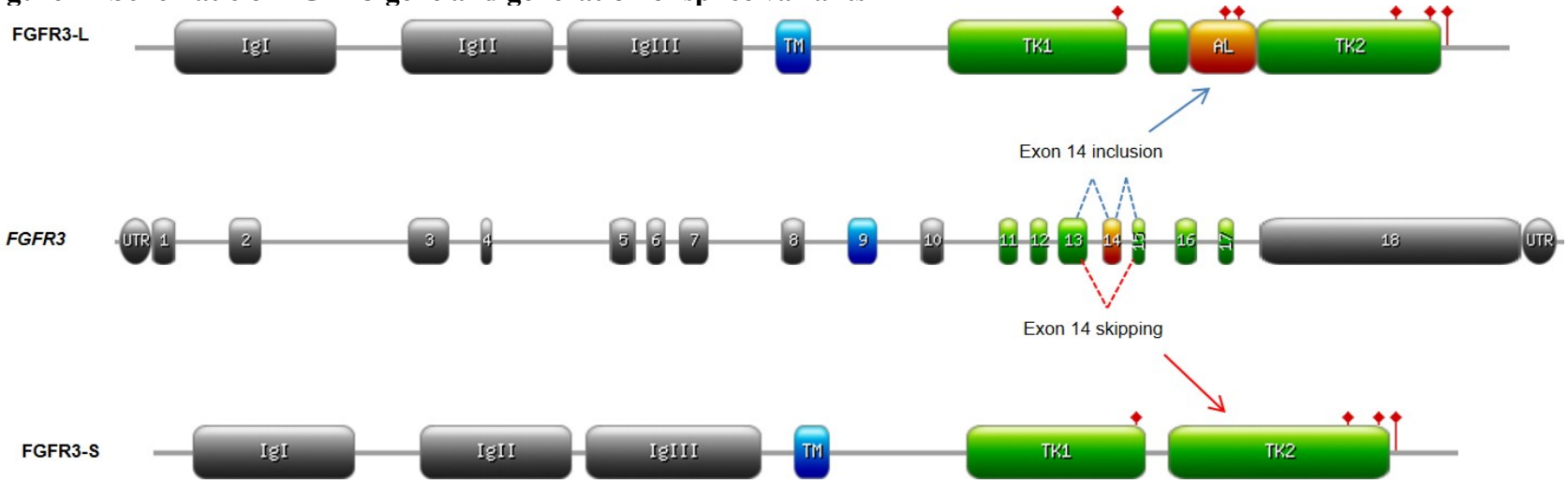

Inclusion of exon 14 (top) generates the long isoform (FGFR3-L) containing the activation loop (AL) in the C-terminal kinase domain. Exon skipping of exon 14 results in a shorter isoform (FGFR3-S) that is missing the AL and tyrosines 643 and 644. Key: Ig-like domains (grey), transmembrane domain (TM) (blue), tyrosine kinase domains (TK) (green), activation loop (AL) (orange), tyrosine residues that are phosphorylated for kinase activation (red flags).

B. Generation of stable cell lines

Next, we generated cell lines that stably overexpressed FGFR3-S, FGFR3-L, or a vector control. These cell lines were used in later experiments to analyze the effect of each variant *in vitro* and *in vivo*.

FGFR3-S, FGFR3-L, or a *lacZ*-containing control vector were transfected into two EA cell lines (PC-3 and LNCaP) and used in Chapter 4. V5 and His tags were added to the 3' end of each gene of interest for the purpose of measuring expression levels of transfected versus endogenous gene expression. *FGFR3-L* and *FGFR3-S* were cloned into pcDNA3.1+ vector with G418S resistance (**Table 15**). As these cell lines will be compared directly, equal expression of FGFR3-S, FGFR3-L, and β-Galactosidase was required to ensure continuous expression of the transfected vector. Correct and equal expression of the tagged FGFR3 variants were determined by RT-PCR, using internal *FGFR3* primers that amplified exons 12-16 and primers amplifying exon 16-V5 tag. Protein expression was confirmed by western blot analysis using antibodies to the His or V5 tag (**Table 16, Table 17, Figure 12**). Expression of *lacZ* in control transfected cells was determined by RT-PCR, using internal *lacZ* and V5 primers, and western blot, using a V5 tag antibody (**Table 16, Table 17, Figure 13**). Cell lines were incubated with G418S throughout maintenance and *in vitro* experiments.

Two AA cell lines, MDA PCa 2b and RC77 T/E overexpressing *FGFR3*-S or a vector control were generated for use in Chapter 5. As the RC77 T/E cell line was immortalized under G418S selection (Theodore et al. 2010), pcDN3.1+ vectors with hygromycin resistance were used. As described previously, overexpression of FGFR3-S was confirmed via RT-PCR, using internal *FGFR3* and V5 tag primers, and by western

blot analysis, using a V5 antibody (**Table 16, Table 17, Figure 14**). Expression of the empty vector control was validated via RT-PCR using primers specific to the pcDNA3.1+ vector (**Table 16, Figure 15**). Stable cell lines were incubated with hygromycin throughout maintenance and *in vitro* experiments.

Table 15 Vectors used for stable cell line transfection

Vector	Insert	Selective Antibiotic	Cell line
pcDNA3.1+	lacZ-V5-His	G418S (150µg/ml, 200µg/ml)	PC-3, LNCaP
pcDNA3.1+	FGFR3-L-V5-His	G418S (150µg/ml, 200µg/ml)	PC-3, LNCaP
pcDNA3.1+	FGFR3-S-V5-His	G418S (150µg/ml, 200µg/ml)	PC-3, LNCaP
pcDNA3.1+	N/A	Hygromycin (200µg/ml, 150µg/ml)	MDA PCa 2b, RC77 T/E
pcDNA3.1+	FGFR3-S-V5-His	Hygromycin (200µg/ml, 150µg/ml)	MDA PCa 2b, RC77 T/E

Vector name, insert, selective antibiotic, and cell line used for transfection.

Table 16 Primers used for stable cell line transfection confirmation

Primer Pair	Target	Expected size (bp)
exon12F-exon16R	*FGFR3-L*	662
	FGFR3-S	539
exon16F-V5R	*FGFR3* (transfected)	460
lacZ-V5R	*lacZ*	264
T7-BGH	pcDNA3.1+ (no insert)	170

Primer pairs, intended gene target for PCR, and expected size of PCR product used to verify expression of correct gene of interest for stable cell line transfections.

Table 17 Antibodies used for stable cell line transfection confirmation

Antibody	Target	Expected size (KDa)
His or V5 tag	FGFR3-L, -S	110-120
V5 tag	β-Galactosidase	116

Antibodies, intended protein target, and expected size of band of western blot used to verify expression of correct proteins of interest for stable cell line transfections.

Figure 12 PC-3+L, PC-3+S, LNCaP+L, LNCaP+S transfection screen

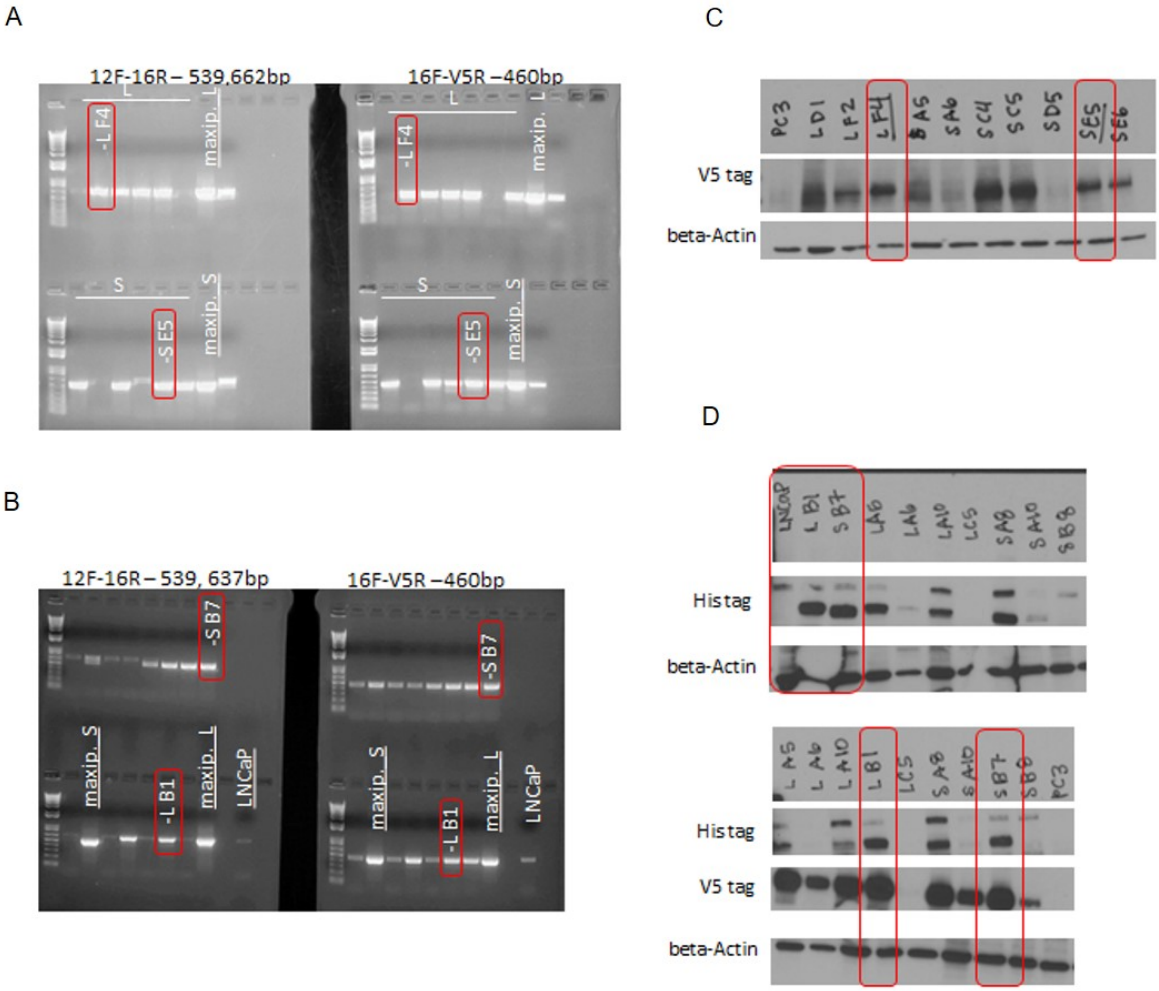

Agarose gels showing RT-PCR screening of PC-3+L and PC-3+S (A) and LNCaP+L and LNCaP+S (B) colonies. Colonies were screened for expression of the correct *FGFR3* variant (12F-16R primers) and V5 tag (16F-V5R primers). The final colonies selected for future experiments are outlined in red (PC-3+L F4, PC-3+S E5, LNCaP+L B1, LNCaP+S B7). Positive controls, labeled maxip. L or maxip. S, were maxiprep DNA of *FGFR3-L* and *FGFR3-S* vectors. Expected size of each primer pair are shown above gels. Western blots of RT-PCR positive PC-3 (C) and LNCaP (D) transfected cell lines were screened with V5 and/or His tag antibodies. β-actin was used as a loading control. The final colonies selected for future experiments are outlined in red. Negative controls were untransfected PC-3 or LNCaP cells.

Figure 13 PC-3+vector, LNCaP+vector transfection screen

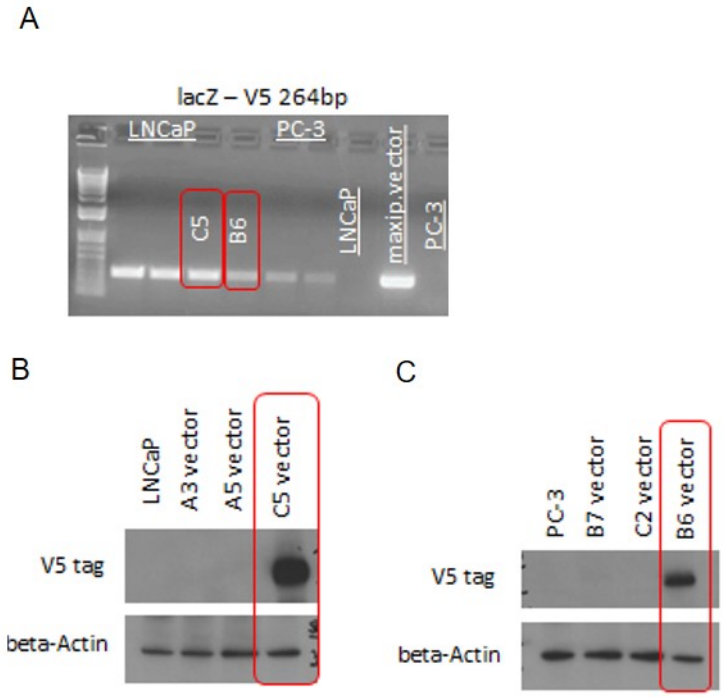

A) Agarose gel showing RT-PCR screening of LNCaP+vector and PC-3+vector colonies. Colonies were screened for expression of *lacZ* and V5 tag (lacZ-V5). The final colonies selected for future experiments are outlined in red (LNCaP+vector C5, PC-3+vector B6). Positive control, labeled maxip.vector, was maxiprep DNA of *laz* vector. Negative controls were untransfected LNCaP and PC-3 cell lines. Expected PCR product size is shown above gel. Western blots of RT-PCR positive LNCaP (B) and PC-3 (C) transfected cell lines were screened with V5 tag antibody. β-actin was used as a loading control. The final colonies selected for future experiments are outlined in red. Negative controls were untransfected PC-3 or LNCaP cells.

Figure 14 MDA PCa 2b+S, RC77 T/E+S transfection screen

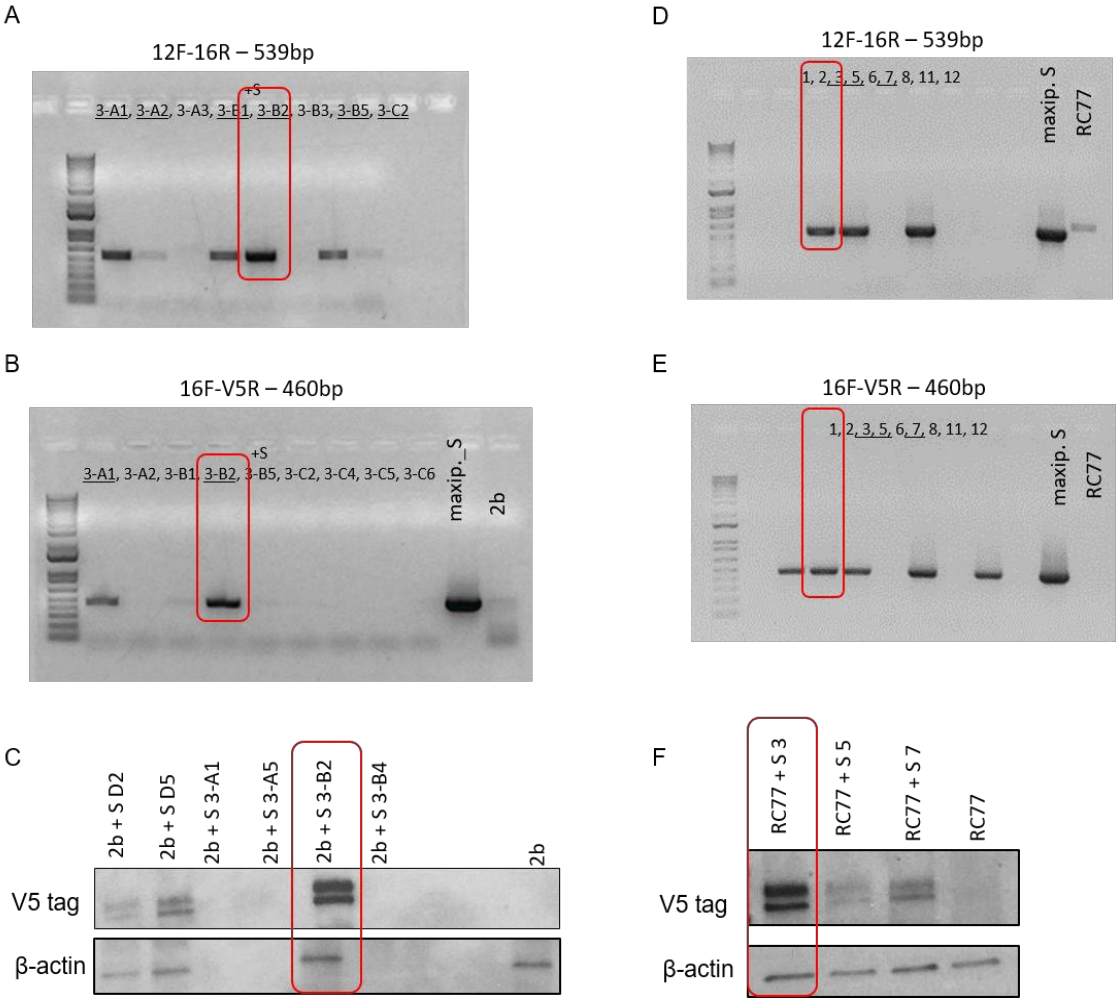

Agarose gels showing RT-PCR screening of MDA PCa 2b+S (A,B) RC77 T/E+S (D,E) colonies. Colonies were screened for expression of the correct *FGFR3* variant (12F-16R primers) (A,D) and V5 tag (16F-V5R primers) (B,E). The final colonies selected for future experiments are outlined in red (MDA PCa 2b+S 3-B2, RC77 T/E+S 3). Positive controls, labeled maxip._S, were maxiprep DNA of *FGFR3-S* vectors. Expected size of each primer pair are shown above gels. Western blots of RT-PCR positive MDA PCa 2b (C) and RC77 T/E (F) transfected cell lines were screened with V5 tag antibody. β-actin was used as a loading control. The final colonies selected for future experiments are outlined in red. Negative controls were untransfected MDA PCa 2b or RC77 T/E cells.

Figure 15 MDA PCa 2b+vector, RC77 T/E+vector transfection screen

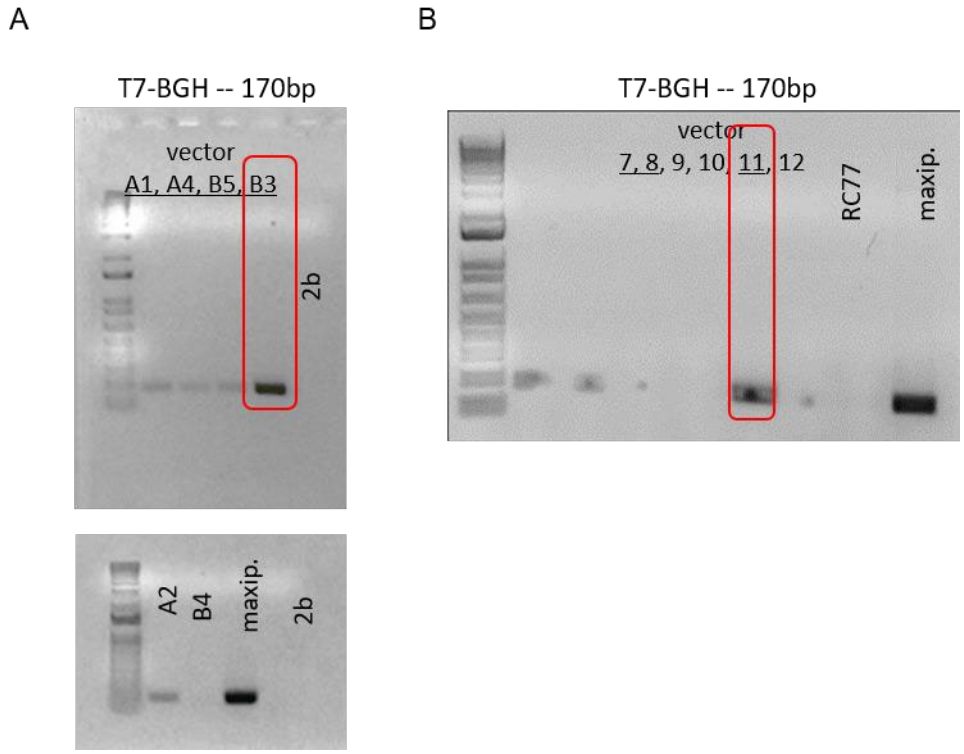

A) Agarose gel showing RT-PCR screening of MDA PCa 2b+vector and RC77 T/E+vector colonies. Colonies were screened for expression of pcDNA3.1+ vector (T7-BGH). The final colonies selected for future experiments are outlined in red (MDA PCa 2b+vector B3, RC77 T/E+vector 11). Positive control, labeled maxip., was DNA pcDNA3.1+ vector maxiprep DNA. Negative controls were untransfected MDA PCa 2b and RC77 T/E cell lines. Expected PCR product size is shown above gel.

A. FGFR3 expression in AA and EA specimens

Previous studies, including our Affymetrix exon array data, have shown that 1) FGFR3 is expressed in PCa tissue and 2) there is no significant difference in total FGFR3 expression between AA and EA PCa (Hernández et al. 2009; Lo Iacono et al. 2016; Pilié et al. 2017; Wan et al. 2014; Wang et al. 2015; Wang et al. 2017). We confirmed these findings in our own patient cohort by performing immunohistochemistry (IHC) on AA and EA PCa specimens (**Figure 16**). In agreement with the literature, we saw positive staining of total FGFR3 in PCa specimens and no significant difference in expression between racial groups.

Figure 16 Expression of total FGFR3 was not significantly different in AA and EA PCa specimens

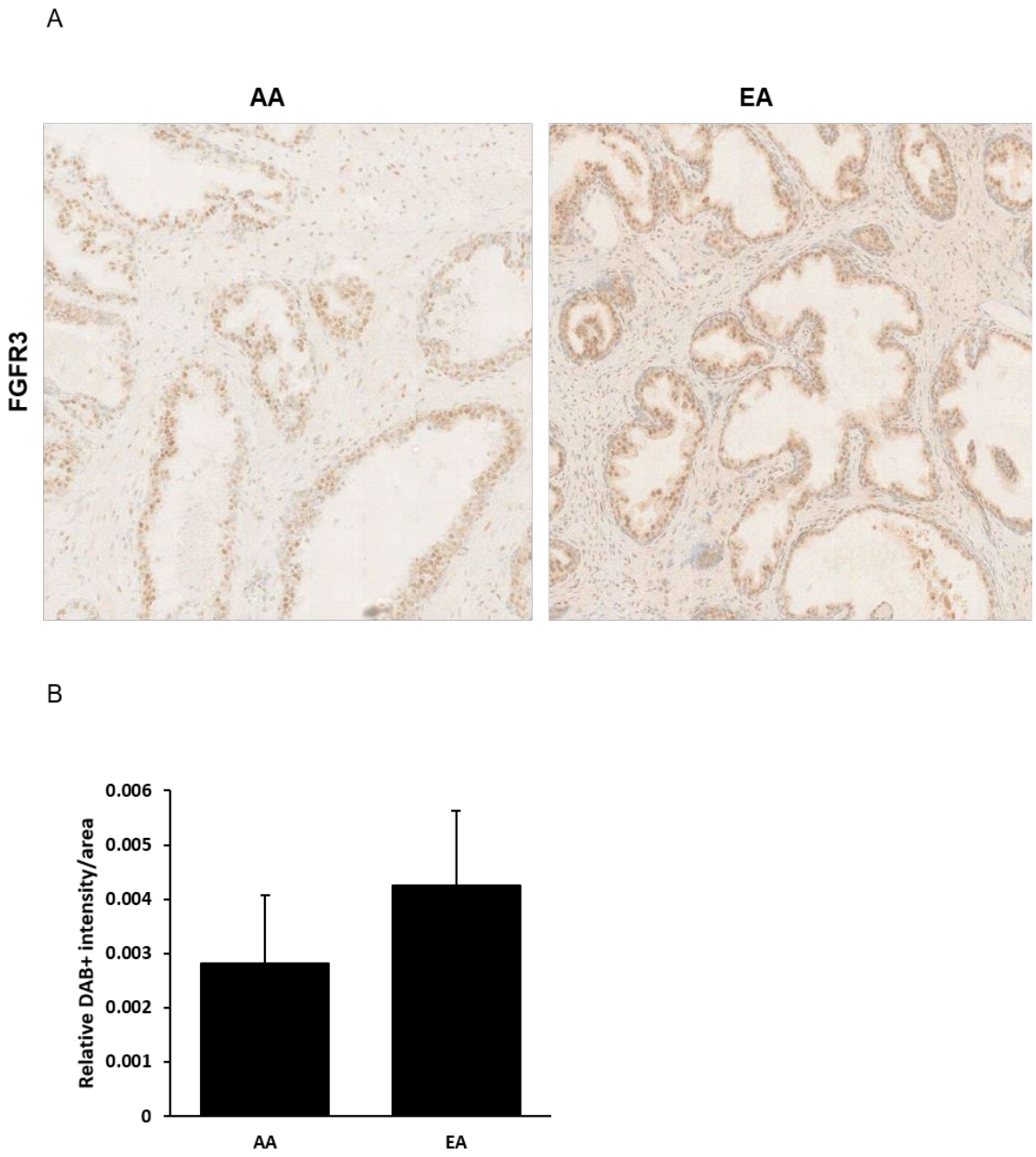

A) Representative images of IHC of AA (n=4) and EA (n=4) PCa specimens. Total FGFR3 was stained with DAB+ chromagen (brown) and counterstained with hematoxylin (blue). B) Quantification of relative DAB+ chromagen staining/area from patient specimens. Data are represented as mean±SEM, n=4 independent experiments, unpaired t-test, *$p<0.05$.

Chapter 4: Determination of oncogenicity of FGFR3-S compared to FGFR3–L

A. *FGFR3-S* expression correlates with poor PCa patient prognosis

B. FGFR3-S confers an oncogenic advantage *in vitro*

C. FGFR3-S signaling is more active and resistant to dovitinib compared to FGFR3-L

D. FGFR3-S is resistant to dovitinib in xenograft models of tumor growth and metastasis

A. *FGFR3-S* expression correlates with poor PCa patient prognosis

To assess the clinical relevance of the *FGFR3-S* variant, prostate, colon, and breast cancer patient expression data from The Cancer Genome Atlas (TCGA) database were analyzed for *FGFR3-S/-L* expression ratios in relation to patient survival. A significant decrease in survival ($p = 0.04$) was observed in patients harboring PCa specimens containing a high *FGFR3-S/-L* expression ratio (n=550) (**Figure 17**). Neither colon (albeit trending towards significance; n=328) nor breast cancer (n=1,203) patient survival significantly correlated with the *FGFR3-S/-L* expression ratio. Patient groups were not stratified by race/ethnicity due to insufficient information.

Figure 17 Prostate cancer patients with high FGFR3-S/-L ratios have decreased survival

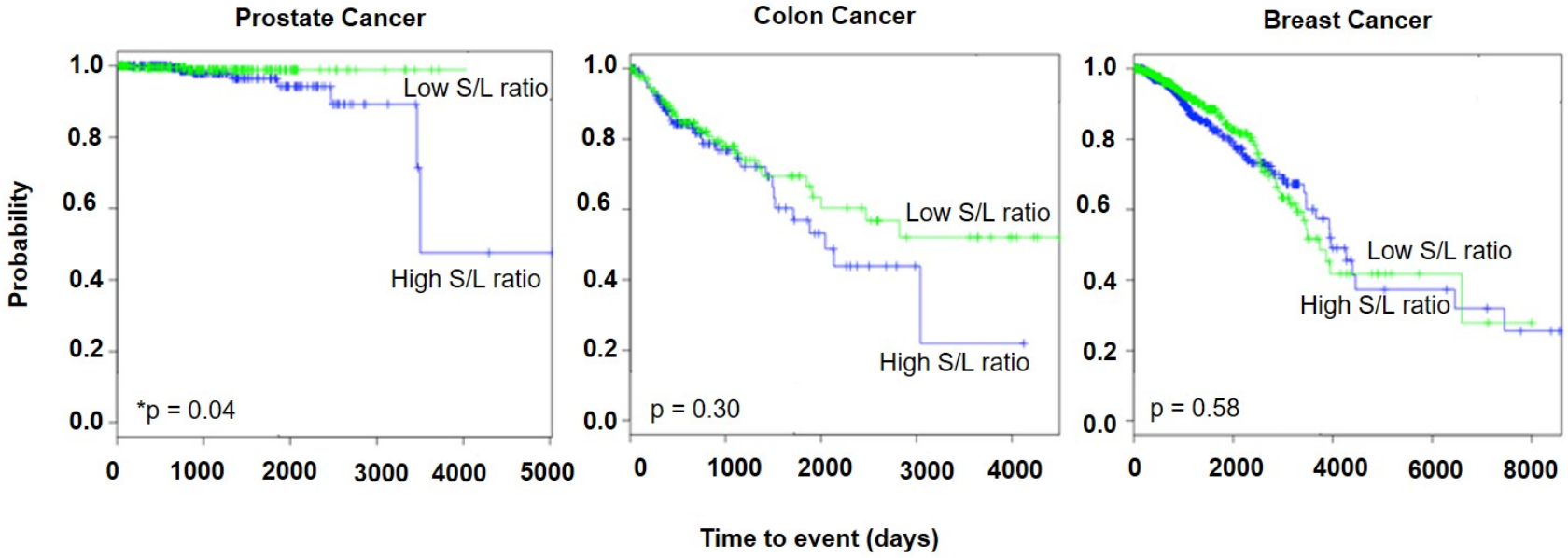

Kaplan-Meier survival curves plotting disease-free survival of prostate cancer (n=550), colon cancer (n=328), and breast cancer (n=1,203) patients with high or low *FGFR3-S/-L* expression ratios. RNA-Seq data was obtained from TCGA and is not stratified by race, stage, or grade. Log-rank test, *p<0.05.

B. FGFR3-S confers an oncogenic advantage *in vitro*

As normal cells evolve to a cancerous phenotype, they acquire characteristics that promote growth and survival (Hanahan and Weinberg 2000, 2011). These "hallmarks of cancer" include sustained proliferative signaling, active cell migration, increased invasive potential, resistance to apoptosis, and reduced sensitivity to cytotoxic and targeted therapies. To better understand the effects of the short isoform on these oncogenic properties, we devised *in vitro* experiments using the EA PCa cells lines stably overexpressing FGFR3-L or FGFR3-S generated in chapter 3.

We first measured bromodeoxyuridine (BrdU) incorporation as a marker of proliferation. In this assay, the thymidine analog BrdU is incorporated into newly synthesized DNA strands in actively proliferating cells. BrdU immunolabeling can then be analyzed as a measure of cell proliferation. EA PCa cells overexpressing FGFR3-S (PC-3+S and LNCaP+S) exhibited a 2- to 3-fold increased baseline proliferative capability compared to cells overexpressing FGFR3-L (PC-3+L, LNCaP+L) and vector control (PC-3+vector, LNCaP+vector) (**Figure 18A**). We then tested the effects of treatment with 0.001-100μM of the small molecule inhibitor (SMI) dovitinib on proliferation. Dovitinib is a multi-kinase inhibitor that targets FGFR1-3, VEGFR 1-3, PDGFRβ, c-Kit, and FLT3 at nanomolar levels (André et al. 2013; Hoon Lee et al. 2005; Konecny et al. 2013; Trudel et al. 2005). In PC-3+L and LNCaP+L cells, dovitinib inhibited proliferation in a dose dependent manner with IC_{50} values of 0.90 ± 0.28μM and 0.39 ± 0.28μM, respectively (**Figure 18B-C, Table 18, Table 19**). By comparison, both PC-3+S and LNCaP+S cells were relatively resistant to dovitinib-mediated

inhibition of proliferation with a rightward shift in the dose-response curves and IC_{50} values of 7.53 ± 2.23μM and 11.14 ± 0.83μM, respectively.

Next, we employed the Boyden chamber assay to measure migratory activity. Aberrant cell migration is an initial step in tumor metastasis. The Boyden chamber assay measures the migration of cells towards a chemoattractant through a porous membrane. Baseline migration was significantly lower in PC-3+L, LNCaP+L, PC-3+vector, and LNCaP+vector cells compared to +S overexpression cells (**Figure 19A**). Additionally, +S cells were relatively resistant to dovitinib inhibition, displaying greater migratory capacity compared to +L cells at 4 out of 6 tested inhibitor concentrations (**Figure 19B-C**). Cells overexpressing the -L isoform (+L cells) exhibited a 4- to 6-fold lower IC_{50} compared to +S cells (**Table 18, Table 19**). These data support the hypothesis that the -S isoform is more oncogenic and relatively resistant to SMI treatment compared to the -L isoform.

Given that +S cells exhibited greater migratory capacity compared to +L cells, we next evaluated the invasive potential in these lines as measured by Matrigel assay at both baseline and with dovitinib treatment. Invasion through the extracellular matrix and into a secondary site is a distinct characteristic of tumor cells. In this assay, the ability of cells to invade through a coated porous membrane mimicking the basement membrane is measured. Overexpression of either the -L or -S isoform conferred an oncogenic advantage compared to vector control cells at baseline (**Figure 20A**). Baseline invasion between +L and +S cells was not significantly different, whereas both cell lines exhibited a 1.8- to 2.6-fold greater ability to invade compared to +vector cells. The invasive capacity of +S cells appeared to be more resistant to the inhibitory effects of dovitinib

compared to +L cells, albeit significant differences in invasion were observed only at 1 and 10μM (**Figure 20B-C**). Notwithstanding, the IC_{50} value of dovitinib in +L cells was approximately 6-times lower compared to +S cells (**Table 18, Table 19**). These results suggest that the FGFR3-S isoform may be playing a more prominent role in cell proliferation and migration versus invasion in AA PCa aggressiveness.

To examine the effects of *FGFR3* splice variants on apoptosis, we treated +vector, +L, and +S cells with docetaxel, a standard chemotherapy treatment for PCa, and measured caspase 3/7 activity. Aberrant cell survival through evasion of apoptosis is a key feature in cancer development and progression. Activation of caspases is one of the main biological changes that occurs when apoptosis is triggered. As both extrinsic and intrinsic pathways converge on caspase 3/7 activation, measurement of caspase 3/7 activity via cleavage of a luminogenic substrate is a useful measure of apoptotic activity. At baseline, +S cells exhibited a 50-70% decrease in caspase 3/7 activity compared to +L and +vector cells (**Figure 21A**). Both +vector and +L cells demonstrated increasing caspase 3/7 activity with increasing doses of docetaxel (**Figure 21B,C,E,F**). Notably, PC-3+S and LNCaP+S cells were completely resistant to docetaxel-induced apoptosis (**Figure 21D,G**). The combination of docetaxel and dovitinib did not have an additive effect on caspase 3/7 activity (**Figure 22**). Taken together, these findings suggest FGFR3-S is more resistant to the apoptotic effects of SMI (dovitinib) and taxane (docetaxel) treatment.

Figure 18 FGFR3-S is resistant to dovitinib-mediated inhibition of proliferation

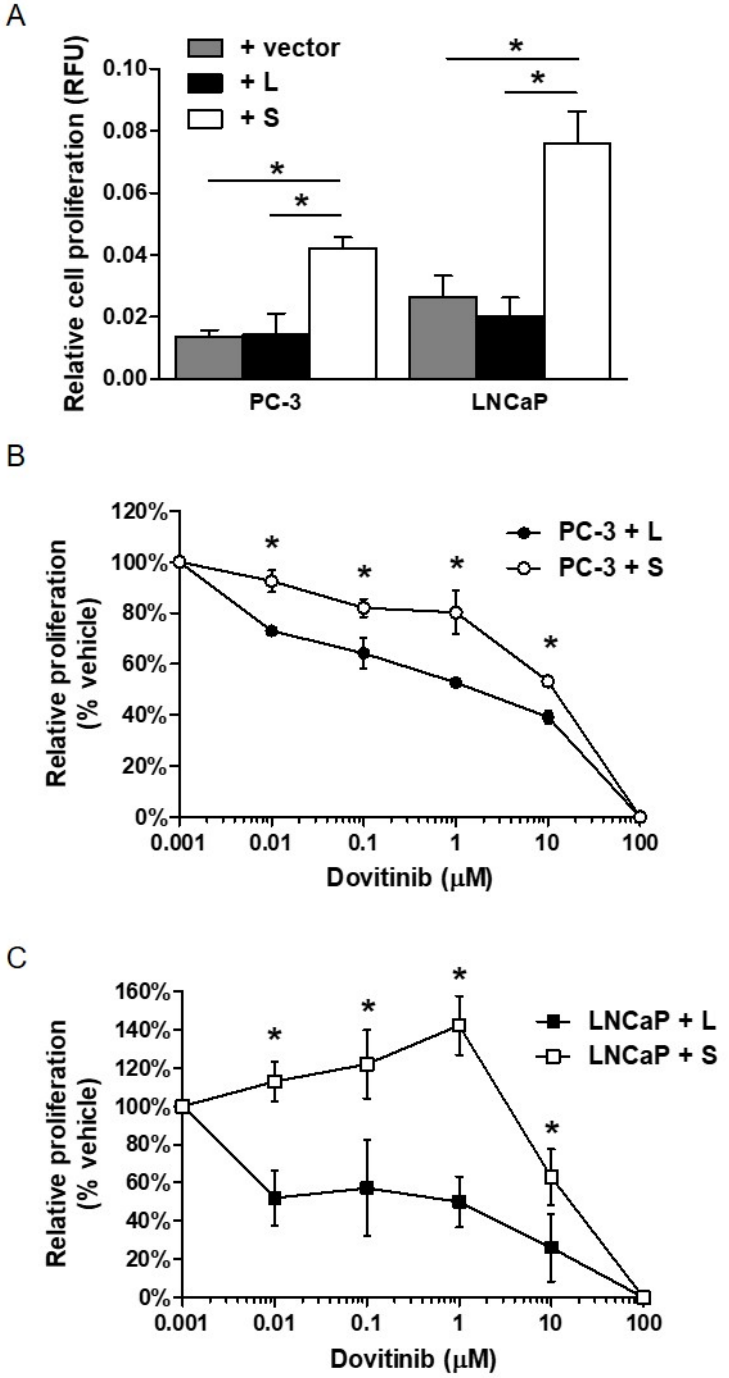

A) Baseline proliferation via BrdU incorporation of EA cell lines PC-3 and LNCaP ectopically overexpressing vector control, FGFR3-L, and FGFR3-S. Relative proliferation in PC-3 (B) and LNCaP (C) overexpressing FGFR3-L and FGFR3-S with increasing doses of dovitinib. Data are represented as mean±SEM, n=3-4 independent experiments, one-way ANOVA with Tukey post-hoc or unpaired t-test, *$p<0.05$.

Figure 19 FGFR3-S is resistant to dovitinib-mediated inhibition of migration

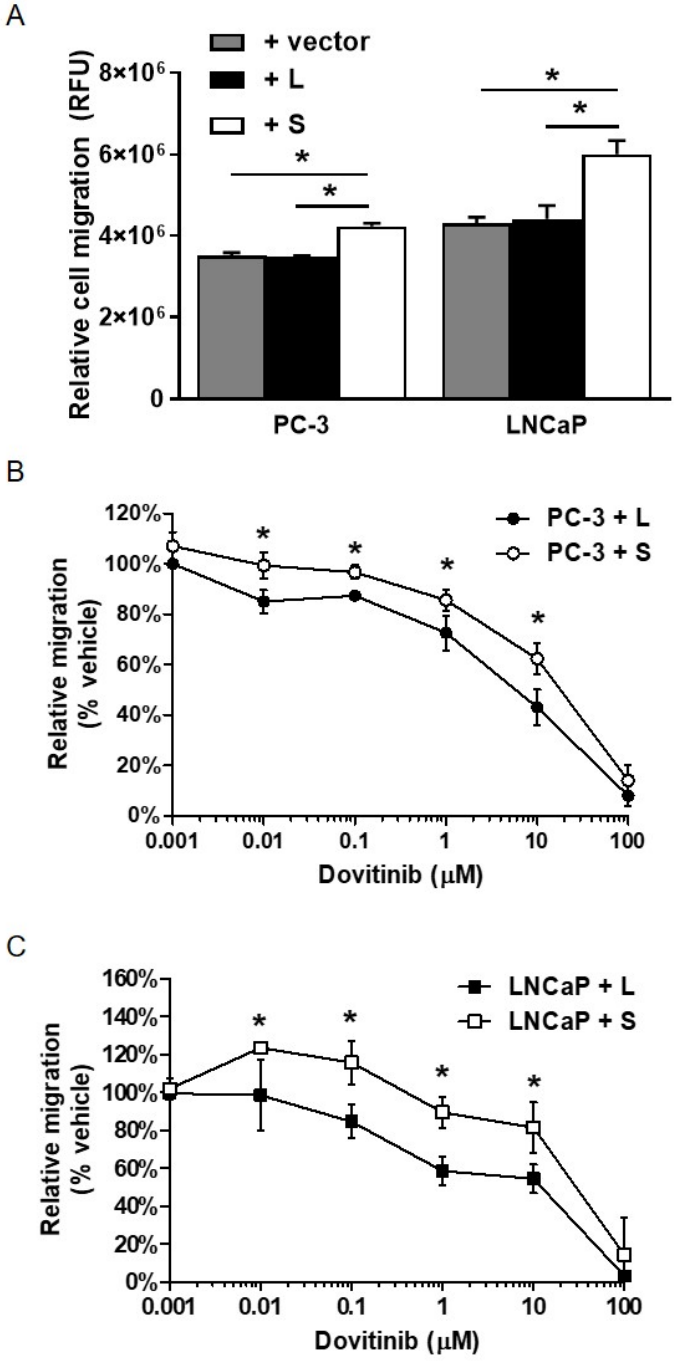

A) Baseline migration via Boyden chamber assay of PC-3 and LNCaP cells overexpressing vector control, FGFR3-L, and FGFR3-S. Relative migration in PC-3 (B) and LNCaP (C) overexpressing FGFR3-L and FGFR3-S with increasing doses of dovitinib. Data are represented as mean±SEM, n=3-4 independent experiments, one-way ANOVA with Tukey post-hoc or unpaired t-test, *$p<0.05$.

Figure 20 FGFR3-S is resistant to dovitinib-mediated inhibition of invasion

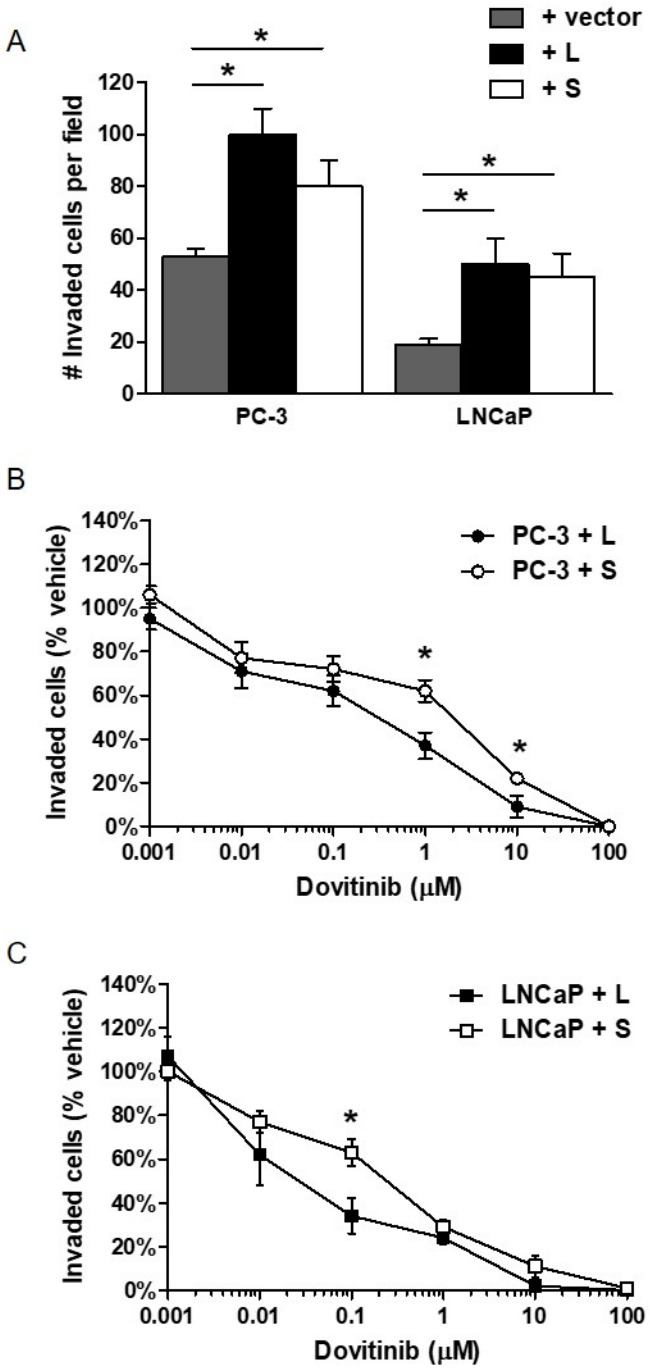

A) Baseline invasion via Matrigel assay of PC-3 and LNCaP cells overexpressing vector control, FGFR3-L, and FGFR3-S. Invaded cells shown as percent vehicle in PC-3 (B) and LNCaP (C) cells overexpressing FGFR3-L and FGFR3-S with increasing doses of dovitinib. Data are represented as mean±SEM, n=3-4 independent experiments, one-way ANOVA with Tukey post-hoc or unpaired t-test, *$p<0.05$.

Table 18 IC_{50} values calculated for PC-3+L, PC-3+S *in vitro* assays

IC_{50}	Proliferation (μM)	Migration (μM)	Invasion (μM)
PC-3 + L	0.90 ± 0.28	2.47 ± 0.64	0.22 ± 0.08
PC-3 + S	7.53 ± 2.23	9.82 ± 1.89	1.26 ± 0.40
t-test	*p < 0.05	*p < 0.05	*p < 0.05

Calculated IC_{50} values for dovitinib in proliferation, migration, and invasion assays. Data are represented as mean±SEM, n=3-4 independent experiments, unpaired t-test. All groups were statistically significant, *p<0.05.

Table 19 IC_{50} values calculated for LNCaP+L, LNCaP+S *in vitro* assays

IC_{50}	Proliferation (μM)	Migration (μM)	Invasion (μM)
LNCaP + L	0.39 ± 0.28	1.35 ± 0.58	0.04 ± 0.01
LNCaP + S	11.14 ± 0.83	8.13 ± 1.71	0.25 ± 0.04
t-test	*p < 0.05	*p < 0.05	*p < 0.05

Calculated IC_{50} values for dovitinib in proliferation, migration, and invasion assays. Data are represented as mean±SEM, n=3-4 independent experiments, unpaired t-test. All groups were statistically significant, *p<0.05.

Figure 21 FGFR3-S is resistant to docetaxel-mediated activation of caspase 3/7 activity

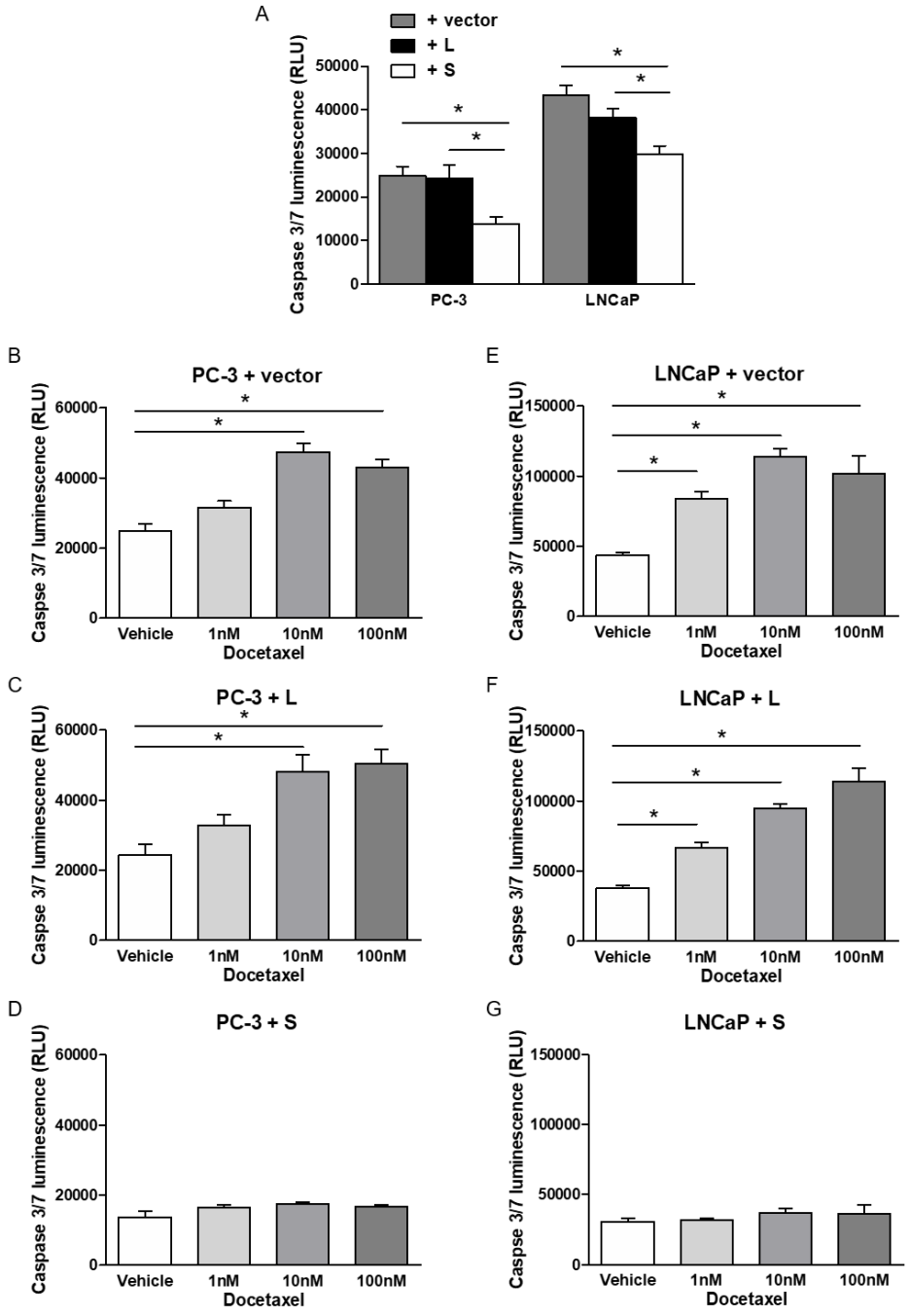

A) Baseline caspase 3/7 activity via luminescence of EA cell lines PC-3 and LNCaP ectopically overexpressing vector control, FGFR3-L, and FGFR3-S. Relative caspase 3/7 activity in PC-3 and LNCaP cells overexpressing vector (B,E), FGFR3-L (C,F), and FGFR3-S (D,G) with increasing concentrations of docetaxel. Data are represented as mean±SEM, n=3-6 independent experiments, one-way ANOVA with Dunnett post-hoc, *$p<0.05$.

Figure 22 Dovitinib does not augment docetaxel-induced caspase activity

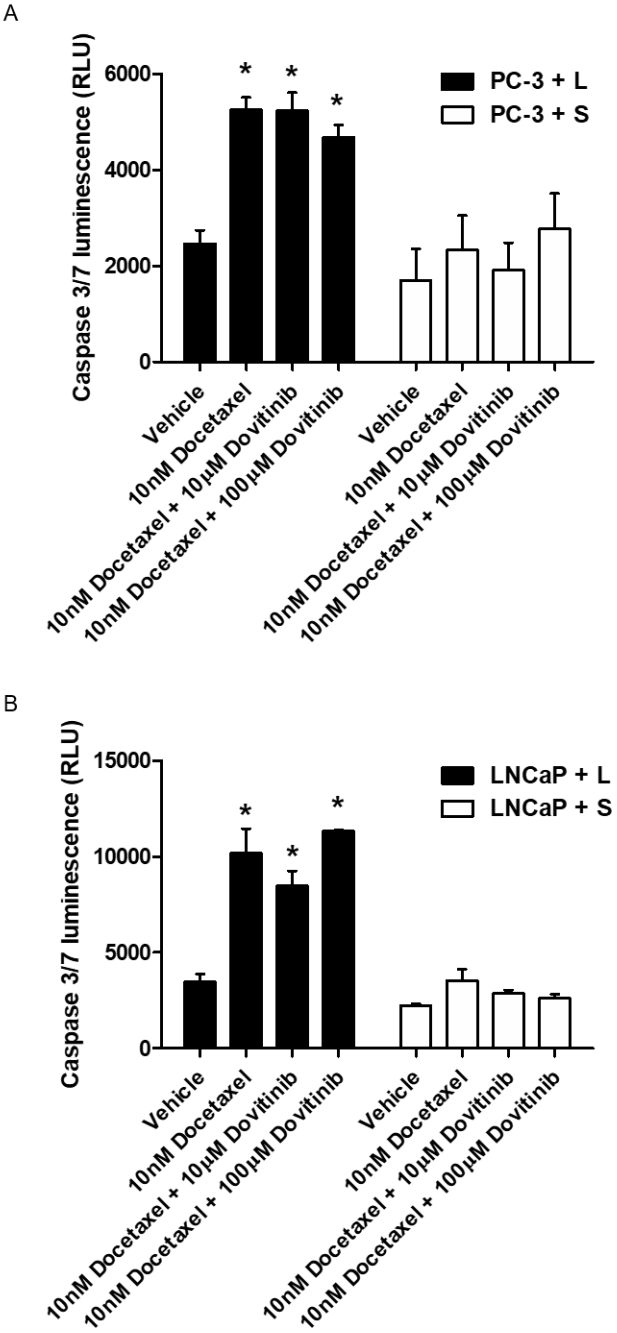

Relative caspase 3/7 activity of PC-3 (A) and LNCaP (B) cells overexpressing FGFR3-L and FGFR3–S with docetaxel treatment alone or in combination with dovitinib. Data are represented as mean±SEM, n=2-3 independent experiments, one-way ANOVA with Dunnett post-hoc, *$p<0.05$.

C. FGFR3-S signaling is more active and less sensitive to dovitinib compared to FGFR3-L

In order to determine potential differences in downstream oncogenic signaling between FGFR3-S and FGFR3-L isoforms, +S and +L cells were treated with vehicle or 10μM dovitinib and subjected to western blot analysis. Equivalent levels of FGFR3 isoform expression were confirmed in each cell line with a V5 tag antibody (**Figure 23**). We investigated activation of three proteins in known FGFR3 signaling pathways: AKT (PI3K/AKT pathway), STAT3 (STAT pathway), and ribosomal protein S6 (S6) (PI3K/AKT) (Dudka, Sweet, and Heath 2010; Li et al. 2016). At baseline, +S cells exhibited 1.46- to 2.24-fold greater phosphorylation of Tyr577 of FGFR3, a residue that is a marker of receptor tyrosine kinase activity (Furdui et al. 2006) compared with +L cells (**Figure 23**). Moreover, baseline +S cells displayed a 1.5- to 2.6-fold greater phosphorylation of downstream signaling proteins AKT (Ser473, Thr308), STAT3 (Tyr705), and S6 (Ser235/236) compared to +L cells. Dovitinib treatment induced a 50-67% decrease in FGFR3-L phosphorylation at Tyr577, as well as a 30-60% decrease in phosphorylation of AKT, STAT3, and S6 in +L cells. In contrast, the phosphorylation status of FGFR3-S, AKT, STAT3, and S6 in +S cells treated with dovitinib were comparable to vehicle treated cells. These data demonstrate that FGFR3-S activity and downstream signaling are not effectively inhibited by dovitinib treatment.

We next measured FGFR3-L and FGFR3-S activity using a cell-free kinase assay that quantified ADP production (**Figure 24**). In this assay, the intracellular domains of each receptor (-L: aa 397-end, -S: aa 397-end minus aa 613-653) were incubated with a kinase substrate and ATP. ADP (converted from ATP during the kinase reaction) was

then converted to ATP which was then converted to light via a luciferase/luciferin reaction. The amount of luminescence correlates ADP amount and, thus, kinase activity. Increasing concentrations of recombinant FGFR3-L correlated with an increase in luminescence and, thus, kinase activity (**Figure 25**). Recombinant FGFR3-S, however, displayed no kinase activity in this assay. Other assay formats will need to be explored to determine a better method for understanding the increased signaling capacity of FGFR3-S.

Figure 23 FGFR3-S exhibits increased downstream signaling via western blot analysis

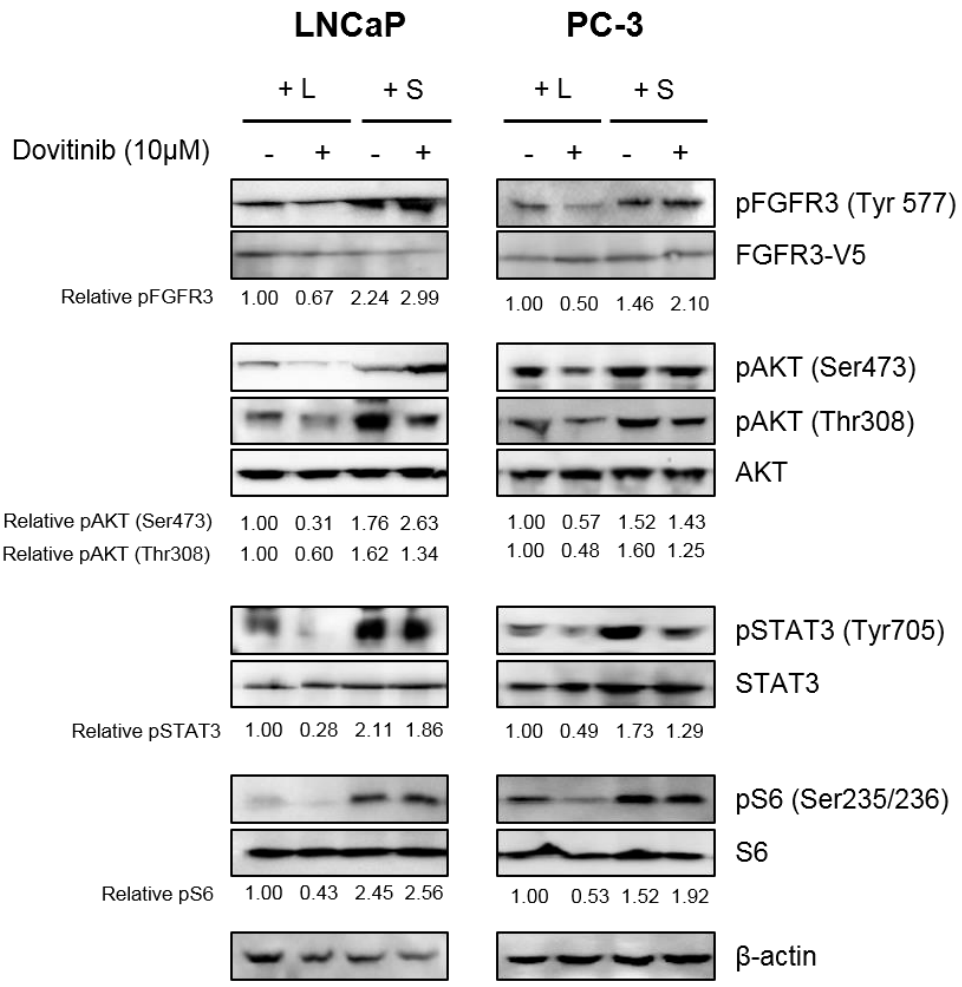

Western blots following treatment of cells overexpressing FGFR3-L and FGFR-3 with and without dovitinib treatment (10μM, 72hrs). Activation of FGFR3 was assessed via phosphorylation status of FGFR3 (Tyr577). V5 antibody was used to confirm equal expression of V5-tagged FGFR3. Activation of PI3K/AKT pathway was assessed via phosphorylation status of AKT and S6. Activation of STAT pathway was assessed via phosphorylation status of STAT3. β-actin was used as a loading control. Data are representative of n=3 independent experiments.

Figure 24 Cell-free kinase assay protocol

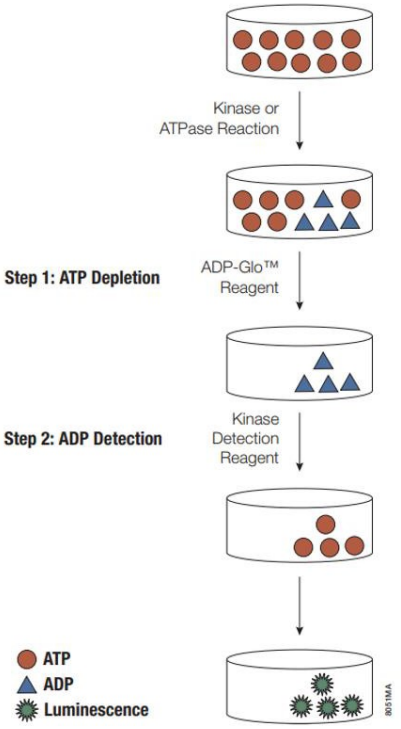

Schematic of the cell-free kinase assay protocol modified from Promega.

Figure 25 FGFR3-S shows no activity in cell-free kinase assay

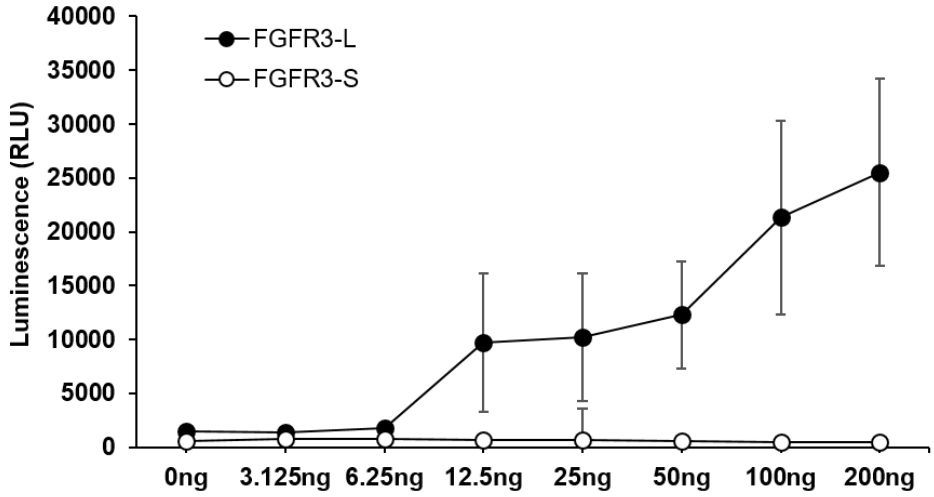

Kinase activity of intracellular domains of FGFR3-L and FGFR3-S as measured by ADP production. Data are represented as mean±SEM, n=2-4 independent experiments, unpaired t-test, *p<0.05.

D. FGFR3-S is resistant to dovitinib inhibition of tumor growth in xenograft models

The above findings suggest that the FGFR-S isoform is more oncogenic and exhibits resistance to SMI treatment compared to FGFR3-L. To further substantiate these *in vitro* results, we employed a xenograft mouse model to investigate the effects of *FGFR3* splice variants on tumor growth *in vivo* (**Figure 26**). We evaluated tumor growth by subcutaneous injection of $2x10^6$ PC-3+S or PC-3+L cells into the right hind flank of 3-6 week old NOD/SCID male mice. When tumors grew to a size of $3mm^3$, 30 days of daily *p.o.* treatment with 0.9% saline or 30mg/kg dovitinib was initiated. First, to determine if there were differences in the rate of tumor development between PC-3+L and PC-3+S cells, we measured the time it took for tumors to reach $3mm^3$. Mice injected with PC-3+L cells developed tumors significantly later than mice injected with PC-3+S cells, 20±0.55 days versus 16.4±0.67, respectively (**Figure 27A**). Dovitinib treatment significantly reduced the tumor volume in mice injected with PC- 3+L compared to saline treatment (**Figure 27B-C**). At day 30, the average PC-3+L tumor volume in mice treated with saline was over 2-fold greater than in mice treated with dovitinib. In contrast, dovitinib treatment had no significant effect on tumor volume in mice injected with PC-3+S cells compared to mice treated with saline. Additionally, the tumor volume in saline treated mice with PC-3+S cells was over two times greater than in mice harboring PC-3+L xenografts. All tumor specimens showed positive IHC staining with an anti-His tag antibody, confirming the tumors were derived from PC-3+L or PC- 3+S cells (**Figure 27D**).

Figure 26 Outline of mouse model experiments

A

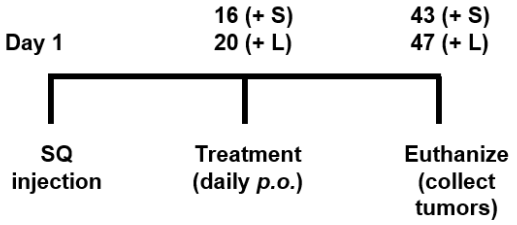

B

Cell line	Treatment (n=10-12)
PC-3 + L	0.9% saline
PC-3 + L	30mg/kg dovitinib
PC-3 + S	0.9% saline
PC-3 + S	30mg/kg dovitinib

A) PC-3+L or PC-3+S cells were subcutaneously (SQ) injected on day 1 of tumor growth study. Daily oral (*p.o.*) treatments of saline or dovitinib began when tumors reached $3mm^3$, at day 16 for animals injected with PC-3+S cells and at day 20 for those injected with PC-3+L cells. Animals were euthanized after 30 days of treatment and tumors were dissected. B) List of cell lines and treatments used in the study.

Figure 27 FGFR3-S is resistant to dovitinib-mediated inhibition of tumor growth

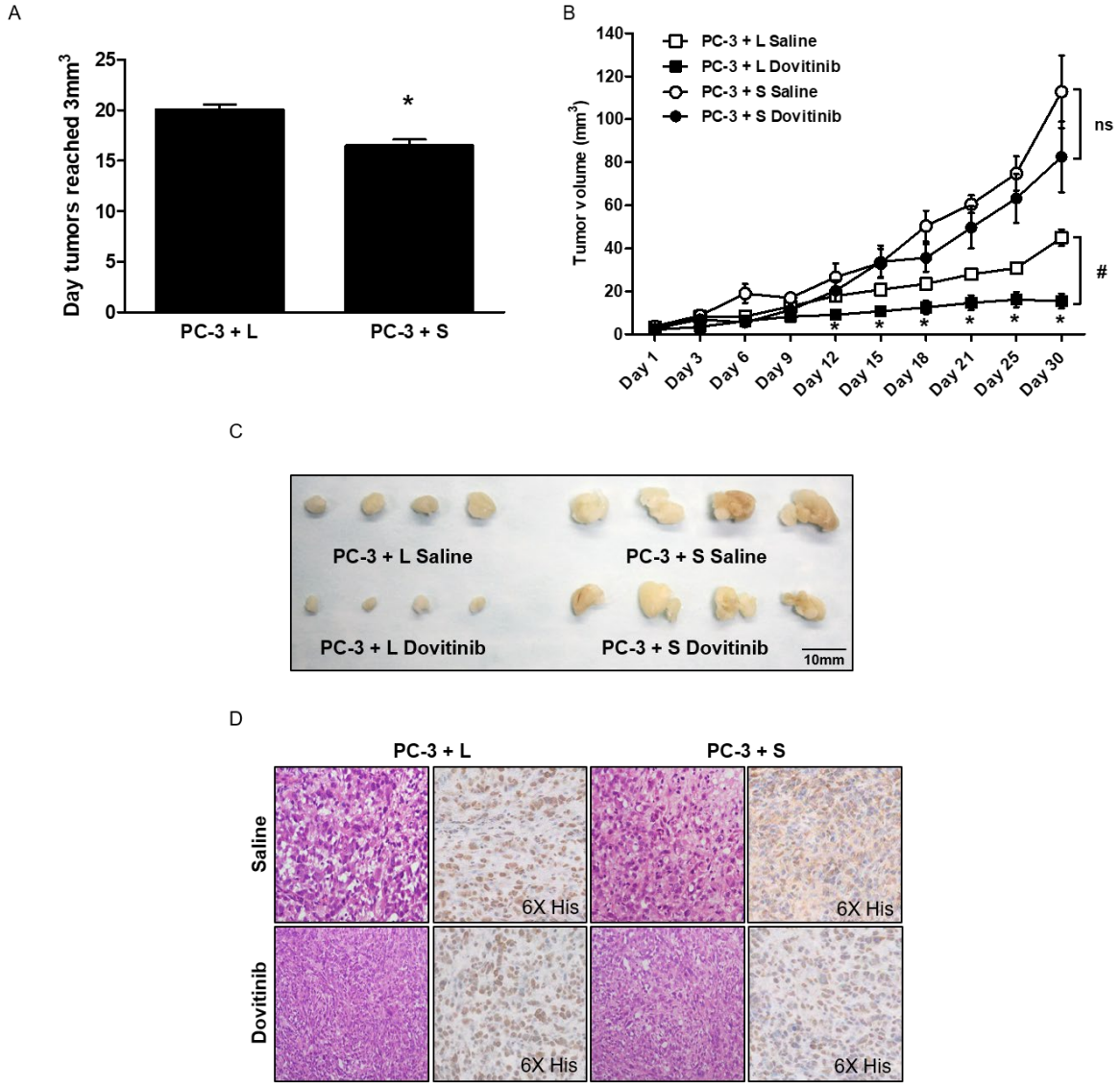

A) Day tumor xenografts of PC-3+L or PC-3+S cells reached 3mm^3. Data is represented as mean±SEM, n=20-21, unpaired t-test, *p<0.05. B) Volume of PC-3+L or PC-3+S tumor xenografts from day 1-30 of daily *p.o.* treatment of 0.9% saline or 30 mg/kg dovitinib. Data is represented as mean±SEM, n=10-11, one-way ANOVA with Tukey post hoc, #p<0.05, unpaired t-test, *p<0.05. C) Representative tumor xenografts (D) and H&E staining and IHC with His tag (brown) and hematoxylin (blue) (D) of tumor xenografts from each treatment group dissected on day 30 of treatment.

Chapter 5: Determination of differential expression of splicing factors and their contribution to *FGFR3* splicing patterns

A. Splicing factors are upregulated in AA versus EA PCa

B. SRSF2 and hnRNPF are splicing factors of interest

C. Knockdown of splicing factors leads to *FGFR3* splice switching and decreased oncogenicity

D. Overexpression of FGFR3-S rescues splicing factor knockdown phenotype

A. Splicing factors are upregulated in AA PCa

Following the identification and characterization of the novel FGFR3-S variant, we next investigated which upstream factors may play a role in generating the more oncogenic short isoform of *FGFR3*. One well known group of splicing modulators are RNA binding proteins (RBPs), such as SFs. To evaluate the expression of SFs in patient samples, we returned to previously generated Affymetrix array data (Wang et al. 2017) and compared total expression of known SFs in AA and EA PCa specimens. We identified seven SFs that were predicted to have significantly increased gene expression in AA (n=15) versus EA (n=20) PCa specimens: *SRSF1*, *SRSF2*, *SRSF7*, *HNRNPF*, *HNRNPR*, *DDX5*, and *DDX21* (**Figure 28**).

Validation of increased SF expression was confirmed in a separate patient cohort via immunohistochemistry (IHC). All seven splicing factors showed increased nuclear and cytoplasmic staining of epithelial prostate cancer cells of AA (n=19) versus EA (n=19-21) PCa specimens (**Figure 29A**). Additionally, when the DAB+ chromagen staining intensity per area was quantitated and binned into four groups from low (Score 1) to high staining (Score 4) (Varghese et al. 2014), SF staining was significantly higher in AA compared to EA PCa specimens (**Figure 29B-D**).

We also assessed SF expression in two AA PCa cell lines (MDA PCa 2b and RC77 T/E) and three EA PCa cell lines (VCaP, LNCaP, and PC-3) via immunocytochemistry (ICC) (**Figure 30**). Both AA cell lines showed increased expression of SFs compared to EA PCa cells.

Figure 28 Gene expression of splicing factors in AA and EA PCa specimens

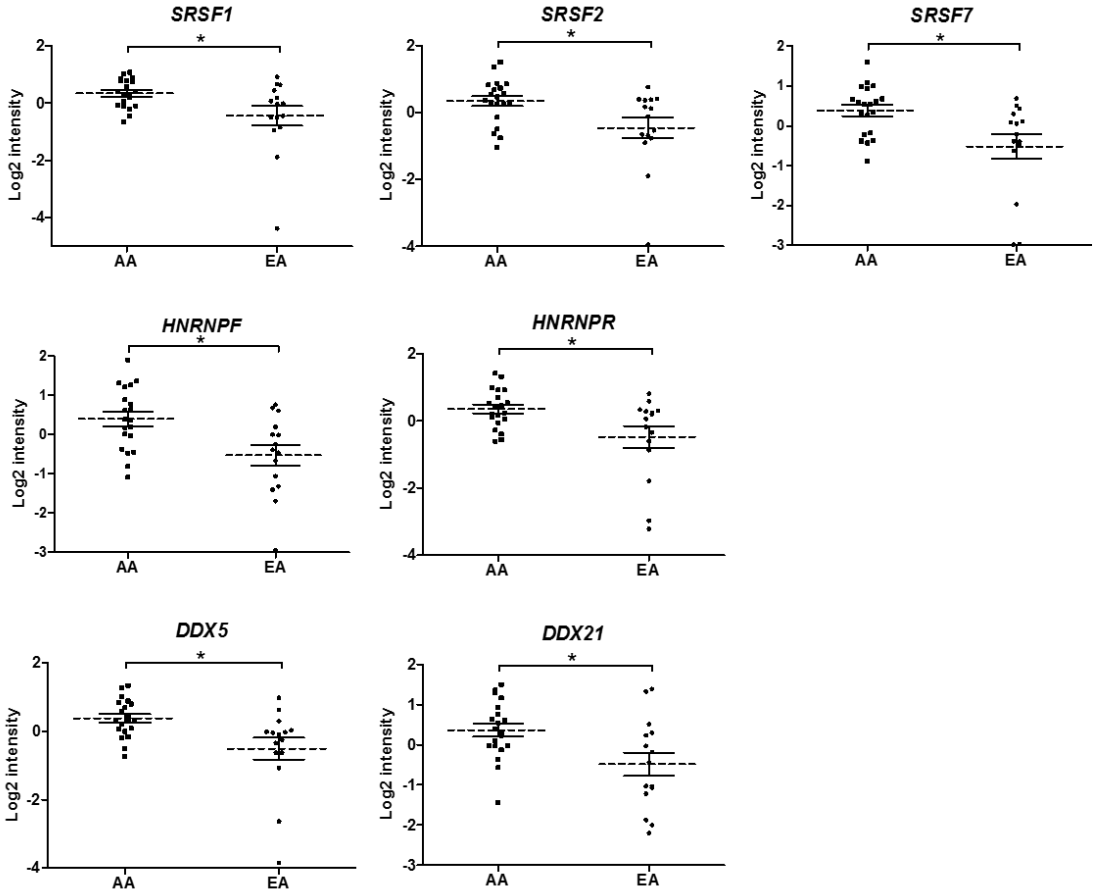

Microarray data showing gene expression of splicing factors in AA (n=15) and EA (n=20) PCa specimens. Data represented with median (dotted line) and SEM, unpaired t-test, *$p < 0.05$.

Figure 29 Differential expression of SF in AA vs EA PCa specimens

A

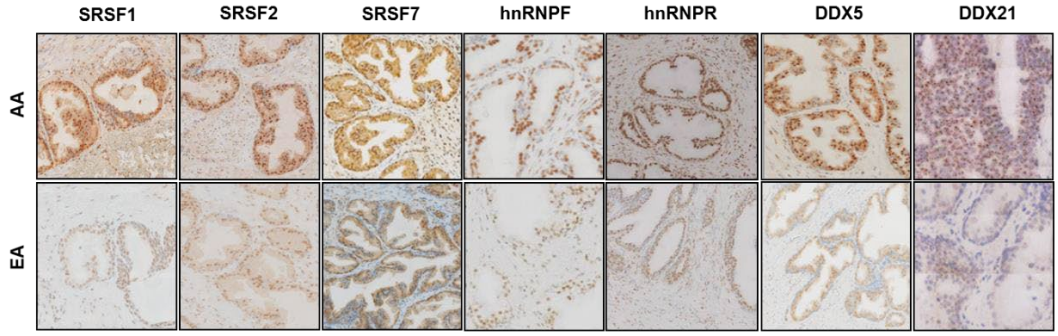

B

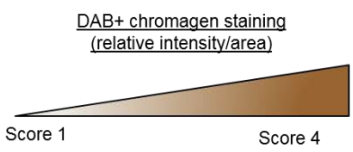

C

	SRSF1*		SRSF2*		SRSF7*		hnRNPF*		hnRNPR*		DDX5*		DDX21*	
	AA	EA	AA	EA	AA	EA	AA	EA	AA	EA	AA	EA	AA	EA
Score 1	2	14	0	10	2	10	1	14	0	15	1	10	5	17
Score 2	3	3	4	6	6	4	2	5	1	0	3	3	12	3
Score 3	10	2	8	2	1	4	11	0	10	1	7	2	2	0
Score 4	4	1	7	1	10	1	5	0	8	5	8	4	0	0
total n	19	20	19	19	19	19	19	19	19	21	19	19	19	20

D

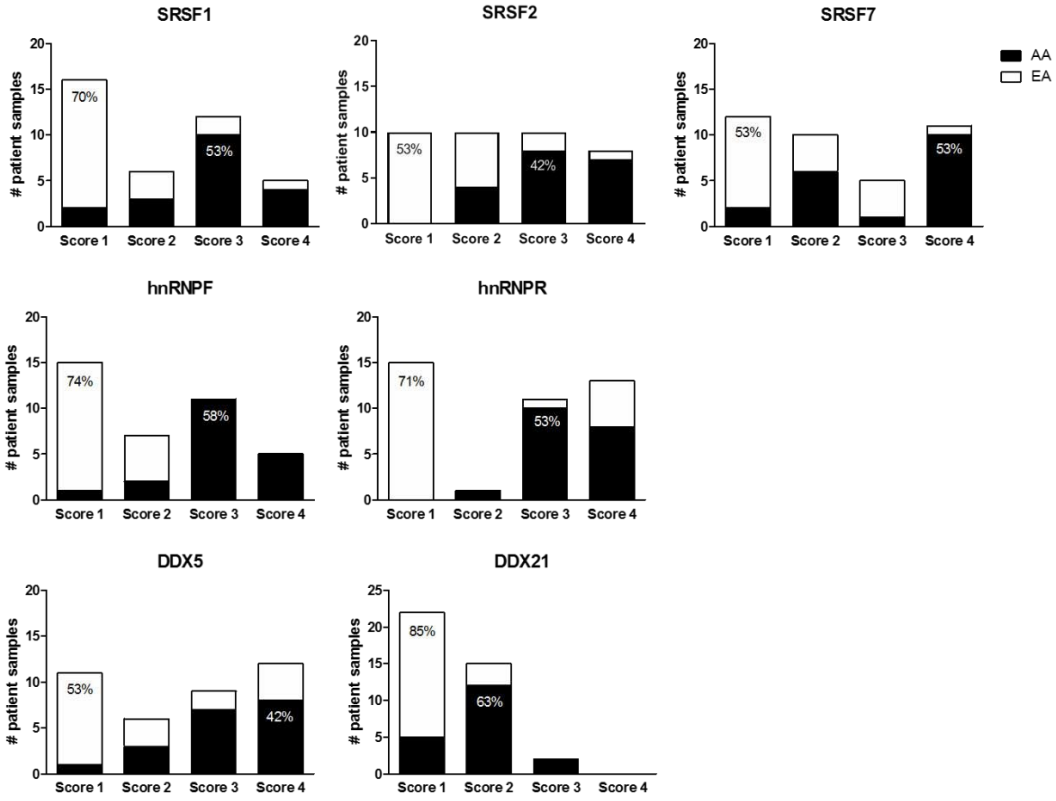

A) Representative IHC of AA (top; n=19) and EA (bottom; n=19-21) paraffin-embedded PCa specimens of SFs (brown) and nuclei (hematoxylin). B) Schematic of relative DAB+ chromagen intensity/area in relation to scoring of IHC specimens. Quantitated staining/area for each image was binned into four groups (Score 1-4). C) Number of patients per score for each ethnic group for each SF. Chi-square test, *p<0.05. D) Graphic representation of data in C). Scores that include the largest percentages of each group of labeled within the bar.

Figure 30 SFs are differentially expressed in AA versus EA PCa cell lines

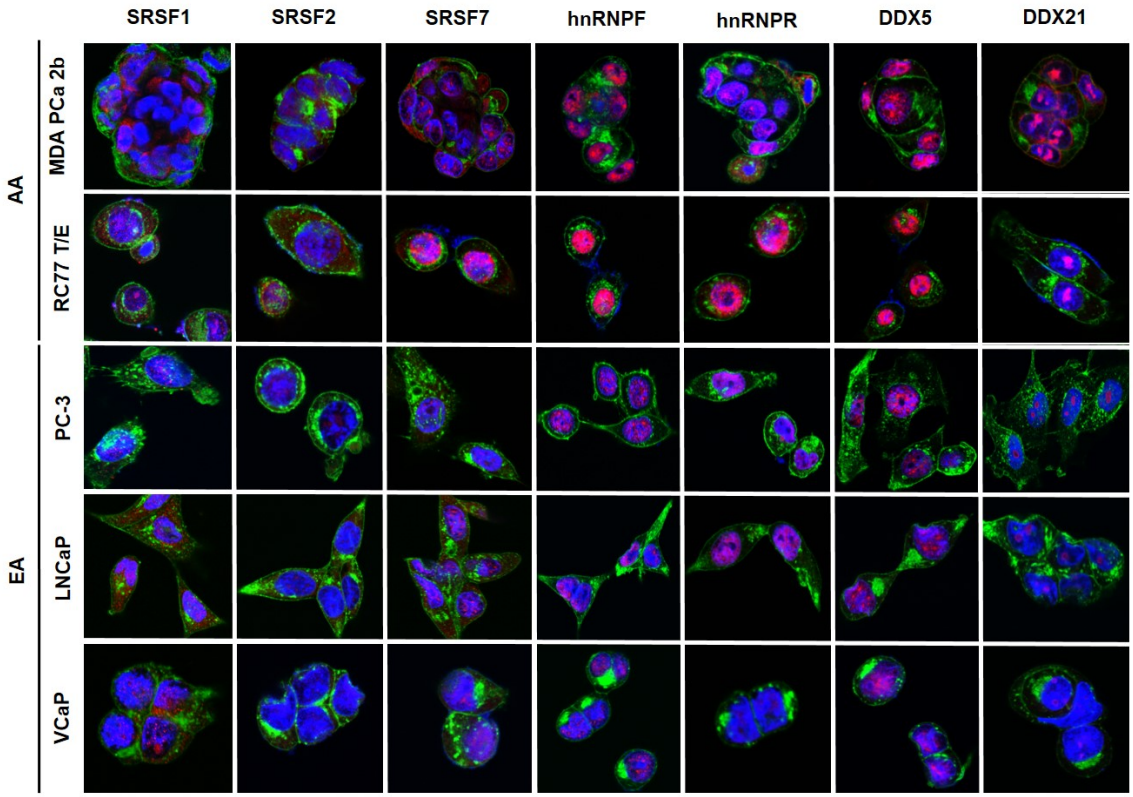

Immunocytochemistry of SFs in AA (MDA PCa 2b, RC77 T/E) and EA (PC-3, LNCaP, VCaP) PCa cells. Key: SFs (Alexa 594, pink), cell outline with WGA (Alexa 488, green), nuclei with DAPI (λ405, blue), n=3-4.

B. SRSF2 and hnRNPF are splicing factors of interest

We next wanted to determine which SFs were directly involved in exon 14 skipping of *FGFR3*. To do so, we employed a bioinformatics approach using the predicted binding sites of each SF. We hypothesized that the SF with the most predicted binding sites flanking and within the sequence of exon 14 would be contributing the greatest role in skipping of exon 14. We utilized the SF-RNA binding site database SpliceAid-F to identify SFs that had putative binding sites in the exonic and intronic sequence space around exon 14 (**Figure 31A**). Of the seven SFs identified, three were predicted to have binding sites in or around exon 14: SRSF1 (n=3 predicted sites), SRSF2 (n=10), and hnRNPF (n=23) (**Figure 31B**). Due to the large number of predicted sites, we selected SRSF2 and hnRNPF as our SFs of interest.

Figure 31 SRSF1, SRSF2, and hnRNPF have predicted binding sites in exon 14 sequence space

A

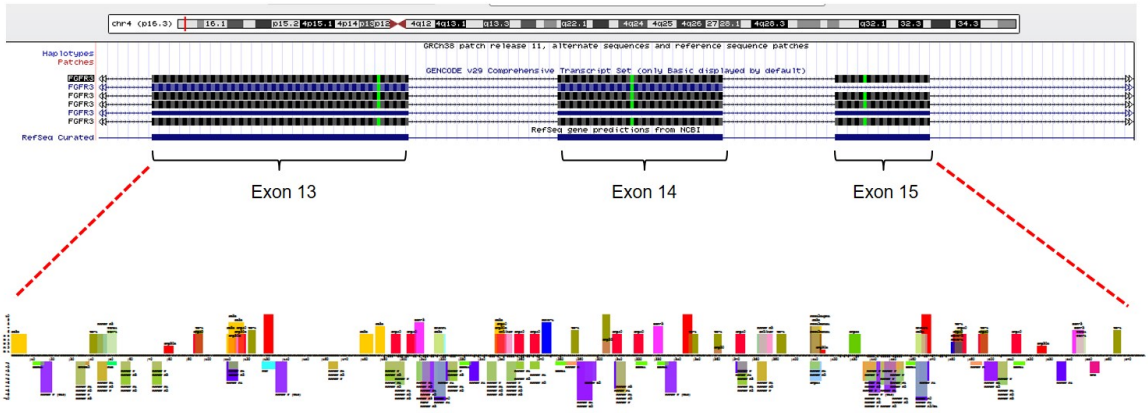

B

	Length (bp)	# SRSF1 binding sites	# SRSF2 binding sites	# hnRNPF binding sites
Exon 13	191	1	6	6
Intron 13-14	110	1	2	5
Exon 14	123	1	1	3
Intron 14-15	83	0	1	9
Exon 15	71	0	0	0
total		**3**	**10**	**23**

A) *FGFR3* sequence (exon 13-exon 15 with introns) (top) and SFs with predicted binding sites (bottom) within those sequences. *FGFR3* sequence space retrieved from the UCSC Genome Browser (Kent et al. 2002). SF binding sites were predicted using SpliceAid-F (Giulietti et al. 2013). B) Number of predicted binding sites of SRSF1, SRSF2, and hnRNPF within each exon and intron around exon 14. SRSF2 and hnNRPF were selected for further investigation and are outlined in red.

C. Knockdown of splicing factors leads to *FGFR3* splice switching and decreased oncogenicity

In order to validate the direct role of SRSF2 and hnRNPF in the skipping of exon 14 during processing of the pre-*FGFR3* mRNA, we knocked down expression of each SF in AA PCa cell lines and performed RT-PCR to examine the expression of *FGFR3-L* and *FGFR3-S*. MDA PCa 2b and RC77 T/E AA cell lines predominantly expressed *FGFR3-S* in control nonsense siRNA (siNS) cells. For targeted knockdown of individual SFs, two separate siRNAs for each SF were employed to take into account potential off-target effects. SiRNA-mediated knockdown of *SRSF2* and *HNRNPF* caused splice switching from predominant -*S* to -*L* variant expression (**Figure 32**). SF knockdown significantly decreased the *FGFR3-S/-L* ratio over 3-fold. These results suggest SRSF2 and hnRNPF are directly involved in exon 14 skipping events.

To better understand the effects of the SF knockdown on AA PCa, we treated AA cell lines with siRNAs to knockdown expression of *SRSF2* and *HNRNPF* and evaluated the functional consequences in *in vitro* assays. We first assessed the invasive potential in these cell lines as measured by Matrigel assay following control siNS treatment and targeted siRNA-mediated knockdown of *SRSF2* and *HNRNPF*. In this assay, knockdown of either SF by two different siRNAs significantly decreased invasion by 1.25 to 2.5-fold in both cell lines (**Figure 33A**). Next, we measured BrdU incorporation as a measure of proliferation. Again, knockdown of either SFs significantly reduced the proliferative capability by 40-60% (**Figure 33B**). Finally, in order to test the effects of SF knockdown on apoptosis, we measured caspase 3/7 luminescence. Compared to siNS control treatment, knockdown of *SRSF2* and *HNRNPF* in AA PCa cell lines significantly

increased caspase 3/7 luminescence by approximately 50%, indicating apoptosis of PCa cell lines (**Figure 33C**). Knockdown efficiency was determined by western blot analysis to ensure that a decrease of SF protein levels occurred following treatment of cells with the siRNAs (**Figure 34).** Taken together, these findings suggest SRSF2 and hnRNPF are directly influencing the splicing of exon 14.

Figure 32 SF knockdown causes splice switching from *FGFR3-S* to *FGFR3-L* variant

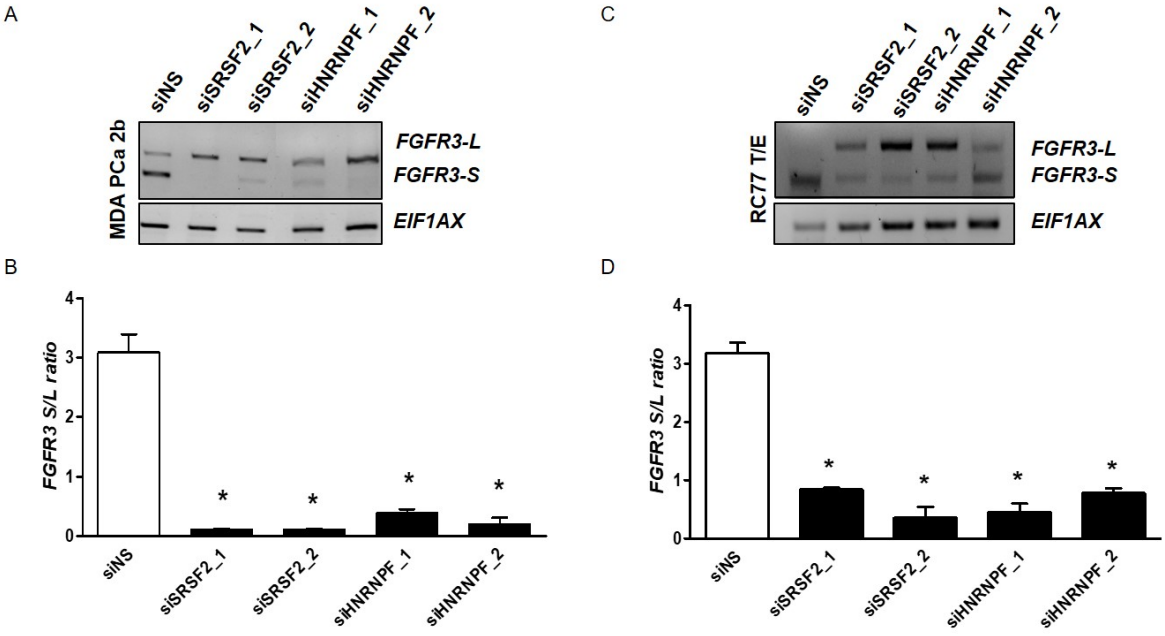

Representative RT-PCR of *FGFR3* variants following siRNA-mediated knockdown of *SRSF2* and *HNRNPF* compared to control siNS-treated MDA PCa 2b (A) and RC77 T/E (C) cells. Quantification of *FGFR3 S/L* expression ratios in MDA PCa 2b (B) and RC77 T/E (D) cells. Data are represented as mean±SEM, n=3-7 independent experiments, one-way ANOVA with Dunnett post-hoc or unpaired t-test, *p<0.05.

Figure 33 Splicing factor knockdown decreases oncogenicity of AA PCa

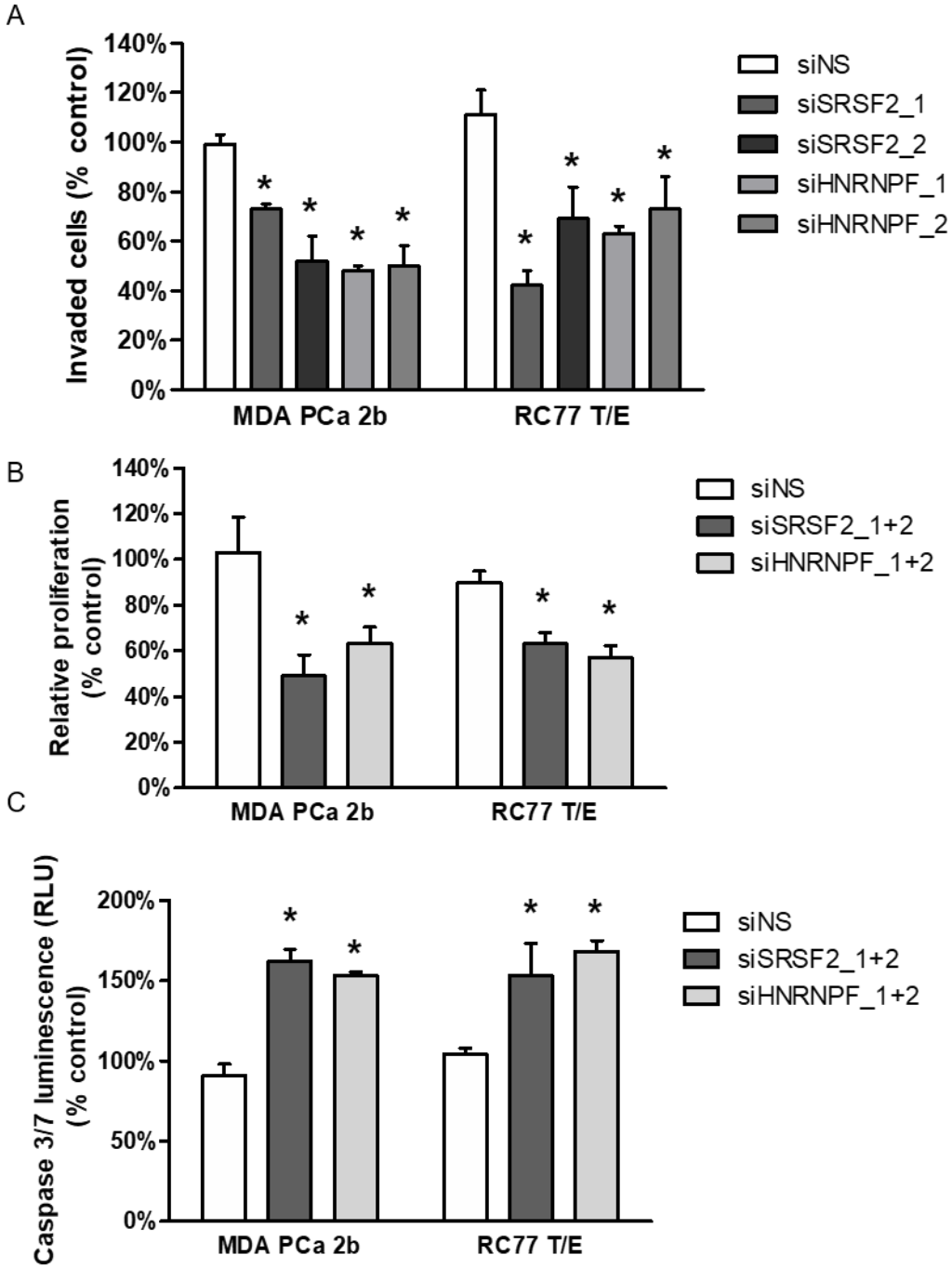

Relative invasion (A), proliferation (B), and caspase 3/7 luminescence (C) in MDA PCa 2b and RC77 T/E AA cell lines after treatment is siRNAs against *SRSF2*, *HNRNPF*, and a nonsense control (siNS). Data are represented as mean±SEM, n=3-7 independent experiments, one-way ANOVA with Dunnett post-hoc or unpaired t-test, *$p<0.05$.

Figure 34 Western blot confirms knockdown of splicing factors

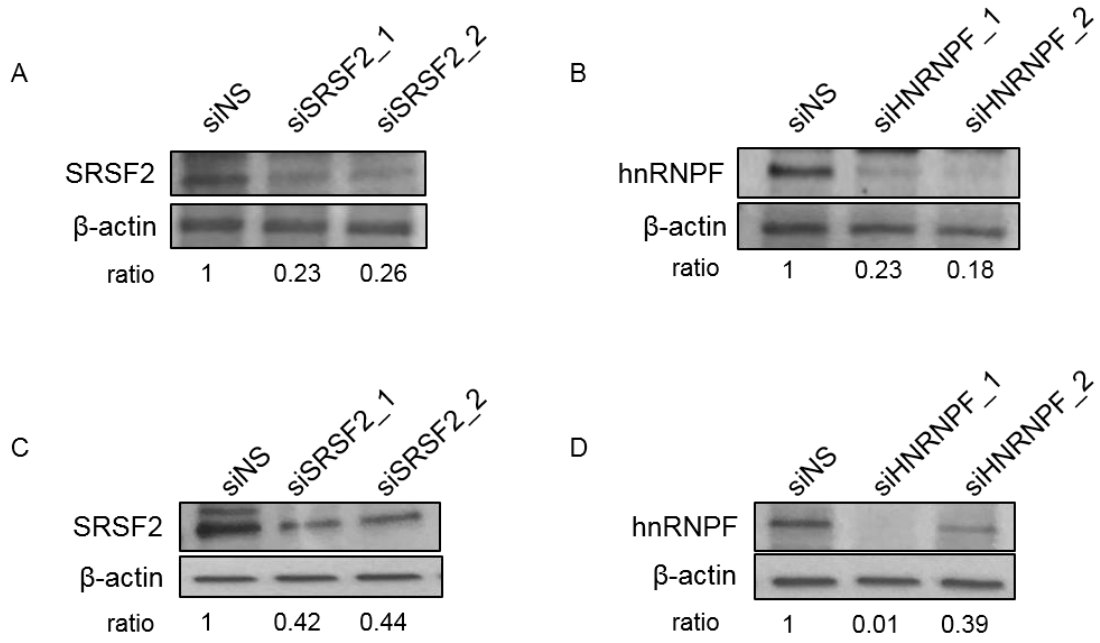

Representative blots of SF knockdown in MDA PCa 2b (A,B) and RC77 T/E (C,D) cell lines. Knockdown efficiency of two individual siRNAs per SF were normalized to β-actin and compared to siNS control treated cells.

D. Overexpression of FGFR3-S rescues splicing factor knockdown phenotype

In order to confirm the role of SRSF2 and hnRNPF in FGFR3-S-mediated exon 14 skipping and oncogenesis, we devised *in vitro* rescue experiments using the AA PCa cells lines stably overexpressing FGFR3-S generated in Chapter 3. If these SFs are directly responsible for skipping of exon 14, we hypothesized that the decrease in oncogenicity of AA PCa cell lines as a consequence of SF knockdown (**Figure 33**) would be phenotypically "rescued" in SF knockdown experiments of cells that stably overexpressed FGFR3-S ectopically.

We first measured invasion by Matrigel assay at baseline and with SF siRNA-mediated knockdown. In this assay, AA PCa cells overexpressing FGFR3-S (MDA PCa 2b+S and RC77 T/E+S) exhibited 1.75- to 2-fold increase in baseline invasion compared to cells overexpressing a vector control (MDA PCa 2b+vector and RC77 T/E+vector) (**Figure 35A**). We then tested the effect of SF knockdown on invasion. In MDA PCa 2b+vector and RC77 T/E+vector cells, knockdown of either *SRSF2* or *HNRNPF* significantly decreased invasion by 30-60% compared to siNS-treated control cells (**Figure 35B-C**). By comparison, neither MDA PCa 2b+S nor RC77 T/E+S cells showed any significant loss of invasive phenotype after successful SF knockdown (**Figure 35B-C**).

Next, we measured BrdU incorporation as an index of proliferation. Baseline proliferation was significantly higher in MDA PCa 2b+S and RC77 T/E+S cells compared to empty vector control (+vector) cells (**Figure 36A**). Control cells overexpressing the empty vector exhibited significantly lower invasive capacity

following knockdown of SFs (**Figure 36B-C**). The invasive capacity of +S cells with SF knockdown was unchanged compared to siNS-treated cells (**Figure 36B-C**).

To examine the effect of SF knockdown on apoptosis, we treated +vector and +S cells with siRNAs targeting *SRSF2* or *HNRNPF* and measured caspase3/7 activity. At baseline, +S cells exhibited a 2- to 3-fold decrease in caspase 3/7 activity compared to +vector cells (**Figure 37A**). MDA PCa 2b+vector and RC77 T/E+vector cells demonstrated significantly increased caspase 3/7 activity with SF knockdown (**Figure 37B-C**). By comparison, ectopic stable overexpression of FGFR3-S decreased caspase3/7 activity to baseline, rescuing the phenotype observed in +vector expressing control cells (**Figure 37B-C**). Knockdown efficiency was determined by western blot analysis (**Figure 38, Figure 39**). Together, these data suggest SRSF2 and hnRNPF are directly involved in skipping of exon 14 and, thus, are playing a crucial role in the increased oncogenicity of AA PCa.

Figure 35 FGFR3-S overexpression rescues splicing factor knockdown-mediated inhibition of invasion

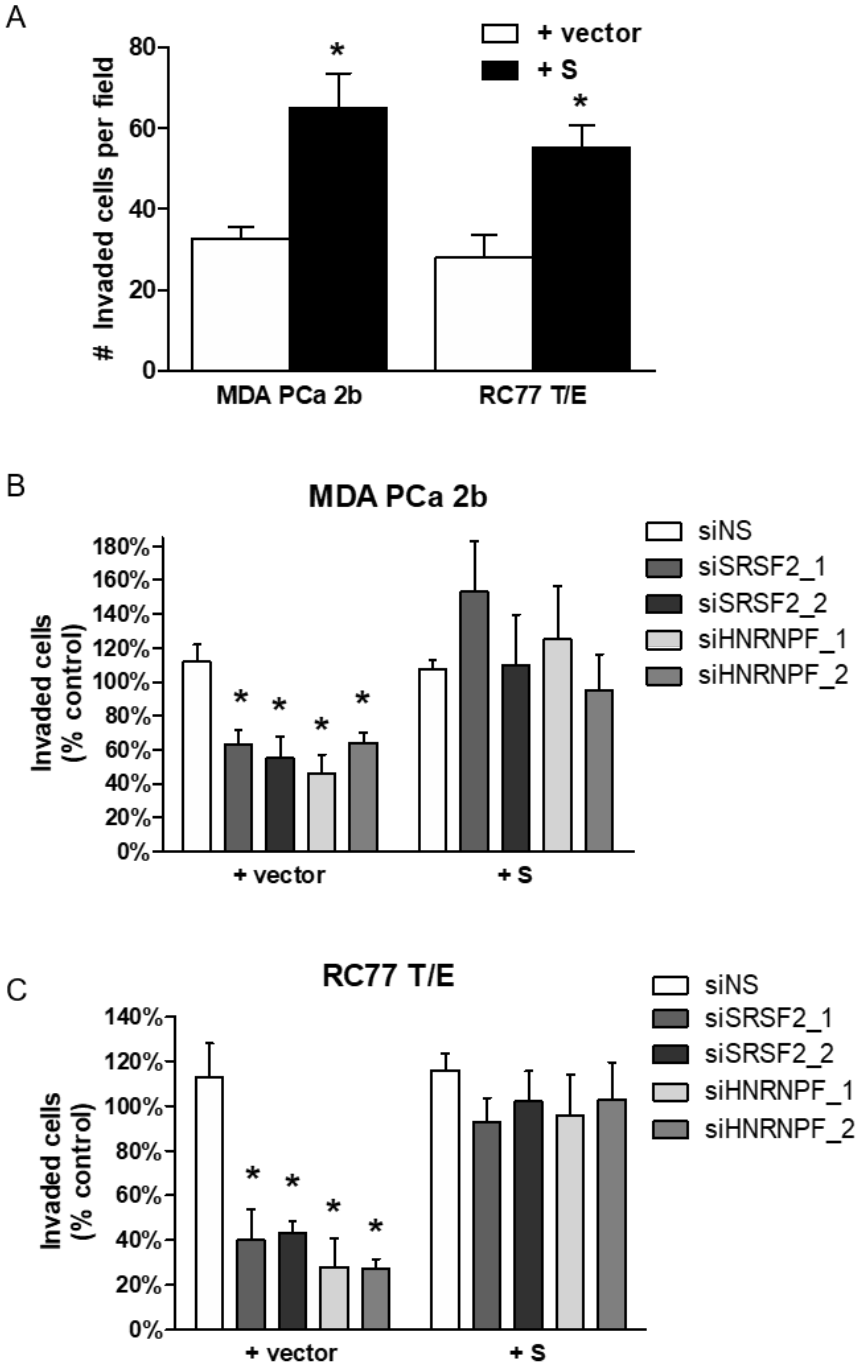

A) Baseline invasion via Matrigel assay of AA cell lines MDA PCa 2b and RC77 T/E cells ectopically overexpressing vector control or FGFR3-S. Invaded cells shown as percent vehicle in MDA PCa 2b (B) and RC77 T/E (C) cells overexpressing vector or FGFR3-S with treatment with a control siRNA (siNS) and two separate siRNAs targeting *SRSF2* and *HNRNPF*. Data are represented as mean±SEM, n=3-6 independent experiments, unpaired t-test or one-way ANOVA with Dunnet post-hoc, *p<0.05.

Figure 36 FGFR3-S overexpression rescues splicing factor knockdown-mediated inhibition of proliferation

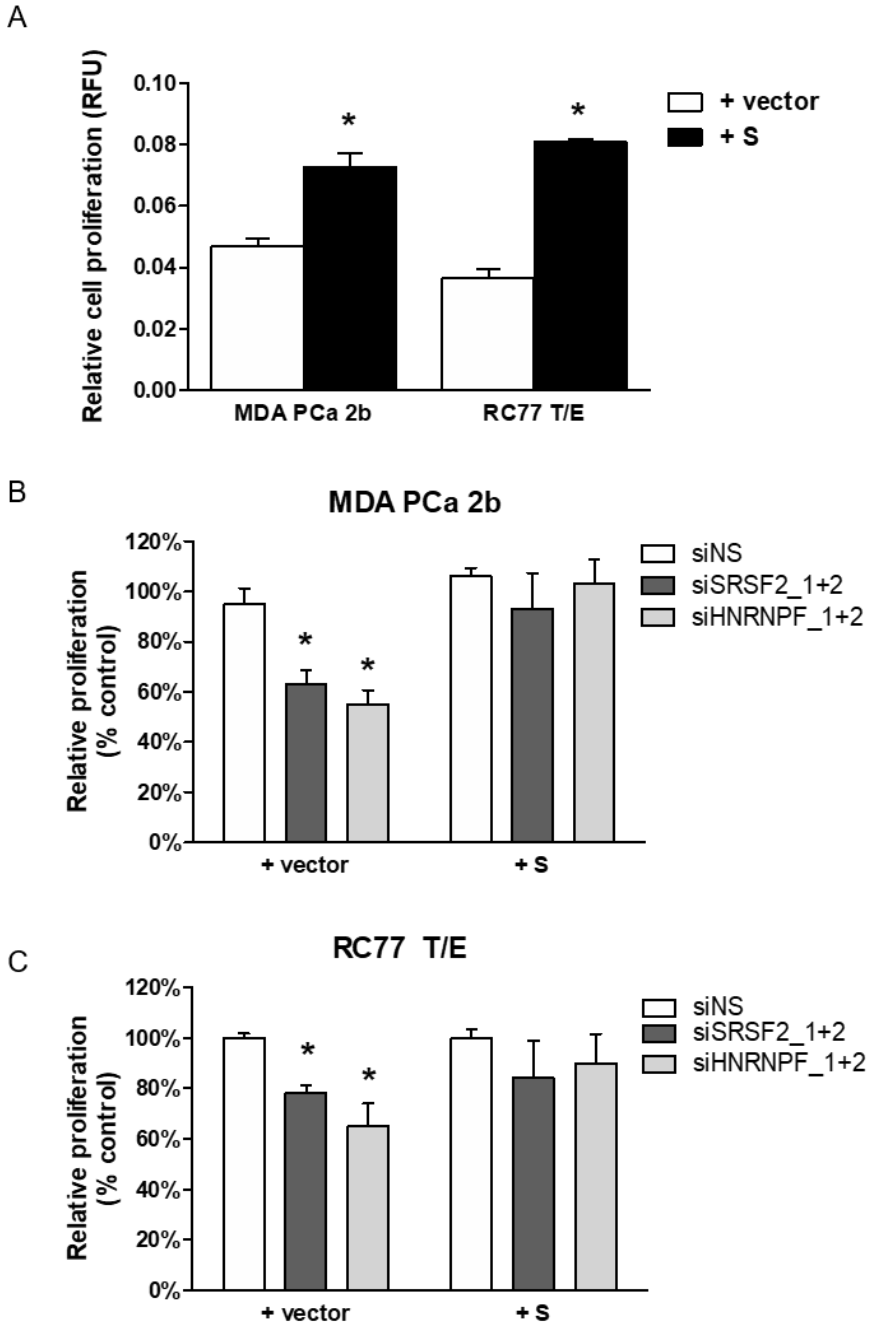

A) Baseline proliferation via BrdU incorportation of AA cell lines MDA PCa 2b and RC77 T/E cells ectopically overexpressing vector control or FGFR3-S. Invaded cells shown as percent vehicle in MDA PCa 2b (B) and RC77 T/E (C) cells overexpressing vector or FGFR3-S with treatment with a control siRNA (siNS) and two combined siRNAs targeting *SRSF2* and *HNRNPF*. Data are represented as mean±SEM, n=3-6 independent experiments, unpaired t-test or one-way ANOVA with Dunnet post-hoc, *$p<0.05$.

Figure 37 FGFR3-S overexpression rescues splicing factor knockdown-mediated caspase 3/7 activation

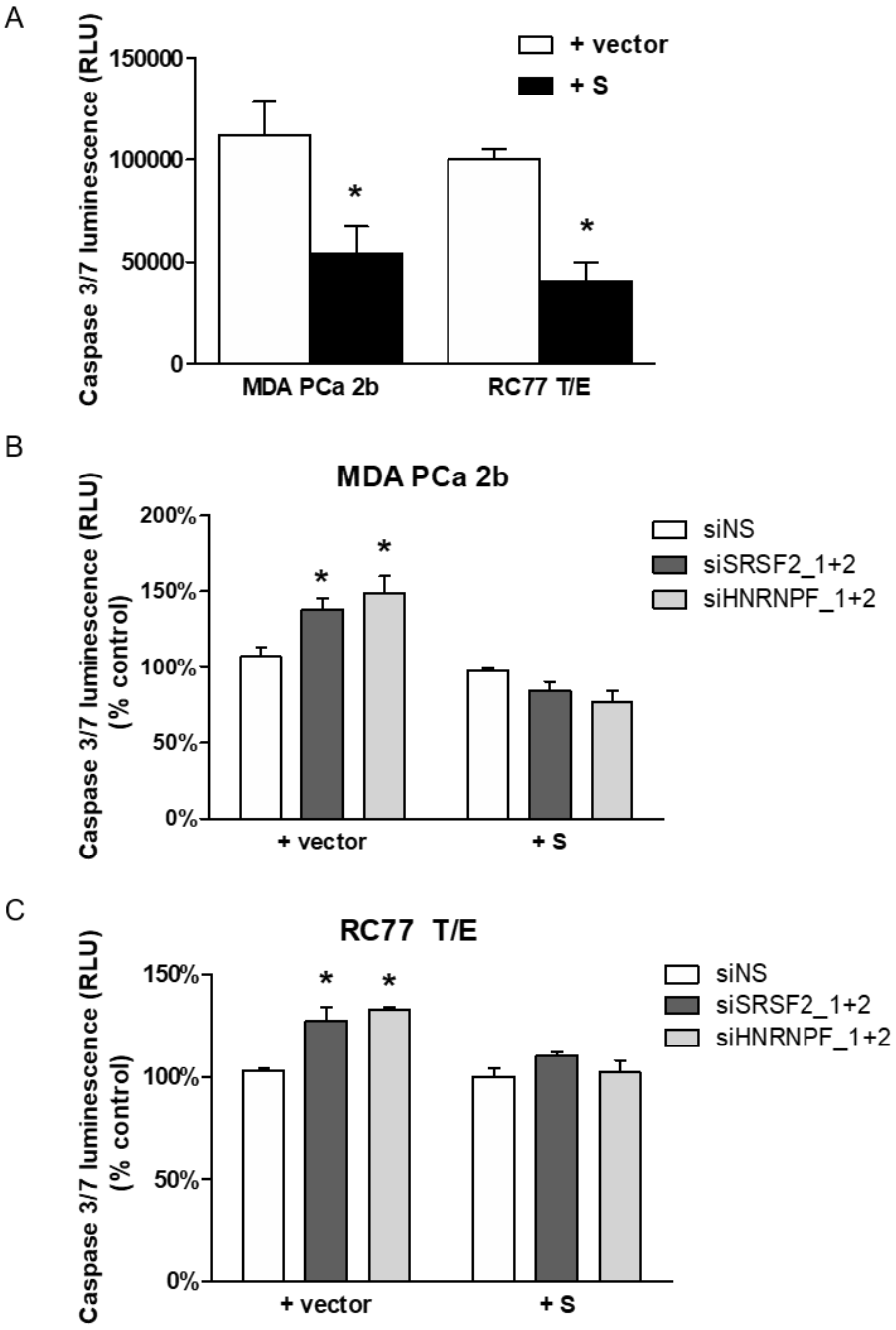

A) Baseline caspase 3/7 activity via luminescence of AA cell lines MDA PCa 2b and RC77 T/E cells ectopically overexpressing vector control or FGFR3-S. Invaded cells shown as percent vehicle in MDA PCa 2b (B) and RC77 T/E (C) cells overexpressing vector or FGFR3-S with treatment with a control siRNA (siNS) and two combined siRNAs targeting *SRSF2* and *HNRNPF*. Data are represented as mean±SEM, n=3-6 independent experiments, unpaired t-test or one-way ANOVA with Dunnet post-hoc, *$p<0.05$.

Figure 38 Western blot confirms knockdown of splicing factors in MDA PCa 2b transfected cells

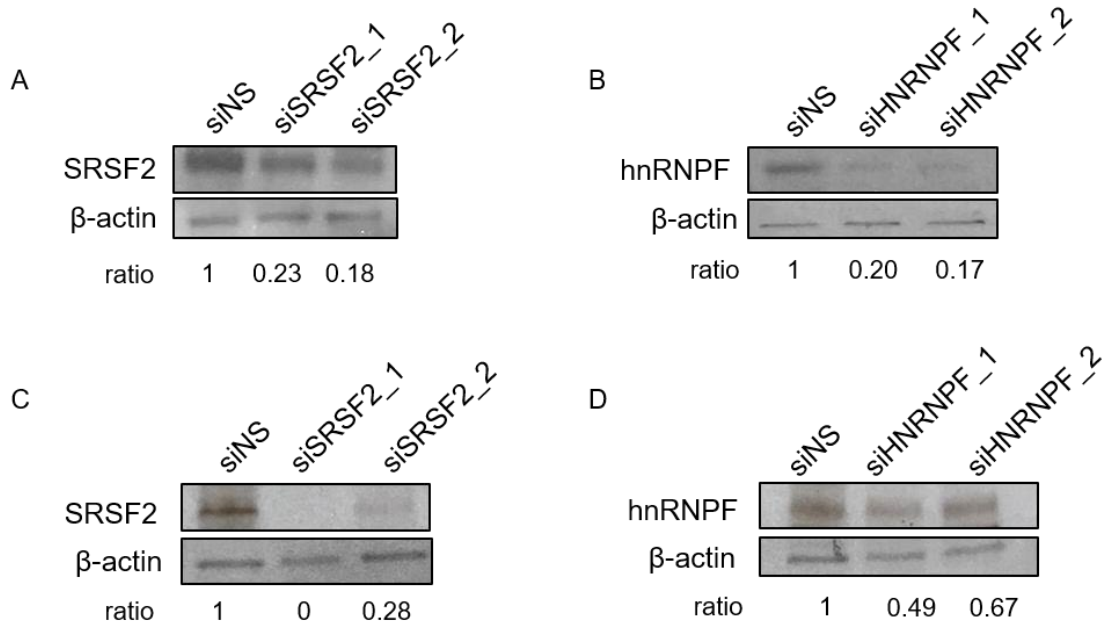

Representative blots of SF knockdown in MDA PCa 2b+vector (A,B) and MDA PCa 2b+S (C,D) cell lines. Knockdown efficiency of two individual siRNAs per SF were normalized to β-actin and compared to siNS control treated cells.

Figure 39 Western blot confirms knockdown of splicing factors in RC77 T/E transfected cells

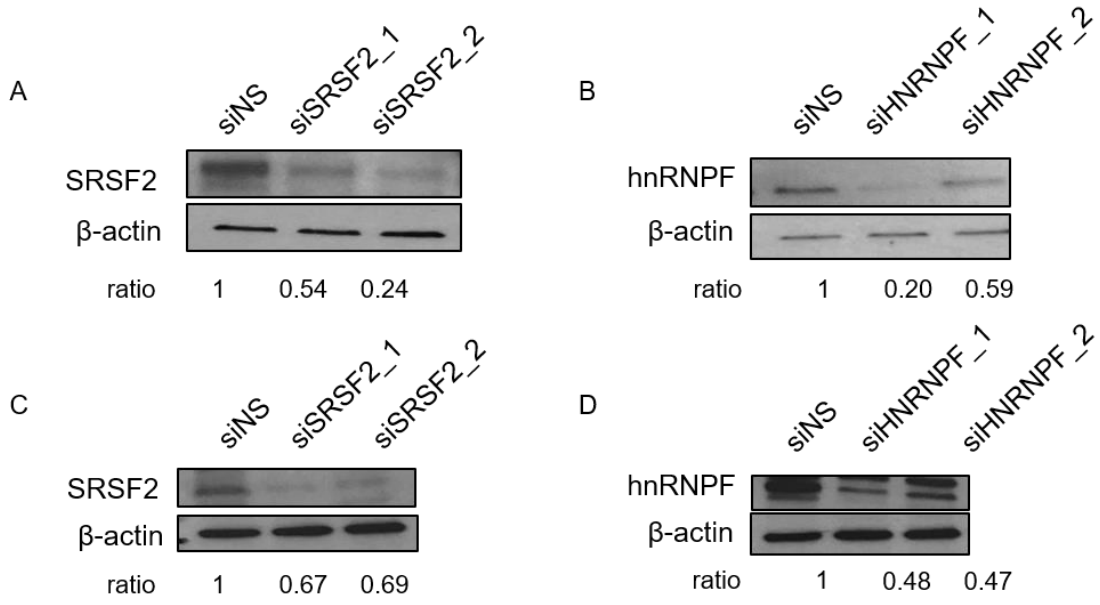

Representative blots of SF knockdown in RC77 T/E+vector (A,B) and RC77 T/E+S (C,D) cell lines. Knockdown efficiency of two individual siRNAs per SF were normalized to β-actin and compared to siNS control treated cells.

Chapter 6: Discussion

Prior studies have highlighted the clinical significance of receptor tyrosine kinase (RTK) alterations in cancer. A splice variant of the BCR-ABL fusion, *BCR-ABL35INS*, retains 35 intronic nucleotides, causing a frameshift and pre-mature termination (O'Hare et al. 2011). This fusion isoform is resistant to imatinib, a tyrosine kinase inhibitor (TKI) used to treat chronic myelogenous leukemia (Lee et al. 2008). In melanoma, a 61 kDa isoform encoded by a *BRAF* splice variant missing exons 4-8 lacks the RAS-binding domain, resulting in constitutive isoform dimerization and kinase activity and resistance to the inhibitor vemurafenib (Poulikakos et al. 2011). A splice variant of *BIM* (*BIM-γ*), encoding a protein that lacks the BH3 domain, has been identified as a mechanism for TKI (e.g. imatinib, gefitinib) resistance in chronic myeloid leukemia (CML) (Ko et al. 2016; Liu et al. 2017; Ng et al. 2012).

In prostate cancer (PCa), splice variants of the androgen receptor (*AR*) are known to promote oncogenesis and drug resistance. The *ARv7* variant encodes an AR isoform that is androgen-independent and is more resistant to anti-androgen therapies, such as abiraterone and enzalutamide (Antonarakis et al. 2014). The *ARv567es* variant codes for an AR isoform that is constitutively active, androgen-independent, and reduces sensitivity of PCa cells to taxanes, such as docetaxel (Zhang et al. 2015). In addition, ARv567es has increased expression in bone metastases in metastatic castration resistant PCa (mCRPC) (Hörnberg et al. 2011).

Fibroblast growth factor receptor (FGFR) signaling is of clinical importance in PCa, especially aggressive PCa. Inhibition of FGFR signaling by AZ8010, a pan-FGFR inhibitor, in PCa cell lines and xenografts in mouse models inhibits ERK signaling,

invasion, proliferation, and tumor growth (Feng et al. 2012). Additionally, combination treatment of FGFR and AKT inhibitors reduces cell proliferation and invasion, decreases angiogenesis *in vivo*, and decreases STAT3 activation (Feng et al. 2016). AR-inhibition has been suggested to shift PCa to a subtype of CRPC known as the AR-independent, neuroendocrine PCa (NEPC) negative phenotype. AR-dependence is bypassed in PCa cell lines and patient specimens by elevating FGFR autocrine signaling and FGFR/MAPK pathway activity (Bluemn et al. 2017).

The individual roles of FGFR1, FGFR2, FGFR3, and various FGFR isoforms encoded by AS variants in PCa development, progression, and/or disparities is currently poorly understood. Increased expression of *FGFR1* has been connected with poorly differentiated PCa (Kwabi-Addo, Ozen, and Ittmann 2004). Splice switching of the third Ig-like domain of *FGFR2* from IIIb to IIIc variants occurs as PCa progresses. The FGFR2IIIb isoform is exclusively expressed in normal prostate epithelium, while FGFR2IIIc is predominantly expressed in PCa (Kwabi-Addo et al. 2001). *FGFR3* is expressed in both normal and cancerous prostate tissue (Feng et al. 2016; Kwabi-Addo et al. 2001). Previously, *FGFR3* mutations have been linked to low-grade PCa. Exons 7, 10, and 15 of *FGFR3* have revealed polymorphisms (F386L), missense mutations (S249C, F384L, F386L, A393E), and frameshift mutations in low-risk or low-grade PCa (Hernández et al. 2009; Lo Iacono et al. 2016; Pilié et al. 2017). Other studies, however, have found no *FGFR3* mutations in PCa specimens when analyzing these hotspot mutation sites (Koufou et al. 2010; Zuiverloon et al. 2011).

In chapter 3 we cloned and confirmed the loss of exon 14 in the *FGFR3-S* variant (**Figure 9**). This is the first confirmed example of an AS event in the intracellular kinase

domain of *FGFR3.* Three other splice events within *FGFR3* have been previously identified, all of which take place within the Ig-like domains: IIIb (inclusion of exon 8, exclusion of exon 9), IIIc (inclusion of exon 9, exclusion of exon 8), and Δ7-9 variant (skipping of exons 7-9) (Avivi, Yayon, and Givol 1993; Li et al. 2016). Exon 14 of *FGFR3* encodes the activation loop (A-loop), a 41 amino acid dynamic loop that, in the inactive conformation, covers the substrate binding pocket of the C-terminal intracellular kinase domain (Bunney et al. 2015) (**Figure 11**). The A-loop contains two key Tyr residues (Tyr 647, Tyr648) that, when phosphorylated: 1) disengage the kinase domain's molecular brake and help stabilize the kinase in the active state; 2) upregulate kinase activity; and 3) expose a docking site for downstream signaling proteins.

Activating mutations in the A-loop, such as K650E, can generate constitutive FGFR3 signaling by stabilizing the A-loop in the active state, even in the absence of phosphorylation of the two key tyrosine residues (Byron et al. 2013; Huang et al. 2013; Karp, Sparks, and Cowburn 2017; Patani et al. 2016; Webster and Donoghue 1996). FGFR3 dimers, stabilized by transmembrane and intracellular interactions, have been shown to exist in the absence of ligand, as per the pre-formed RTK model (Sarabipour and Hristova 2016). *FGFR3* mutations can trap the receptor in a closely packed dimer structure, which stabilize and increase receptor signaling even in the absence of agonist binding. Our *in vitro* and *in vivo* results in chapter 4 demonstrate that the in-frame loss of the A-loop (including Tyr647 and Tyr648) generates an FGFR3 isoform with increased oncogenic activity, measured by cell proliferation (**Figure 18A**), migration (**Figure 19A**), caspase 3/7 activity (**Figure 21A**), downstream signaling (**Figure 23**) and tumor growth (**Figure 27**). Increased time in the active state has also been shown to decrease the

efficacy of small molecule inhibitors (SMIs), including dovitinib, that preferentially bind the inactive form of FGFRs (Bunney et al. 2015; Patani et al. 2016). FGFR3-S-overexpressing cells showed significant resistance to dovitinib-mediated inhibition of proliferation (**Figure 18B-C**), migration (**Figure 19B-C**), invasion (**Figure 20B-C**), downstream signaling (**Figure 23**), and tumor growth (**Figure 27B-C**). Based on these results, we hypothesize that FGFR3-S "samples" the active conformation more frequently than FGFR3-L, and, as a result, dovitinib has a lower affinity for FGFR3-S. This would explain the decreased sensitivity of the short isoform to dovitinib treatment compared to the long isoform.

We attempted a cell-free kinase assay to evaluate the activity of recombinant intracellular domains of both FGFR3-L and FGFR3-S (e.g. intracellular domain containing the tyrosine kinase domains minus the ligand binding and transmembrane domains) (**Figure 25**). We postulate that the apparent lack of enzymatic activity of the intracellular domain of FGFR3-S in this assay may be due to the use of only the intracellular portion and not the full-length RTK. Other studies investigating FGFR3 tyrosine kinase activity utilized the full-length receptor in membrane-derived lipid particles (Sarabipour and Hristova 2016). This allows conformational changes and interactions between the extracellular, transmembrane, and intracellular kinase domains to occur. The orientation of the entire kinase, including transmembrane separation, conformational changes, and monomer versus dimer status, play a role in receptor phosphorylation, activation, and signaling. Future studies into the mechanism of FGFR3-S activity will need to investigate dimer structures, receptor orientation, and conformation sampling using the full-length receptor and fluorescence resonance

energy transfer (FRET) techniques (e.g. quantitative imaging-FRET (QI-FRET)).

Dovitinib is a multi-target RTK SMI that has shown modest anti-tumor activity in preclinical and clinical models of solid tumors, including PCa (Choi et al. 2018; Pecqueux et al. 2018; Wan et al. 2014; Yadav et al. 2017). Studies evaluating dovitinib as a therapeutic option for CRPC and bone metastases have highlighted FGFR signaling as a mediator in stromal-epithelial cell interactions in the bone microenvironment (Wan et al. 2014). Dovitinib treatment appears to inhibit the FGFR paracrine loop between PCa cells and osteoblasts and has moderate inhibitory effects on bone metastases and skeletal pain in patient studies (Choi et al. 2018). While dovitinib failed a critical Phase III trial in metastatic renal cell carcinoma, recent efforts have been taken to identify and select potential responders (e.g. patients with driver FGFR alterations) in future clinical trials ("MPI – Oncology Venture exercises option to inlicense Dovitinib a Phase 3 Multi Tyrosine Kinase Inhibitor" 2018). This work suggests dAS of *FGFR3* may also need to be taken into account when selecting potential responders for clinical trials. Going forward, *FGFR* molecular profiling for mutations and/or splice variants will be crucial in identifying whether FGFR inhibitors will be an effective therapeutic choice (Patani et al. 2016; Porta et al. 2017).

Treatment with dovitinib has been shown to cause differentiation of PCa cells to a neuroendocrine (NE) phenotype (Yadav et al. 2017). NE cells are located within the prostate in small numbers and support the growth and development of normal and cancerous prostate tissue (Abrahamsson 1999). The population of NE cells has been known to increase in number post treatment and is associated with increased aggressiveness, drug resistance, and poor patient survival (Terry et al. 2013; Wang et al.

2014). Of interest would be future experiments to explore if FGFR3-S-overexpressing cells model a NE phenotype to promote aggressiveness. Expression analysis of markers that correlate with NEPC, including chromogranin A (CHGA), neuron-specific enolase 2 (NSE), neural cell adhesion molecule 1 (NCAM), synaptophysin (SYP), and the SF serine/arginine repetitive matrix 4 (SRRM4), by mRNA profiling, immunocytochemistry (ICC), or fluorescence- activated cell sorting (FACS) would be instructive in characterizing FGFR3-S-expressing PCa cells (Li et al. 2019).

In chapter 4 we examined FGFR3 signaling via signal transduction through PI3K/AKT and STAT3 pathways at baseline and with dovitinib inhibition. FGFR3-S-overexpressing cells showed increased activation of FGFR3, AKT, STAT3, and S6 compared to FGFR3-L-expressing cells (**Figure 23**). Dovitinib treatment resulted in decreased phosphorylation of these molecules in FGFR3+L cells compared to vehicle treated cells (**Figure 23**). The phosphorylation status of FGFR3 and downstream signaling molecules was comparable in FGFR3+S cells after vehicle and dovitinib treatment (**Figure 23**). In future studies, investigation of other known FGFR3-linked pathways, such as the RAS/MAPK and PLCγ pathways, will be informative as to how FGFR3-S promotes PCa aggressiveness. There are conflicting reports regarding what pathways are initiated by active and constitutively active FGFR3 (Agazie et al. 2003; Fafilek et al. 2018; Hart, Robertson, and Donoghue 2001; Li et al. 1999; Salazar et al. 2014). Elucidating which pathways are and are not directly activated by FGFR3-S will be beneficial in identifying more effective therapeutics for AA PCa. The efficacy of other FGFR inhibitors (e.g. FGFR-specific SMI, mAbs, etc.), as well as the effect of agonist binding (e.g. FGF2 or FGF8 to emulate autocrine signaling) will provide further insights.

DNA methylation, post-translation modifications of histones (e.g. methylation, acetylation, phosphorylation, and ubiquitination), and miRNAs are the major regulators of gene expression at the epigenetic and post-transcriptional levels. Changes in epigenetic patterns can influence the expression of tumor suppressor genes and oncogenes by altering the structure and accessibility of DNA, especially in promoter regions. There is evidence that epigenetic changes appear earlier and more consistently during cancer progression than genetic/mutational changes (Reis, Vargas, and Lemos 2016). In general, cancer cells, including PCa, trend towards overall hypomethylation within genes (lack of methylation leading to increased gene expression) but have increased methylation (hypermethylation) at CpG islands (Biswas and Rao 2017; Nowacka-Zawisza and Wiśnik 2017). However, any aberration in epigenetics can lead to oncogenesis. As a result, drugs inhibiting members of the epigenetic pathway (e.g. DNA methyltransferase, histone acetyltransferase, histone deacetylase) are promising cancer therapeutics (Biswas and Rao 2017).

Studies have shown that DNA methylation status differs between African American (AA) and European American (EA) PCa. AA PCa specimens have significantly increased DNA methylation, including of promoter regions, compared to EA PCa (Kwabi-Addo et al. 2010; Devaney et al. 2015). Further investigation into the methylation status of *FGFR3* and genes related to splicing (e.g. splicing factor (SF) genes, SF kinase genes) in normal and cancerous prostate tissues in different racial groups is warranted. Similarly, a firm understanding of epigenetic regulation of histones and miRNAs in PCa and PCa disparities is lacking. Research into these race-related differences in epigenetics and response to epigenetic drugs will be important for PCa

health disparities.

While studies focusing on PCa disparities have increased over the past 10 years, the RNA splicing landscape has not been fully characterized as a potential mechanism for race-related PCa aggressiveness. Recently, expression of the RNA binding protein *HNRNPH1* was found to correlate with AR expression and disease progression (Yang et al. 2016). This correlation was significant in AA, but not EA, PCa patients. *HNRNPH1* expression was determined to be regulated by the tumor suppressor miR-122 and dihydrotestosterone (DHT). HnRNPH1 complexes with AR and NCoA-2 to upregulate AR expression in a hormone-dependent and -independent manner, suggesting a role for the ligand-independent AR splice isoform, ARv7. Another study investigated the effect of treating *TP53* wildtype AA cells (MDA PCa 2b and RC77T) with IL-6 (Teslow et al. 2018). Treatment with IL-6 downregulated expression of *TP53* and induced expression of a splice variant of *MBD2*. The MBD2_v2 isoform lacks the NuRD-recruiting coiled-coil domain and the intrinsically disordered region (IDR), both of which are crucial for binding to methylated DNA. Finally, our laboratory has identified a splice variant of *PIK3CD* that is expressed more prominently in AA (Wang et al. 2017). This splice isoform of p110δ was missing 56 amino acids located in the catalytic domain and has increased proliferation, invasion, and resistance to the SMI idelalisib.

We confirmed differential expression of SFs between AA and EA PCa in chapter 5. Seven SFs have increased expression in AA PCa compared to EA PCa patient specimens and cell lines (**Figure 28, Figure 29, Figure 30**), two of which we identified as being directly involved in exon 14 skipping (**Figure 32**). Knockdown of *SRSF2* and *HNRNPF* significantly decreased invasion and proliferation and increased caspase 3/7

activity in AA PCa cell lines (**Figure 33**). Overexpression of FGFR3-S in AA cell lines restored the phenotypic aggressiveness of AA PCa cell lines after siRNA-mediated knockdown of these SFs (**Figure 35, Figure 36, Figure 37**). Future studies will aim to map the exact binding sites of SRSF2 and hnRNPF to the RNA regions flanking exon 14.

The majority of studies on FGFR signaling in PCa have focused on FGFR1 (Kwabi-Addo et al., 2004; Wan et al., 2014a; Wang et al., 2018; Yang et al., 2013). *FGFR3*, like *FGFR1*, undergoes nearly identical alternative splicing (AS) in the extracellular Ig-like domain. Interestingly, although *FGFR1* and *FGFR3* have almost identical exon 14 sequences, the intronic sequences flanking exon 14 vary dramatically between these two receptor subtypes (**Figure 40**). It is within these intronic sequences that regulation of AS, such as SF binding sites, occurs. Thus, the AS of exon 14 in *FGFR1* and *FGFR3* may be very different. Investigating AS of other members of the FGFR family, especially in other patient subgroups, would be informative.

Figure 40 Comparison of FGFR exon 14 sequences

A

```
FGFR1_ex14      TGCATACACCGAGACCTGGCAGCCAGGAATGTCCTGGTGACAGAGGACAATGTGATGAAGAT
FGFR2_ex14      TGTATTCATCGAGATTTAGCAGCCAGAAATGTTTTGGTAACAGAAAACAATGTGATGAAAAT
FGFR3_ex14      TGCATCCACAGGGACCTGGCTGCCCGCAATGTGCTGGTGACCGAGGACAACGTGATGAAGAT
FGFR4_ex14      TGTATCCACCGGGACCTGGCTGCCCGCAATGTGCTGGTGACTGAGGACAATGTGATGAAGAT
                ** ** **  * **  * ** *** * *****  **** ** **  **** ******** **

FGFR1_ex14      AGCAGACTTTGGCCTCGCACGGGACATTCACCACATCGACTACTATAAAAAGACAACCAAC
FGFR2_ex14      AGCAGACTTTGGACTCGCCAGAGATATCAACAATATAGACTATTACAAAAAGACCACCAAT
FGFR3_ex14      CGCAGACTTCGGGCTGGCCCGGGACGTGCACAACCTCGACTACTACAAGAAGACGACCAAC
FGFR4_ex14      TGCTGACTTTGGGCTGGCCCGCGGCGTCCACCACATTGACTACTATAAGAAAACCAGCAAC
                 ** ***** ** ** **  * *   *  ** *  * ***** ** ** ** ** * ***
```

B

```
FGFR1_AL      CIHRDLAARNVLVTEDNVMKIADFGLARDIHHIDYYKKTTN
FGFR2_AL      CIHRDLAARNVLVTENNVMKIADFGLARDINNIDYYKKTTN
FGFR3_AL      CIHRDLAARNVLVTEDNVMKIADFGLARDVHNLDYYKKTTN
FGFR4_AL      CIHRDLAARNVLVTEDNVMKIADFGLARGVHHIDYYKKTSN
                           :           .::::     :
```

C

	FGFR1 **(bp)**	***FGFR2*** **(bp)**	***FGFR3*** **(bp)**	***FGFR4*** **(bp)**
Exon 13	191	191	191	191
Intron 13-14	968	8,418	110	333
Exon 14	123	123	123	123
Intron 14-15	149	566	83	107
Exon 15	71	71	71	71

A) Nucleotide sequence of exon 14 of *FGFR1*, *FGFR2*, *FGFR3*, and *FGFR4*. Codons coding for key tyrosine residues are highlighted in red. Locations where base is the same in all four receptors are denoted by "*". B) Protein sequence of activation loop (AL) coded by exon 14 of FGFR1, FGFR2, FGFR3, and FGFR4. Key tyrosine resides are highlighted in red. Locations where amino acid is different is denoted by ".:". C) Table comparing lengths of sequence space around exon 14 of *FGFR1*, *FGFR2*, *FGFR3*, and *FGFR4*.

Future studies and considerations

We have designed a construct that uses green fluorescent protein (GFP) as a direct readout of *FGFR3* AS. The *GFP* gene will be separated by intron 13-14, exon 14, and intron 14-15 of *FGFR3* (**Figure 41A**). If skipping of exon 14 occurs, the two halves of *GFP* will be spliced together, resulting in a functional fluorescent protein that fluoresces following excitation by light at a wavelength of 395nm. If exon 14 is not skipped, functional GFP will not be expressed. This construct can be transfected into AA and EA PCa cell lines, with predicted higher exon skipping (and thus functional GFP expression) in AA compared to EA cell lines (**Figure 41B**). Additionally, this construct can be co-transfected with a plasmid construct to overexpress *SRSF2* or *HNRNPF* in EA cell lines. Under this condition, we would hypothesize an increase in exon 14 skipping and subsequent functional GFP expression. In order to further elucidate direct binding of SRSF2 and hnRNPF to the intronic sequences flanking exon 14, we can mutate the predicted binding sites of each SF using the aforementioned GFP construct. We predict that mutating these binding sites will result in decreased SF binding, decreased skipping of exon 14, and decreased functional GFP expression.

Figure 41 FGFR3_GFP construct

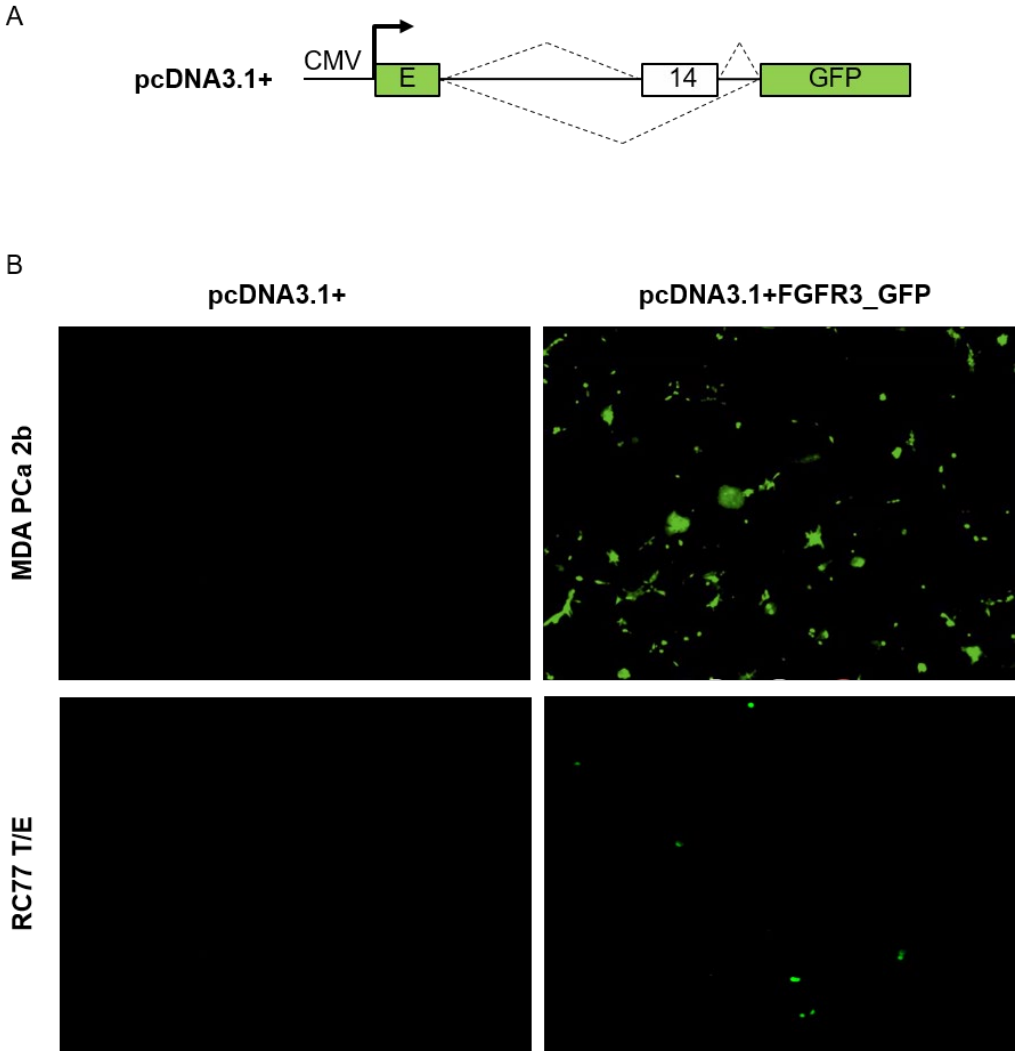

A) Schematic of FGFR3_GFP vector using the CMV promoter. B) Proof of concept transfections of AA cell lines using pcDNA3.1+ (negative control) and pcDNA3.1+FGFR3_GFP showing GFP expression (green). MDA PCa 2b cells are shown post-FACS sorting.

Our results also confirm that dysregulation of AS is a genome-wide phenomenon. "Splicing sickness" has only recently been identified as a characteristic of cancer and cancer disparities. Characterizing the global dysregulated splicing landscape of PCa in different racial/ethnic groups will play an important role in eradicating PCa health disparities. While we have identified specific SFs playing a role in dAS of *FGFR3*, other pre-mRNA targets of SRSF2 and hnNRPF and the upstream regulators of these SFs have yet to be characterized in AA PCa. In addition, other AS modulators remain unknown. For example, our gene expression array data have identified several SFs and SF regulators that are differentially expressed or differentially spliced in AA PCa (**Table 20, Table 21**). CDC-like kinase 2 (CLK2), P21 (RAC1) activated kinase 3 (PAK3), PAK7, SRSF protein kinase 1 (SRPK1), and SRPK2 are all serine-threonine kinases that phosphorylate SRSFs. PAK1 interacting protein 1 (PAK1IP1I) is negative regulator of PAK1 and DDX46, hnRNPR, hnRNPU, and SRSF6 are all RNA binding proteins. Deregulation of these upstream factors may have a direct impact on hundreds of transcripts, including *FGFR3*. Knowledge of the individual dAS variants as well as global changes in AS can provide key information in designing new targets for therapeutic interventions.

Splice-modulating drugs are already being studied as potential therapeutics in cancer (Bates et al. 2017; Gallego-Paez et al. 2017). None of these, however, have been repurposed for PCa disparities. Future experiments exploring the global response of treating AA PCa cell lines with splicing-modulators, such as antisense oligonucleotides (ASOs) and SMIs against SF or SF kinases, will be important in determining if these drugs can be an effective treatment for PCa disparities (Wang and Lee 2018).

Table 20 Differentially expressed genes in AA PCa versus AA normal prostate

Gene Name	Gene Symbol	AA tumor vs AA normal
CDC Like Kinase 2	*CLK2*	↑
DEAD-Box Helicase 46	*DDX46*	↑
PAK1 Interacting Protein 1	*PAK1IP1*	↑
P21 (RAC1) Activated Kinase 3	*PAK3*	↓
Serine and Arginine Rich Splicing Factor 6	*SRSF6*	↑

Table 21 Differentially spliced genes in AA PCa versus EA PCa

Gene Name	Gene Symbol	AA PCa vs EA PCa
Heterogeneous Nuclear Ribonucleoprotein R	*HNRNPR*	↑
Heterogeneous Nuclear Ribonucleoprotein U	*HNRNPU*	↑
P21 (RAC1) Activated Kinase 7	*PAK7*	↓
SRSF Protein Kinase 1	*SRPK1*	↑
SRSF Protein Kinase 2	*SRPK2*	↑

Concluding remarks

In conclusion, we propose a model wherein low expression of specific SFs in EA PCa results in "normal" splicing of *FGFR3*, generating the long isoform containing exon 14 (**Figure 42**). Predominant expression of the FGFR3-L isoform in EA PCa is associated with minimal oncogenic signaling and sensitivity to SMIs and cytotoxic drugs. Aberrant overexpression of SFs, specifically SRSF2 and hnRNPF, in AA PCa leads to skipping of exon 14 of *FGFR3*, generating the short isoform. Predominant expression of the FGFR3-S protein in AA PCa is associated with enhanced oncogenic signaling and increased resistance to dovitinib and docetaxel (**Figure 42**).

The FGFR signaling pathway plays an important role in cancer (and cancer health disparity) risk, development, progression, and therapeutic response. We have, for the first time, identified *FGFR3* splice status as a potential biomarker for prognostic predictions in cancer and cancer health disparities. Development of future targeted therapies and selection of treatments should take into account the predominant *FGFR3* splice variant expression. The identification of seven SFs that have increased expression in AA PCa highlights the global dysregulation of AS in cancers and PCa disparities. Future studies into PCa disparities will need to employ a genome-wide approach to identifying and treating "splicing sickness". Finally, this study highlights the importance of identifying the racial/genetic ancestry of patients, as well as the need to include minority patients in biomedical research studies in order to better understand and treat cancer health disparities.

Figure 42 Proposed mechanism for aberrant splicing of FGFR3 in PCa disparities

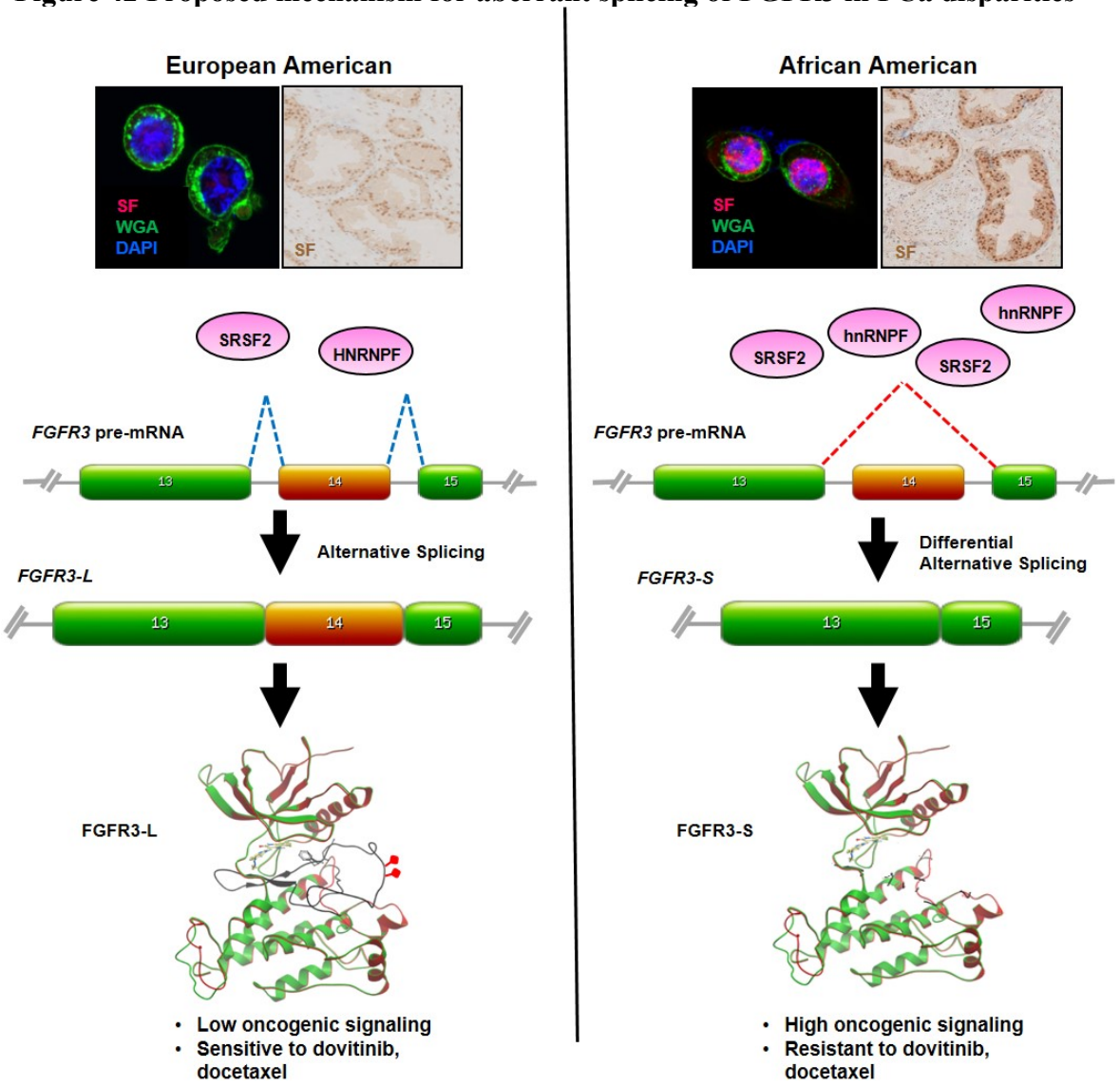

References

Abeler-Dörner, Lucie et al. 2012. "Butyrophilins: An Emerging Family of Immune Regulators." *Trends in Immunology* 33(1): 34–41.

Abrahamsson, P A. 1999. "Neuroendocrine Cells in Tumour Growth of the Prostate."

Agarwal, D et al. 2014. "FGF Receptor Genes and Breast Cancer Susceptibility: Results from the Breast Cancer Association Consortium." *British Journal of Cancer* 110(4): 1088–1100.

Agazie, Yehenew M, Nieves Movilla, Irene Ischenko, and Michael J Hayman. 2003. "The Phosphotyrosine Phosphatase SHP2 Is a Critical Mediator of Transformation Induced by the Oncogenic Fibroblast Growth Factor Receptor 3." *Oncogene* 22(44): 6909–18.

Agrawal, Anant A, Lihau Yu, Peter G Smith, and Silvia Buonamici. 2018. "Targeting Splicing Abnormalities in Cancer." *Current Opinion in Genetics & Development* 48: 67–74.

Ahmadiyeh, Nasim et al. 2010. "8q24 Prostate, Breast, and Colon Cancer Risk Loci Show Tissue-Specific Long-Range Interaction with MYC." *Proceedings of the National Academy of Sciences of the United States of America* 107(21): 9742–46.

Albert, Brian J et al. 2009. "Meayamycin Inhibits Pre-Messenger RNA Splicing and Exhibits Picomolar Activity against Multidrug-Resistant Cells." *Molecular Cancer Therapeutics* 8(8): 2308–18.

Alsafadi, Samar et al. 2016. "Cancer-Associated SF3B1 Mutations Affect Alternative Splicing by Promoting Alternative Branchpoint Usage." *Nature Communications* 7: 10615.

Amin, MB et al., eds. 2017. "Prostate." In *AJCC Cancer Staging Manual*, New York: Springer, 715–25.

André, Fabrice et al. 2013. "Targeting FGFR with Dovitinib (TKI258): Preclinical and Clinical Data in Breast Cancer." *Clinical Cancer Research* 19(13): 3693–3702.

Angevin, Eric et al. 2013. "Phase I Study of Dovitinib (TKI258), an Oral FGFR, VEGFR, and PDGFR Inhibitor, in Advanced or Metastatic Renal Cell Carcinoma." *Clinical Cancer Research* 19(5): 1257–68.

Antonarakis, Emmanuel S et al. 2014. "AR-V7 and Resistance to Enzalutamide and Abiraterone in Prostate Cancer." *New England Journal of Medicine* 371(11): 1028–38.

Araki, Shinsuke et al. 2015. "Inhibitors of CLK Protein Kinases Suppress Cell Growth

and Induce Apoptosis by Modulating Pre-MRNA Splicing" ed. Chunhong Yan. *PLOS ONE* 10(1): e0116929.

Asatiani, Ekatherine et al. 2005. "Deletion, Methylation, and Expression of the NKX3.1 Suppressor Gene in Primary Human Prostate Cancer." *Cancer research* 65(4): 1164–73.

Ateeq, Bushra et al. 2011. "Therapeutic Targeting of SPINK1-Positive Prostate Cancer." *Science Translational Medicine* 3(72): 72ra17.

Attard, Gerhardt et al. 2016. "Prostate Cancer." *The Lancet* 387(10013): 70–82.

Augello, Michael A et al. 2013. "Convergence of Oncogenic and Hormone Receptor Pathways Promotes Metastatic Phenotypes." *The Journal of Clinical Investigation* 123(1): 493–508.

Avivi, A, A Yayon, and D Givol. 1993. "A Novel Form of FGF Receptor-3 Using an Alternative Exon in the Immunoglobulin Domain III." *FEBS letters* 330(3): 249–52.

Babina, Irina S, and Nicholas C Turner. 2017. "Advances and Challenges in Targeting FGFR Signalling in Cancer." *Nature Reviews Cancer* 17(5): 318–32.

Baca, Sylvan C et al. 2013. "Punctuated Evolution of Prostate Cancer Genomes." *Cell* 153(3): 666–77.

Bae, Victoria L et al. 1994. "Tumorigenicity of SV40 T Antigen Immortalized Human Prostate Epithelial Cells: Association with Decreased Epidermal Growth Factor Receptor (EGFR) Expression." *International Journal of Cancer* 58(5): 721–29.

Bae, Victoria L et al.1998. "Metastatic Sublines of an SV40 Large T Antigen Immortalized Human Prostate Epithelial Cell Line." *The Prostate* 34(4): 275–82.

Baralle, Francisco E, and Jimena Giudice. 2017. "Alternative Splicing as a Regulator of Development and Tissue Identity." *Nature Reviews Molecular Cell Biology* 18(7): 437–51.

Barbieri, Christopher E et al. 2012. "Exome Sequencing Identifies Recurrent SPOP, FOXA1 and MED12 Mutations in Prostate Cancer." *Nature Genetics* 44(6): 685–89.

Barbieri, Christopher E et al. 2013. "The Mutational Landscape of Prostate Cancer." *European Urology* 64(4): 567–76.

Barbieri, Christopher E et al. 2017. "The Emergence of Precision Urologic Oncology: A Collaborative Review on Biomarker-Driven Therapeutics." *European Urology* 71(2): 237–46.

Barbieri, Christopher E, and Scott A Tomlins. 2015. "The Prostate Cancer Genome: Perspectives and Potential." *Urologic Oncology: Seminars and Original*

Investigations 33(2): 95–102.

Bates, David O, Jonathan C Morris, Sebastian Oltean, and Lucy F Donaldson. 2017. "Pharmacology of Modulators of Alternative Splicing." *Pharmacological Reviews* 69(1): 63–79.

Beltran, Himisha et al. 2011. "Molecular Characterization of Neuroendocrine Prostate Cancer and Identification of New Drug Targets." *Cancer Discovery* 1(6): 487–95.

Berger, Raanan et al. 2006. "Androgen-Dependent Regulation of Her-2/Neu in Prostate Cancer Cells." *Cancer Research* 66(11): 5723–28.

Biswas, Subhankar, and C. Mallikarjuna Rao. 2017. "Epigenetics in Cancer: Fundamentals and Beyond." *Pharmacology & Therapeutics* 173: 118–34.

Bluemn, Eric G et al. 2017. "Androgen Receptor Pathway-Independent Prostate Cancer Is Sustained through FGF Signaling." *Cancer Cell* 32(4): 474–489.e6.

van Bokhoven, Adrie et al. 2003. "Molecular Characterization of Human Prostate Carcinoma Cell Lines." *The Prostate* 57(3): 205–25.

Bonaventure, J et al. 1996. "Common Mutations in the Fibroblast Growth Factor Receptor 3 (FGFR3) Gene Account for Achondroplasia, Hypochondroplasia, and Thanatophoric Dwarfism." *American Journal of Medical Genetics* 63(1): 148–54.

Brawley, Otis W. 2012. "Prostate Cancer Epidemiology in the United States." *World Journal of Urology* 30(2): 195–200.

Bunney, Tom D et al. 2015. "The Effect of Mutations on Drug Sensitivity and Kinase Activity of Fibroblast Growth Factor Receptors: A Combined Experimental and Theoretical Study." *EBioMedicine* 2(3): 194–204.

Busà, R et al. 2007. "The RNA-Binding Protein Sam68 Contributes to Proliferation and Survival of Human Prostate Cancer Cells." *Oncogene* 26(30): 4372–82.

Byron, Sara A et al. 2013. "The N550K/H Mutations in FGFR2 Confer Differential Resistance to PD173074, Dovitinib, and Ponatinib ATP-Competitive Inhibitors." *Neoplasia* 15(8): 975–88.

Cairns, P et al. 1997. "Frequent Inactivation of PTEN/MMAC1 in Primary Prostate Cancer." *Cancer Research* 57(22): 4997–5000.

Cao, Bo et al. 2014. "Androgen Receptor Splice Variants Activating the Full-Length Receptor in Mediating Resistance to Androgen-Directed Therapy." *Oncotarget* 5(6): 1646–56.

Cappellen, David et al. 1999. "Frequent Activating Mutations of FGFR3 in Human Bladder and Cervix Carcinomas." *Nature Genetics* 23(1): 18–20.

Carstens, RP et al. 1997. “Alternative Splicing of Fibroblast Growth Factor Receptor 2 (FGF-R2) in Human Prostate Cancer.” *Oncogene* 15(25): 3059–65.

Cerami, Ethan et al. 2012. “The CBio Cancer Genomics Portal: An Open Platform for Exploring Multidimensional Cancer Genomics Data: Figure 1.” *Cancer Discovery* 2(5): 401–4.

Chae, Young Kwang et al. 2017. “Inhibition of the Fibroblast Growth Factor Receptor (FGFR) Pathway: The Current Landscape and Barriers to Clinical Application.” *Oncotarget* 8: 16052–74.

Chaudhary, Kumardeep et al. 2018. “Multi-Modal Meta-Analysis of 1494 Hepatocellular Carcinoma Samples Reveals Significant Impact of Consensus Driver Genes on Phenotypes.” *Clinical Cancer Research* 25(2): 463–72.

Chell, V et al. 2013. “Tumour Cell Responses to New Fibroblast Growth Factor Receptor Tyrosine Kinase Inhibitors and Identification of a Gatekeeper Mutation in FGFR3 as a Mechanism of Acquired Resistance.” *Oncogene* 32(25): 3059–70.

Chen, J, and WA A Weiss. 2015. “Alternative Splicing in Cancer: Implications for Biology and Therapy.” *Oncogene* 34(1): 1–14.

Chen, Muhan et al. 2011. “Identification of PHLPP1 as a Tumor Suppressor Reveals the Role of Feedback Activation in PTEN-Mutant Prostate Cancer Progression.” *Cancer Cell* 20(2): 173–86.

Cheng, Liang et al. 1998. “Evidence of Independent Origin of Multiple Tumors From Patients With Prostate Cancer.” *Journal of the National Cancer Institute* 90(3): 233–37.

Ching, Travers et al. 2016. “Pan-Cancer Analyses Reveal Long Intergenic Non-Coding RNAs Relevant to Tumor Diagnosis, Subtyping and Prognosis.” *EBioMedicine* 7: 62–72.

Ching, Travers, Xun Zhu, and Lana X. Garmire. 2018. “Cox-Nnet: An Artificial Neural Network Method for Prognosis Prediction of High-Throughput Omics Data” ed. Florian Markowetz. *PLOS Computational Biology* 14(4): e1006076.

Choi, Yoon Ji et al. 2018. “Phase II Study of Dovitinib in Patients with Castration-Resistant Prostate Cancer (KCSG-GU11-05).” *Cancer Research and Treatment* 50(4): 1252–59.

Chornokur, Ganna, Kyle Dalton, Meghan E Borysova, and Nagi B Kumar. 2011. “Disparities at Presentation, Diagnosis, Treatment, and Survival in African American Men, Affected by Prostate Cancer.” *The Prostate* 71(9): 985–97.

Climente-González, Héctor, Eduard Porta-Pardo, Adam Godzik, and Eduardo Eyras. 2017. “The Functional Impact of Alternative Splicing in Cancer.” *Cell Reports*

20(9): 2215–26.

Conti, David V et al. 2017. “Two Novel Susceptibility Loci for Prostate Cancer in Men of African Ancestry.” *Journal of the National Cancer Institute* 109(8).

Convertini, Paolo et al. 2014. “Sudemycin E Influences Alternative Splicing and Changes Chromatin Modifications.” *Nucleic Acids Research* 42(8): 4947–61.

Coombs, Thomas C et al. 2010. “Identification of Selective Inhibitors of Cdc2-like Kinases 1 and 4 (Clk1, Clk4).” In *Probe Reports from the NIH Molecular Libraries Program*.

Cooperberg, Matthew R. 2013. “Re-Examining Racial Disparities in Prostate Cancer Outcomes.” *Journal of Clinical Oncology* 31(24): 2979–80.

Couture, Frédéric et al. 2017. “PACE4 Undergoes an Oncogenic Alternative Splicing Switch in Cancer.” *Cancer Research* 77(24): 6863–79.

Cronin, Kathleen A, Andrew J Lake, Susan Scott, et al. 2018. “Annual Report to the Nations on the Status of Cancer, part I: National Cancer Statistics.” *Cancer* 124(13): 2785-2800.

David, Charles J, and James L Manley. 2010. “Alternative Pre-MRNA Splicing Regulation in Cancer: Pathways and Programs Unhinged.” *Genes & Development* 24(21): 2343–64.

Debdab, Mansour et al. 2011. “Leucettines, a Class of Potent Inhibitors of Cdc2-like Kinases and Dual Specificity, Tyrosine Phosphorylation Regulated Kinases Derived from the Marine Sponge Leucettamine B: Modulation of Alternative Pre-RNA Splicing.” *Journal of Medicinal Chemistry* 54(12): 4172–86.

DeSantis, Carol E et al. 2016. “Cancer Statistics for African Americans, 2016: Progress and Opportunities in Reducing Racial Disparities.” *CA: A Cancer Journal for Clinicians* 66(4): 290–308.

Devaney, JM et al. 2015. “Genome-Wide Differentially Methylated Genes in Prostate Cancer Tissues from African-American and Caucasian Men.” *Epigenetics* 10(4): 319–28.

Donovan, Michael J, and Carlos Cordon-Cardo. 2013. “Predicting High-Risk Disease Using Tissue Biomarkers.” *Current Opinion in Urology* 23(3): 245–51.

Dudka, Anna A, Steve M M Sweet, and John K Heath. 2010. “Signal Transducers and Activators of Transcription-3 Binding to the Fibroblast Growth Factor Receptor Is Activated by Receptor Amplification.” *Cancer Research* 70(8): 3391–3401.

Dvinge, Heidi, and Robert K Bradley. 2015. “Widespread Intron Retention Diversifies Most Cancer Transcriptomes.” *Genome Medicine* 7(1): 45.

Dvinge, Heidi, Eunhee Kim, Omar Abdel-Wahab, and Robert K Bradley. 2016. "RNA Splicing Factors as Oncoproteins and Tumour Suppressors." *Nature Reviews Cancer* 16(7).

Effenberger, Kerstin A et al. 2015. "The Natural Product N-Palmitoyl-l-Leucine Selectively Inhibits Late Assembly of Human Spliceosomes." *The Journal of Biological Chemistry* 290(46): 27524–31.

Escudier, Bernard et al. 2014. "Phase II Results of Dovitinib (TKI258) in Patients with Metastatic Renal Cell Cancer." *Clinical Cancer Research* 20(11): 3012–22.

Eskens, Ferry ALM et al. 2013. "Phase I Pharmacokinetic and Pharmacodynamic Study of the First-in-Class Spliceosome Inhibitor E7107 in Patients with Advanced Solid Tumors." *Clinical Cancer Research* 19(22): 6296–6304.

Evans, Simon et al. 2008. "Investigating Black-White Differences in Prostate Cancer Prognosis: A Systematic Review and Meta-Analysis." *International Journal of Cancer* 123(2): 430–35.

Fafilek, Bohumil et al. 2018. "The Inositol Phosphatase SHIP2 Enables Sustained ERK Activation Downstream of FGF Receptors by Recruiting Src Kinases." *Science Signaling* 11(548): eaap8608.

Feng, Shu et al. 2012. "Targeting Fibroblast Growth Factor Receptor Signaling Inhibits Prostate Cancer Progression." *Clincal Cancer Research*: OF1-9.

Feng, Shu et al. 2016. "Combination Treatment of Prostate Cancer with FGF Receptor and AKT Kinase Inhibitors." *Oncotarget* 8(4): 6179–92.

Finci, Lorenzo I et al. 2018. "The Cryo-EM Structure of the SF3b Spliceosome Complex Bound to a Splicing Modulator Reveals a Pre-MRNA Substrate Competitive Mechanism of Action." *Genes & Development* 32(3–4): 309–20.

Fischbach, Anna et al. 2015. "Fibroblast Growth Factor Receptor (FGFR) Gene Amplifications Are Rare Events in Bladder Cancer." *Histopathology* 66(5): 639–49.

Fitzgerald, Liesel M et al. 2013. "Germline Missense Variants in the BTNL2 Gene Are Associated with Prostate Cancer Susceptibility." *Cancer Epidemiology, Biomarkers & Prevention* 22(9): 1520–28.

Fitzmaurice, Christina et al. 2017. "Global, Regional, and National Cancer Incidence, Mortality, Years of Life Lost, Years Lived With Disability, and Disability-Adjusted Life-Years for 32 Cancer Groups, 1990 to 2015." *JAMA Oncology* 3(4): 524–48.

Foldynova-Trantirkova, Silvie, William R Wilcox, and Pavel Krejci. 2012. "Sixteen Years and Counting: The Current Understanding of Fibroblast Growth Factor Receptor 3 (FGFR3) Signaling in Skeletal Dysplasias." *Human Mutation* 33(1): 29–41.

Fong, Eliza L S et al. 2016. "A 3D in Vitro Model of Patient-Derived Prostate Cancer

Xenograft for Controlled Interrogation of in Vivo Tumor-Stromal Interactions." *Biomaterials* 77: 164–72.

Freedman, Matthew L et al. 2011. "Principles for the Post-GWAS Functional Characterization of Cancer Risk Loci." *Nature Genetics* 43(6): 513–18.

Fu, Xiang Dong, and Manuel Ares. 2014. "Context-Dependent Control of Alternative Splicing by RNA-Binding Proteins." *Nature Reviews Genetics* 15(10): 689–701.

Furdui, Cristina M, Erin D Lew, Joseph Schlessinger, and Karen S Anderson. 2006. "Autophosphorylation of FGFR1 Kinase Is Mediated by a Sequential and Precisely Ordered Reaction." *Molecular Cell* 21(5): 711–17.

Gallego-Paez, LM et al. 2017. "Alternative Splicing: The Pledge, the Turn, and the Prestige: The Key Role of Alternative Splicing in Human Biological Systems." *Human Genetics* 136(9): 1015–42.

Gammons, M V et al. 2014. "Targeting SRPK1 to Control VEGF-Mediated Tumour Angiogenesis in Metastatic Melanoma." *British Journal of Cancer* 111(3): 477–85.

Gan, Yu et al. 2018. "Roles of Alternative RNA Splicing of the Bif-1 Gene by SRRM4 During the Development of Treatment-Induced Neuroendocrine Prostate Cancer." *EBioMedicine* 31: 267–75.

Gao, Jianjiong et al. 2013. "Integrative Analysis of Complex Cancer Genomics and Clinical Profiles Using the CBioPortal." *Science Signaling* 6(269): pl1.

Ghigna, Claudia et al. 2010. "Pro-Metastatic Splicing of Ron Proto-Oncogene MRNA Can Be Reversed: Therapeutic Potential of Bifunctional Oligonucleotides and Indole Derivatives." *RNA biology* 7(4): 495–503.

Giulietti, Matteo et al. 2013. "SpliceAid-F: A Database of Human Splicing Factors and Their RNA-Binding Sites." *Nucleic Acids Research* 41(Database issue): D125-31.

Gnanapragasam, V J et al. 2003. "FGF8 Isoform b Expression in Human Prostate Cancer." *British Journal of Cancer* 88(9): 1432–38.

Goehe, Rachel Wilson et al. 2010. "HnRNP L Regulates the Tumorigenic Capacity of Lung Cancer Xenografts in Mice via Caspase-9 Pre-MRNA Processing." *Journal of Clinical Investigation* 120(11): 3923–39.

Golan-Gerstl, R et al. 2011. "Splicing Factor HnRNP A2/B1 Regulates Tumor Suppressor Gene Splicing and Is an Oncogenic Driver in Glioblastoma." *Cancer Research* 71(13): 4464–72.

Gonçalves, Vânia, Joana FS Pereira, and Peter Jordan. 2017. "Signaling Pathways Driving Aberrant Splicing in Cancer Cells." *Genes* 9(1): 9.

Gust, Kilian M et al. 2013. "Fibroblast Growth Factor Receptor 3 Is a Rational Therapeutic Target in Bladder Cancer." *Molecular Cancer Therapeutics* 12(7):

1245–54.

Haiman, Christopher A et al. 2007. “Multiple Regions within 8q24 Independently Affect Risk for Prostate Cancer.” *Nature Genetics* 39(5): 638–44.

Haiman, Christopher A et al. 2011. “Genome-Wide Association Study of Prostate Cancer in Men of African Ancestry Identifies a Susceptibility Locus at 17q21.” *Nature Genetics* 43(6): 570–73.

Hallinan, Niamh et al. 2016. “Anti-Tumour Treatment Targeting the Fibroblast Growth Factor Receptor Family in Cancer.” *Cancer Treatment Reviews* 46: 51–62.

Han, Ting et al. 2017. “Anticancer Sulfonamides Target Splicing by Inducing RBM39 Degradation via Recruitment to DCAF15.” *Science* 356(6336): eaal3755.

Han, Ying et al. 2016. “Prostate Cancer Susceptibility in Men of African Ancestry at 8q24.” *Journal of the National Cancer Institute* 108(7): djv431.

Hanahan, Douglas, and Robert A Weinberg. 2000. “The Hallmarks of Cancer.” *Cell* 100(1): 57–70.

Hanahan, Douglas, and Robert A Weinberg. 2011. “Hallmarks of Cancer: The next Generation.” *Cell* 144(5): 646–74.

Hardiman, Gary et al. 2016. “Systems Analysis of the Prostate Transcriptome in African–American Men Compared with European–American Men.” *Pharmacogenomics* 17(10): 1129–43.

Hart, Kristen C, Scott C Robertson, and Daniel J Donoghue. 2001. “Identification of Tyrosine Residues in Constitutively Activated Fibroblast Growth Factor Receptor 3 Involved in Mitogenesis, Stat Activation, and Phosphatidylinositol 3-Kinase Activation.” 12(4): 931–42.

Helsten, T. et al. 2016. “The FGFR Landscape in Cancer: Analysis of 4,853 Tumors by Next-Generation Sequencing.” *Clinical Cancer Research* 22(1): 259–67.

Hensel, Janine, and George N Thalmann. 2016. “Biology of Bone Metastases in Prostate Cancer.” *Urology* 92: 6–13.

Hernández, Silvia et al. 2009. “FGFR3 Mutations in Prostate Cancer: Association with Low-Grade Tumors.” *Modern Pathology* 22(6): 848–56.

Herrera-Abreu, Maria Teresa et al. 2013. “Parallel RNA Interference Screens Identify EGFR Activation as an Escape Mechanism in FGFR3-Mutant Cancer.” *Cancer Discovery* 3(9): 1058–71.

Hong, David et al. 2015. “AZD9150, a next-Generation Antisense Oligonucleotide Inhibitor of *STAT3* with Early Evidence of Clinical Activity in Lymphoma and Lung Cancer.” *Science Translational Medicine* 7(314): 314ra185-314ra185.

Hong, DS et al. 2014. “A Phase I, Open-Label, Single-Arm, Dose-Escalation Study of E7107, a Precursor Messenger Ribonucleic Acid (Pre-MRNA) Splicesome Inhibitor Administered Intravenously on Days 1 and 8 Every 21 Days to Patients with Solid Tumors.” *Investigational New Drugs* 32(3): 436–44.

Hoon Lee, Sang et al. 2005. “In Vivo Target Modulation and Biological Activity of CHIR-258, a Multitargeted Growth Factor Receptor Kinase Inhibitor, in Colon Cancer Models.” *Clinical Cancer Research* 11(10): 3633–41.

Hörnberg, Emma et al. 2011. “Expression of Androgen Receptor Splice Variants in Prostate Cancer Bone Metastases Is Associated with Castration-Resistance and Short Survival” ed. Paul Dent. *PLoS ONE* 6(4): e19059.

Horoszewicz, J S et al. 1983. “LNCaP Model of Human Prostatic Carcinoma.” *Cancer Research* 43(4): 1809–18.

Hsu, Tiffany Y-T et al. 2015. “The Spliceosome Is a Therapeutic Vulnerability in MYC-Driven Cancer.” *Nature* 525(7569): 384–88.

Hu, Zhiyuan, Christopher Yau, and Ahmed Ashour Ahmed. 2017. “A Pan-Cancer Genome-Wide Analysis Reveals Tumour Dependencies by Induction of Nonsense-Mediated Decay.” *Nature Communications* 8: 15943.

Huang, S et al. 2012. “Recurrent Deletion of CHD1 in Prostate Cancer with Relevance to Cell Invasiveness.” *Oncogene* 31(37): 4164–70.

Huang, Sijia et al. 2014. “A Novel Model to Combine Clinical and Pathway-Based Transcriptomic Information for the Prognosis Prediction of Breast Cancer” ed. Andrey Rzhetsky. *PLoS Computational Biology* 10(9): e1003851.

Huang, Zhifeng et al. 2013. “Structural Mimicry of A-Loop Tyrosine Phosphorylation by a Pathogenic FGF Receptor 3 Mutation Zhifeng.” *Structure* 21(10): 1889–96.

Huelga, Stephanie C et al. 2012. “Integrative Genome-Wide Analysis Reveals Cooperative Regulation of Alternative Splicing by HnRNP Proteins.” *Cell Reports* 1(2): 167–78.

Lo Iacono, Marco et al. 2016. “Retrospective Study Testing next Generation Sequencing of Selected Cancer-Associated Genes in Resected Prostate Cancer.” *Oncotarget* 7(12): 14394–404.

Imielinski, Marcin et al. 2012. “Mapping the Hallmarks of Lung Adenocarcinoma with Massively Parallel Sequencing.” *Cell* 150(6): 1107–20.

Jiang, Yuqiu et al. 2010. “Detection of Androgen Receptor Mutations in Circulating Tumor Cells in Castration-Resistant Prostate Cancer.” *Clinical Chemistry* 56(9): 1492–95.

Jue, Joshua Stephen et al. 2017. “Re-Examining PSA Density: Defining the Optimal PSA

Range and Patients for Using PSA Density to Predict Prostate Cancer Using Extended Template Biopsy." *Urology* 105: 123–28.

Jung, Hyunchul et al. 2015. "Intron Retention Is a Widespread Mechanism of Tumor-Suppressor Inactivation." *Nature Genetics* 47(11): 1242–48.

Kaida, Daisuke et al. 2007. "Spliceostatin A Targets SF3b and Inhibits Both Splicing and Nuclear Retention of Pre-MRNA." *Nature Chemical bBology* 3(9): 576–83.

Kaighn, M E et al. 1979. "Establishment and Characterization of a Human Prostatic Carcinoma Cell Line (PC-3)." *Investigative Urology* 17(1): 16–23.

Karp, Jerome M, Samuel Sparks, and David Cowburn. 2017. "Effects of FGFR2 Kinase Activation Loop Dynamics on Catalytic Activity" ed. Marc A. Marti-Renom. *PLOS Computational Biology* 13(2): e1005360.

Katoh, Masaru. 2016a. "FGFR Inhibitors: Effects on Cancer Cells, Tumor Microenvironment and Whole-Body Homeostasis (Review)." *International Journal of Molecular Medicine* 38: 3–15.

Katoh, Masaru. 2016b. "Therapeutics Targeting FGF Signaling Network in Human Diseases." *Trends in Pharmacological Sciences* 37(12): 1081–96.

Kelly, Scott P, William F Anderson, Philip S Rosenberg, and Michale B Cook. 2017. "Past, Current, and Future Incidence Rates and Burden of Metastatic Prostate Cancer in the United States." *European Urology Focus* 4(1): 121–27.

Kent, W James et al. 2002. "The Human Genome Browser at UCSC." *Genome research* 12(6): 996–1006.

Kim, Hyunsoo et al. 2011. "IsoformEx: Isoform Level Gene Expression Estimation Using Weighted Non-Negative Least Squares from MRNA-Seq Data." *BMC Bioinformatics* 12(1): 305.

Kittles, Rick A et al. 2001. "CYP17 Promoter Variant Associated with Prostate Cancer Aggressiveness in African Americans." *Cancer Epidemiology, Biomarkers & Prevention* 10: 943–47.

Ko, Chia-Chen et al. 2014. "Chemical Proteomics Identifies Heterogeneous Nuclear Ribonucleoprotein (HnRNP) A1 as the Molecular Target of Quercetin in Its Anti-Cancer Effects in PC-3 Cells." *The Journal of Biological Chemistry* 289(32): 22078–89.

Ko, Hyun-Kyung et al. 2018. "Loss of an Androgen-Inactivating and Isoform-Specific HSD17B4 Splice Form Enables Emergence of Castration-Resistant Prostate Cancer." *Cell Reports* 22(3): 809–19.

Ko, Tun Kiat et al. 2016. "The BIM Deletion Polymorphism: A Paradigm of a Permissive Interaction between Germline and Acquired TKI Resistance Factors in Chronic

Myeloid Leukemia." *Oncotarget* 7(3): 2721–33.

Konecny, Gottfried E et al. 2013. "Activity of the Fibroblast Growth Factor Receptor Inhibitors Dovitinib (TKI258) and NVP-BGJ398 in Human Endometrial Cancer Cells." *Molecular Cancer Therapeutics* 12(5): 632–42.

Kotake, Yoshihiko et al. 2007. "Splicing Factor SF3b as a Target of the Antitumor Natural Product Pladienolide." *Nature Chemical Biology* 3(9): 570–75.

Kotani, H et al. 2016. "Co-Active Receptor Tyrosine Kinases Mitigate the Effect of FGFR Inhibitors in FGFR1-Amplified Lung Cancers with Low FGFR1 Protein Expression." *Oncogene* 35(27): 3587–97.

Koufou, Stella et al. 2010. "Mutational Activation of FGFR3 Is Not Involved in the Development of Prostate Cancer." *Pathobiology* 77(5): 249–52.

Kuroso, Kazuko et al. 2010. "Immunohistochemical Detection of Fibroblast Growth Factor Receptor 3 in Human Breast Cancer: Correlation with Clinicopathological/Molecular Parameters and Prognosis." *Pathobiology* 77(5): 231–40.

Kwabi-Addo, Bernard, M Ozen, and M Ittmann. 2004. "The Role of Fibroblast Growth Factors and Their Receptors in Prostate Cancer." *Endocrine-Related Cancer* 11: 709 – 724.

Kwabi-Addo, Bernard, F Ropiquet, D Giri, and M Ittmann. 2001. "Alternative Splicing of Fibroblast Growth Factor Receptors in Human Prostate Cancer." *The Prostate* 46(2): 163–72.

Kwabi-Addo, Bernard et al. 2010. "Identification of Differentially Methylated Genes in Normal Prostate Tissues from African American and Caucasian Men." *Clinical Cancer Research* 16(14): 3539–47.

Lapuk, Anna V, Stanislav V Volik, Yuzhuo Wang, and Colin C Collins. 2014. "The Role of MRNA Splicing in Prostate Cancer." *Asian Journal of Andrology* 16(4): 515–21.

Lee, T.-S. et al. 2008. "BCR-ABL Alternative Splicing as a Common Mechanism for Imatinib Resistance: Evidence from Molecular Dynamics Simulations." *Molecular Cancer Therapeutics* 7(12): 3834–41.

Li, C et al. 1999. "A Lys644Glu Substitution in Fibroblast Growth Factor Receptor 3 (FGFR3) Causes Dwarfism in Mice by Activation of STATs and Ink4 Cell Cycle Inhibitors." *Human Molecular Genetics* 8(1): 35–44.

Li, Ke et al. 2016. "Phenotypic and Signaling Consequences of a Novel Aberrantly Spliced Transcript FGF Receptor-3 in Hepatocellular Carcinoma." *Cancer Research*

76(14): 4205–15.

Li, Yinan et al. 2019. “SRRM4 Gene Expression Correlates with Neuroendocrine Prostate Cancer.” *The Prostate* 79(1): 96–104.

Lin, Pei-Chun et al. 2013. “Epigenomic Alterations in Localized and Advanced Prostate Cancer.” *Neoplasia* 15(4): 373–83.

Lindberg, Johan, Daniel Klevebring, et al. 2013. “Exome Sequencing of Prostate Cancer Supports the Hypothesis of Independent Tumour Origins.” *European Urology* 63(2): 347–53.

Lindberg, Johan, Ian G. Mills, et al. 2013. “The Mitochondrial and Autosomal Mutation Landscapes of Prostate Cancer.” *European Urology* 63(4): 702–8.

Liu, Gang et al. 2015. “MED1 Mediates Androgen Receptor Splice Variant Induced Gene Expression in the Absence of Ligand.” *Oncotarget* 6(1): 288–304.

Liu, Jun et al. 2017. “Overcoming Imatinib Resistance Conferred by the *BIM* Deletion Polymorphism in Chronic Myeloid Leukemia with Splice-Switching Antisense Oligonucleotides.” *Oncotarget* 8(44): 77567–85.

Liu, W et al. 2012. “Identification of Novel CHD1-Associated Collaborative Alterations of Genomic Structure and Functional Assessment of CHD1 in Prostate Cancer.” *Oncogene* 31(35): 3939–48.

Liu, Wennuan et al. 2009. “Copy Number Analysis Indicates Monoclonal Origin of Lethal Metastatic Prostate Cancer.” *Nature Medicine* 15(5): 559–65.

Lopez-Beltran, Antonio et al. 2006. “Current Practice of Gleason Grading of Prostate Carcinoma.” *Virchows Archiv : an international journal of pathology* 448(2): 111–18.

Lynch, Henry T. et al. 2016. “Screening for Familial and Hereditary Prostate Cancer.” *International Journal of Cancer* 138(11): 2579–91.

Madan, Vikas et al. 2015. “Aberrant Splicing of U12-Type Introns Is the Hallmark of ZRSR2 Mutant Myelodysplastic Syndrome.” *Nature Communications* 6(1): 6042.

Magi-Galluzzi, Cristina et al. 2011. “TMPRSS2-ERG Gene Fusion Prevalence and Class Are Significantly Different in Prostate Cancer of Caucasian, African-American and Japanese Patients.” *The Prostate* 71(5): 489–97.

Maguire, Sarah L et al. 2015. “*SF3B1* Mutations Constitute a Novel Therapeutic Target in Breast Cancer.” *The Journal of Pathology* 235(4): 571–80.

Martin, Damali N, Adrienne M Starks, and Stefan Ambs. 2013. “Biological Determinants of Health Disparities in Prostate Cancer.” *Current Opinion in Oncology* 25(3): 235–

241.

Mavrou, A et al. 2015. “Serine-Arginine Protein Kinase 1 (SRPK1) Inhibition as a Potential Novel Targeted Therapeutic Strategy in Prostate Cancer.” *Oncogene* 34(33): 4311–19.

Menon, Roopika et al. 2013. “Somatic Copy Number Alterations by Whole-Exome Sequencing Implicates *YWHAZ* and *PTK2* in Castration-Resistant Prostate Cancer.” *The Journal of Pathology* 231(4): 505–16.

Mercatante, Danielle R, James L Mohler, and Ryszard Kole. 2002. “Cellular Response to an Antisense-Mediated Shift of Bcl-x Pre-MRNA Splicing and Antineoplastic Agents.” *The Journal of Biological Chemistry* 277(51): 49374–82.

Mesquita, Diana et al. 2015. “Specific and Redundant Activities of ETV1and ETV4 in Prostate Cancer Aggressiveness Revealed by Co-Overexpression Cellular Contexts.” *Oncotarget* 6(7): 5217–36.

“MPI – Oncology Venture Exercises Option to Inlicense Dovitinib a Phase 3 Multi Tyrosine Kinase Inhibitor.” 2018. *Oncology Venture*.

Muenke, M et al. 1997. “A Unique Point Mutation in the Fibroblast Growth Factor Receptor 3 Gene (FGFR3) Defines a New Craniosynostosis Syndrome.” *American Journal of Human Genetics* 60(3): 555–64.

Munkley, Jennifer et al. 2015. “The Androgen Receptor Controls Expression of the Cancer-Associated STn Antigen and Cell Adhesion through Induction of ST6GalNAc1 in Prostate Cancer.” *Oncotarget* 6(33): 34358–74.

Nadiminty, Nagalakshmi et al. 2015. “NF-KB2/P52:C-Myc:HnRNPA1 Pathway Regulates Expression of Androgen Receptor Splice Variants and Enzalutamide Sensitivity in Prostate Cancer.” *Molecular Cancer Therapeutics* 14(8): 1884–95.

Navone, N M et al. 1997. “Establishment of Two Human Prostate Cancer Cell Lines Derived from a Single Bone Metastasis.” *Clinical Cancer Research* 3(12 Pt 1): 2493–2500

Ng, King Pan et al. 2012. “A Common BIM Deletion Polymorphism Mediates Intrinsic Resistance and Inferior Responses to Tyrosine Kinase Inhibitors in Cancer.” *Nature Medicine* 18(4): 521–28.

Noone, AM et al., eds. 2018. “SEER Cancer Statistics Review, 1975-2015 - SEER Statistics.”

Nowacka-Zawisza, Maria, and Ewelina Wiśnik. 2017. “DNA Methylation and Histone Modifications as Epigenetic Regulation in Prostate Cancer.” *Oncology Reports* 38(5): 2587–96.

O'Hare, T. et al. 2011. "The BCR-ABL35INS Insertion/Truncation Mutant Is Kinase-Inactive and Does Not Contribute to Tyrosine Kinase Inhibitor Resistance in Chronic Myeloid Leukemia." *Blood* 118(19): 5250–54.

Olender, Jacqueline, and Norman H Lee. 2019. "Role of Alternative Splicing in Prostate Cancer Aggressiveness and Drug Resistance in African Americans." *Advances in Experimental Medicine and Biology*: (in press).

Olshavsky, Nicholas A et al. 2010. "Identification of ASF/SF2 as a Critical, Allele-Specific Effector of the Cyclin D1b Oncogene." *Cancer Research* 70(10): 3975–84.

Oltean, Sebastian et al. 2006. "Alternative Inclusion of Fibroblast Growth Factor Receptor 2 Exon IIIc in Dunning Prostate Tumors Reveals Unexpected Epithelial Mesenchymal Plasticity." *PNAS* 103(38): 14116–21.

Oltean, Sebastian, and David O. Bates. 2014. "Hallmarks of Alternative Splicing in Cancer." *Oncogene* 33(46): 5311–18.

Ornitz, David M, and Nobuyuki Itoh. 2015. "The Fibroblast Growth Factor Signaling Pathway." *WIREs Developmental Biology* 4(3): 215–66.

Otto, Tobias et al. 2009. "Stabilization of N-Myc Is a Critical Function of Aurora A in Human Neuroblastoma." *Cancer Cell* 15(1): 67–78.

Palanisamy, Nallasivam et al. 2010. "Rearrangements of the RAF Kinase Pathway in Prostate Cancer, Gastric Cancer and Melanoma." *Nature Medicine* 16(7): 793–98.

Pandit, Shatakshi et al. 2013. "Genome-Wide Analysis Reveals SR Protein Cooperation and Competition in Regulated Splicing." *Molecular Cell* 50(2): 223–35.

Paronetto, Maria Paola et al. 2010. "Alternative Splicing of the Cyclin D1 Proto-Oncogene Is Regulated by the RNA-Binding Protein Sam68." *Cancer Research* 70(1): 229–39.

Patani, Harshnira et al. 2016. "Landscape of Activating Cancer Mutations in FGFR Kinases and Their Differential Responses to Inhibitors in Clinical Use." *Oncotarget* 7(17): 24252–68.

Pecqueux, Carine et al. 2018. "FGF-2 Is a Driving Force for Chromosomal Instability and a Stromal Factor Associated with Adverse Clinico-Pathological Features in Prostate Cancer." *Urologic Oncology* 36(8): 365.e15-365.e26.

Pilié, Patrick G. et al. 2017. "Germline Genetic Variants in Men with Prostate Cancer and One or More Additional Cancers." *Cancer* 123(20): 3925–32.

Porta, Rut et al. 2017. "FGFR a Promising Druggable Target in Cancer: Molecular Biology and New Drugs." *Critical Reviews in Oncology/Hematology* 113: 256–67.

Poulikakos, Poulikos I. et al. 2011. "RAF Inhibitor Resistance Is Mediated by Dimerization of Aberrantly Spliced BRAF(V600E)." *Nature* 480(7377): 387–90.

Powell, Isaac J. 2007. "Epidemiology and Pathophysiology of Prostate Cancer in

Powell, Isaac J. 2013. "Genes Associated with Prostate Cancer Are Differentially Expressed in African American and European American Men." *Cancer Epidemiology, Biomarkers & Prevention* 22(5): 891–97.

Powell, Isaac J, and Aliccia Bollig-Fischer. 2013. "Minireview: The Molecular and Genomic Basis for Prostate Cancer Health Disparities." *Molecular Endocrinology* 27(6): 879–91.

"Prostate Cancer." 2019. *The American Cancer Society*. www.cancer.org/cancer/prostate-cancer.

Rajan, Prabhakar, David J Elliott, Craig N Robson, and Hing Y Leung. 2009. "Alternative Splicing and Biological Heterogeneity in Prostate Cancer." *Nature Reviews Urology* 6(8): 454–60.

Rebbeck, Timothy R. 2017a. "Prostate Cancer Disparities by Race and Ethnicity: From Nucleotide to Neighborhood." *Cold Spring Harbor Perspectives in Medicine*: a030387.

Rebbeck, Timothy R. 2017b. "Prostate Cancer Genetics: Variation by Race, Ethnicity, and Geography." *Seminars in Radiation Oncology* 27(1): 3–10.

Reis, Adriana H. O., Fernando R. Vargas, and Bernardo Lemos. 2016. "Biomarkers of Genome Instability and Cancer Epigenetics." *Tumor Biology* 37(10): 13029–38.

Rennel, E et al. 2008. "The Endogenous Anti-Angiogenic VEGF Isoform, VEGF165b Inhibits Human Tumour Growth in Mice." *British Journal of Cancer* 98(7): 1250–57.

Rhodes, David A., Walter Reith, and John Trowsdale. 2016. "Regulation of Immunity by Butyrophilins." *Annual Review of Immunology* 34(1): 151–72.

Robbins, A S, A S Whittemore, and D H Thom. 2000. "Differences in Socioeconomic Status and Survival among White and Black Men with Prostate Cancer." *American Journal of Epidemiology* 151(4): 409–16.

Robbins, Christiane M et al. 2011. "Copy Number and Targeted Mutational Analysis Reveals Novel Somatic Events in Metastatic Prostate Tumors." *Genome Research* 21(1): 47–55.

Robinson, Dan et al. 2015. "Integrative Clinical Genomics of Advanced Prostate Cancer." *Cell* 161(5): 1215–28.

Rohmann, Edyta et al. 2006. “Mutations in Different Components of FGF Signaling in LADD Syndrome.” *Nature Genetics* 38(4): 414–17.

Rose, Amy E et al. 2010. “Copy Number and Gene Expression Differences between African American and Caucasian American Prostate Cancer.” *Journal of Translational Medicine* 8(1): 70.

Rosen, Philip et al. 2012. “Clinical Potential of the ERG Oncoprotein in Prostate Cancer.” *Nature Reviews Urology* 9(3): 131–37.

Ross, Sarah J et al. 2017. “Targeting KRAS-Dependent Tumors with AZD4785, a High-Affinity Therapeutic Antisense Oligonucleotide Inhibitor of KRAS.” *Science Translational Medicine* 9(394): eaal5253.

Rossbach, Oliver et al. 2014. “Crosslinking-Immunoprecipitation (ICLIP) Analysis Reveals Global Regulatory Roles of HnRNP L.” *RNA Biology* 11(2): 146–55.

Rosty, Christophe et al. 2005. “Clinical and Biological Characteristics of Cervical Neoplasias with FGFR3 Mutation.” *Molecular Cancer* 4(1): 15.

Rubin, Mark A, and Francesca Demichelis. 2018. “The Genomics of Prostate Cancer: Emerging Understanding with Technologic Advances.” *Modern Pathology* 31(S1): S1-11.

Rubin, Mark A, Christopher A Maher, and Arul M Chinnaiyan. 2011. “Common Gene Rearrangements in Prostate Cancer.” *Journal of clinical oncology : official journal of the American Society of Clinical Oncology* 29(27): 3659–68.

Ryan, Michael et al. 2016. “TCGASpliceSeq a Compendium of Alternative MRNA Splicing in Cancer.” *Nucleic Acids Research* 44(D1): D1018-22.

Sahadevan, K et al. 2007. “Selective Over-Expression of Fibroblast Growth Factor Receptors 1 and 4 in Clinical Prostate Cancer.” *The Journal of Pathology* 213(1): 82–90.

Salazar, Lisa et al. 2014. “Fibroblast Growth Factor Receptor 3 Interacts with and Activates TGFβ-Activated Kinase 1 Tyrosine Phosphorylation and NFκB Signaling in Multiple Myeloma and Bladder Cancer” ed. Hari K. Koul. *PLoS ONE* 9(1): e86470.

Sarabipour, Sarvenaz, and Kalina Hristova. 2016. “Mechanism of FGF Receptor Dimerization and Activation.” *Nature Communications* 7: 10262.

Schumacher, Fredrick R et al. 2007. “A Common 8q24 Variant in Prostate and Breast Cancer from a Large Nested Case-Control Study.” *Cancer Research* 67(7): 2951–56.

Sebestyén, Endre et al. 2016. “Large-Scale Analysis of Genome and Transcriptome

Alterations in Multiple Tumors Unveils Novel Cancer-Relevant Splicing Networks." *Genome Research* 26(6): 732–44.

Seiler, Michael et al. 2018. "H3B-8800, an Orally Available Small-Molecule Splicing Modulator, Induces Lethality in Spliceosome-Mutant Cancers." *Nature Medicine* 24: 497–504.

Seol, Dai-Wu, and Timothy R Billiar. 1999. "A Caspase-9 Variant Missing the Catalytic Site Is an Endogenous Inhibitor of Apoptosis." *The Journal of Biological Chemistry* 274(4): 2072–76.

Sharma, Ankur et al. 2010. "The Retinoblastoma Tumor Suppressor Controls Androgen Signaling and Human Prostate Cancer Progression." *The Journal of Clinical Investigation* 120(12): 4478–92.

Shuch, Brian et al. 2004. "Racial Disparity of Epidermal Growth Factor Receptor Expression in Prostate Cancer." *Journal of Clinical Oncology* 22(23): 4725–29.

Shultz, J. C. et al. 2011. "SRSF1 Regulates the Alternative Splicing of Caspase 9 Via A Novel Intronic Splicing Enhancer Affecting the Chemotherapeutic Sensitivity of Non-Small Cell Lung Cancer Cells." *Molecular Cancer Research* 9(7): 889–900.

Sidarovich, Anzhalika et al. 2017. "Identification of a Small Molecule Inhibitor That Stalls Splicing at an Early Step of Spliceosome Activation." *eLife* 6.

Siegel, Rebecca L., Kimberly D. Miller, and Ahmedin Jemal. 2019. "Cancer Statistics, 2019." *CA: A Cancer Journal for Clinicians* 69(1): 7–34.

Siegel, Rebecca L, Kimberly D Miller, and Ahmedin Jemal. 2015. "Cancer Statistics, 2015." *CA: a cancer journal for clinicians* 65(1): 5–29.

Siqueira, Raoni Pais et al. 2015. "Potential Antileukemia Effect and Structural Analyses of SRPK Inhibition by N-(2-(Piperidin-1-Yl)-5-(Trifluoromethyl)Phenyl)Isonicotinamide (SRPIN340)" ed. Emanuele Buratti. *PLOS ONE* 10(8): e0134882.

Soret, J. et al. 2005. "Selective Modification of Alternative Splicing by Indole Derivatives That Target Serine-Arginine-Rich Protein Splicing Factors." *Proceedings of the National Academy of Sciences* 102(24): 8764–69.

Spratt, Daniel E. et al. 2016. "Racial/Ethnic Disparities in Genomic Sequencing." *JAMA Oncology* 2(8): 1070.

Sramkoski, R. Michael et al. 1999. "A New Human Prostate Carcinoma Cell Line, 22Rv1." *In Vitro Cellular & Developmental Biology - Animal* 35(7): 403–9.

Stockley, Jacqueline et al. 2015. "The RNA-Binding Protein Sam68 Regulates Expression and Transcription Function of the Androgen Receptor Splice Variant

AR-V7." *Scientific Reports* 5(1): 13426.

Stoyanova, Tanya et al. 2013. "Prostate Cancer Originating in Basal Cells Progresses to Adenocarcinoma Propagated by Luminal-like Cells." *Proceedings of the National Academy of Sciences* 110(50): 20111–16.

Sun, Shihua et al. 2010. "Castration Resistance in Human Prostate Cancer Is Conferred by a Frequently Occurring Androgen Receptor Splice Variant." *The Journal of Clinical Investigation* 120(8): 2715–30.

Supek, Fran et al. 2014. "Synonymous Mutations Frequently Act as Driver Mutations in Human Cancers." *Cell* 156(6): 1324–35.

Taioli, Emanuela et al. 2013. "Polymorphisms in CYP17 and CYP3A4 and Prostate Cancer in Men of African Descent." *The Prostate* 73(6): 668–76.

Tan, Li et al. 2014. "Development of Covalent Inhibitors That Can Overcome Resistance to First-Generation FGFR Kinase Inhibitors." *Proceedings of the National Academy of Sciences* 111(45): E4869-77..

Tang, Deliang et al. 2013. "Methylation of the RARB Gene Increases Prostate Cancer Risk in Black Americans." *The Journal of Urology* 190(1): 317–24.

Taylor, Barry S. et al. 2010. "Integrative Genomic Profiling of Human Prostate Cancer." *Cancer Cell* 18(1): 11–22.

Terry, Stéphane et al. 2013. "Cross Modulation between the Androgen Receptor Axis and Protocadherin-PC in Mediating Neuroendocrine Transdifferentiation and Therapeutic Resistance of Prostate Cancer." *Neoplasia* 15(7): 761–72.

Teslow, Emily A. et al. 2018. "Exogenous IL-6 Induces MRNA Splice Variant MBD2_v2 to Promote Stemness in TP53 Wild-Type, African American PCa Cells." *Molecular Oncology*.

Theodore, Shaniece et al. 2010. "Establishment and Characterization of a Pair of Non-Malignant and Malignant Tumor Derived Cell Lines from an African American Prostate Cancer Patient." *International Journal of Oncology* 37(6): 1477–82.

Theodore, Shaniece C. et al. 2014. "MicroRNA Profiling of Novel African American and Caucasian Prostate Cancer Cell Lines Reveals a Reciprocal Regulatory Relationship of *MiR-152* and DNA Methyltransferase 1." *Oncotarget* 5(11): 3512–25.

Theodore, Shaniece C, Johng S Rhim, Timothy Turner, and Clayton Yates. 2010. "MiRNA 26a Expression in a Novel Panel of African American Prostate Cancer Cell Lines." *Ethnicity and Disease* 20(1 Suppl 1): S1-96–100.

Tomlins, Scott A. et al. 2007. "Distinct Classes of Chromosomal Rearrangements Create Oncogenic ETS Gene Fusions in Prostate Cancer." *Nature* 448(7153): 595–99.

Tomlins, Scott A et al. 2005. “Recurrent Fusion of TMPRSS2 and ETS Transcription Factor Genes in Prostate Cancer.” *Science (New York, N.Y.)* 310(5748): 644–48.

Tomlinson, DC, O Baldo, P Harnden, and MA Knowles. 2007. “FGFR3 Protein Expression and Its Relationship to Mutation Status and Prognostic Variables in Bladder Cancer.” *The Journal of Pathology* 213(1): 91–98.

Tosoian, Jeffrey J. et al. 2017. “Prevalence and Prognostic Significance of PTEN Loss in African-American and European-American Men Undergoing Radical Prostatectomy.” *European Urology* 71(5): 697–700.

Trudel, Suzanne et al. 2005. “CHIR-258, a Novel, Multitargeted Tyrosine Kinase Inhibitor for the Potential Treatment of t(4;14) Multiple Myeloma.” *Blood* 105(7): 2941–48.

Tummala, Ramakumar, Wei Lou, Allen C Gao, and Nagalakshmi Nadiminty. 2017. “Quercetin Targets HnRNPA1 to Overcome Enzalutamide Resistance in Prostate Cancer Cells.” *Molecular Cancer Therapeutics* 16(12): 2770–79.

Tyson, Mark D., and Erik P. Castle. 2014. “Racial Disparities in Survival for Patients With Clinically Localized Prostate Cancer Adjusted for Treatment Effects.” *Mayo Clinic Proceedings* 89(3): 300–307.

Uehara, Taisuke et al. 2017. “Selective Degradation of Splicing Factor CAPERα by Anticancer Sulfonamides.” *Nature Chemical Biology* 13(6): 675–80.

Uzor, Simon et al. 2018. “Autoregulation of the Human Splice Factor Kinase CLK1 through Exon Skipping and Intron Retention.” *Gene* 670: 46–54.

Varghese, Frency, Amirali B Bukhari, Renu Malhotra, and Abhijit De. 2014. “IHC Profiler: An Open Source Plugin for the Quantitative Evaluation and Automated Scoring of Immunohistochemistry Images of Human Tissue Samples.” ed. Syed A. Aziz. *PloS one* 9(5): e96801.

Vu, Ngoc T. et al. 2013. “HnRNP U Enhances Caspase-9 Splicing and Is Modulated by AKT-Dependent Phosphorylation of HnRNP L.” *Journal of Biological Chemistry* 288(12): 8575–84.

Wainstein, Mark A et al. 1994. “CWR22: Androgen-Dependent Xenograft Model Derived from a Primary Human Prostatic Carcinoma1.” *Cancer Research* 54(23): 6049–52.

Wallace, T. A. et al. 2008. “Tumor Immunobiological Differences in Prostate Cancer between African-American and European-American Men.” *Cancer Research* 68(3): 927–36.

Wan, Xinhai et al. 2014. “Prostate Cancer Cell-Stromal Cell Crosstalk via FGFR1 Mediates Antitumor Activity of Dovitinib in Bone Metastases.” *Science*

Translational Medicine 6(252): 252ra122.

Wang, Bi-Dar et al. 2013. "Androgen Receptor-Target Genes in African American Prostate Cancer Disparities." *Prostate Cancer* 2013: 1–15.

Wang, Bi-Dar et al. 2015. "Identification and Functional Validation of Reciprocal MicroRNA-MRNA Pairings in African American Prostate Cancer Disparities." *Clinical Cancer Research* 21(21): 4970–84.

Wang, Bi-Dar et al. 2017. "Alternative Splicing Promotes Tumour Aggressiveness and Drug Resistance in African American Prostate Cancer." *Nature Communications* 8(15921): 1–14.

Wang, Bi-Dar, and Norman H Lee. 2018. "Aberrant RNA Splicing in Cancer and Drug Resistance." *Cancers* 10(11): pii: E458.

Wang, Cong et al. 2018. "Ectopic Fibroblast Growth Factor Receptor 1 Promotes Inflammation by Promoting Nuclear Factor-KB Signaling in Prostate Cancer Cells." *Journal of Biological Chemistry* 293: 14839–49.

Wang, Eric T. et al. 2008. "Alternative Isoform Regulation in Human Tissue Transcriptomes." *Nature* 456(7221): 470–76.

Wang, Hai Tao et al. 2014. "Neuroendocrine Prostate Cancer (NEPC) Progressing From Conventional Prostatic Adenocarcinoma: Factors Associated With Time to Development of NEPC and Survival From NEPC Diagnosis—A Systematic Review and Pooled Analysis." *Journal of Clinical Oncology* 32(30): 3383–90.

Wang, J et al. 2015. "Ligand-Associated ERBB2/3 Activation Confers Acquired Resistance to FGFR Inhibition in FGFR3-Dependent Cancer Cells." *Oncogene* 34(17): 2167–77.

Wang, Xi et al. 2009. "A Luminal Epithelial Stem Cell That Is a Cell of Origin for Prostate Cancer." *Nature* 461(7263): 495–500.

Wang, Xiaofei et al. 2015. "Gene Expression Profiling Analysis of Castration-Resistant Prostate Cancer." *Medical Science Monitor* 21: 205–12.

Wang, Yang et al. 2014. "The Splicing Factor RBM4 Controls Apoptosis, Proliferation, and Migration to Suppress Tumor Progression." *Cancer Cell* 26(3): 374–89.

Webster, M K, and D J Donoghue. 1996. "Constitutive Activation of Fibroblast Growth Factor Receptor 3 by the Transmembrane Domain Point Mutation Found in Achondroplasia." *The EMBO Journal* 15(3): 520–27.

Wei, Runmin et al. 2016. "Meta-Dimensional Data Integration Identifies Critical Pathways for Susceptibility, Tumorigenesis and Progression of Endometrial

Cancer." *Oncotarget* 7(34): 55249–63.

Will, Cindy L, and Reinhard Lührmann. 2011. "Spliceosome Structure and Function." *Cold Spring Harbor Perspectives in Biology* 3(7): a003707.

Wongpalee, Somsakul Pop, and Shalini Sharma. 2014. "The Pre-MRNA Splicing Reaction." In *Methods in Molecular Biology*, 3–12.

Woods-Burnham, Leanne et al. 2017. "The 22Rv1 Prostate Cancer Cell Line Carries Mixed Genetic Ancestry: Implications for Prostate Cancer Health Disparities Research Using Pre-Clinical Models." *The Prostate* 77(16): 1601–8.

Woolard, J et al. 2004. "VEGF165b, an Inhibitory Vascular Endothelial Growth Factor Splice Variant: Mechanism of Action, in Vivo Effect on Angiogenesis and Endogenous Protein Expression." *Cancer Research* 64: 7822–35.

Wu, Jennifer N. et al. 2014. "No Improvement Noted in Overall or Cause-Specific Survival for Men Presenting with Metastatic Prostate Cancer over a 20-Year Period." *Cancer* 120(6): 818–23.

Wu, Yi-Mi et al. 2013. "Identification of Targetable FGFR Gene Fusions in Diverse Cancers." *Cancer Discovery* 3(6): 636–47.

Xin, Xiaohua et al. 2006. "CHIR-258 Is Efficacious in a Newly Developed Fibroblast Growth Factor Receptor 3-Expressing Orthotopic Multiple Myeloma Model in Mice." *Clinical Cancer Research* 12(16): 4908–15.

Xu, Kexin et al. 2012. "EZH2 Oncogenic Activity in Castration-Resistant Prostate Cancer Cells Is Polycomb-Independent." *Science* 338(6113): 1465–69.

Yadav, Shalini S. et al. 2017. "Induction of Neuroendocrine Differentiation in Prostate Cancer Cells by Dovitinib (TKI-258) and Its Therapeutic Implications." *Translational Oncology* 10(3): 357–66.

Yadav, Shalini S et al. 2015. "Next-Generation Sequencing Technology in Prostate Cancer Diagnosis, Prognosis, and Personalized Treatment." *Urologic Oncology: Seminars and Original Investigations* 33(6): 267.e1-267.e13.

Yang, Feng et al. 2013. "FGFR1 Is Essential for Prostate Cancer Progression and Metastasis." *Cancer Research* 73(12).

Yang, Y. et al. 2016. "Dysregulation of MiR-212 Promotes Castration Resistance through HnRNPH1-Mediated Regulation of AR and AR-V7: Implications for Racial Disparity of Prostate Cancer." *Clinical Cancer Research* 22(7): 1744–56.

Yoshida, Kenichi et al. 2011. "Frequent Pathway Mutations of Splicing Machinery in Myelodysplasia." *Nature* 478(7367): 64–69.

Yoza, K et al. 2016. “Biophysical Characterization of Drug-Resistant Mutants Offibroblast Growth Factor Receptor 1.” *Genes to Cells* 21: 1049–58.

Zhang, Guanyi et al. 2015. “Androgen Receptor Splice Variants Circumvent AR Blockade by Microtubule-Targeting Agents.” *Oncotarget* 6(27): 23358–71.

Zhou, Zhihong, and Xiang-Dong Fu. 2013. “Regulation of Splicing by SR Proteins and SR Protein-Specific Kinases.” *Chromosoma* 122(3): 191–207.

Zuiverloon, Tahlita C.M. et al. 2011. “No Evidence of FGFR3 Mutations in Prostate Cancer.” *The Prostate* 71(6): 637–41.

Appendix

1) Permission to reuse portions of Figure 2 and Figure 3 for **Figure 1** from Cronin, Kathleen A, Andrew J Lake, Susan Scott, et al. 2018. "Annual Report to the Nations on the Status of Cancer, part I: National Cancer Statistics." *Cancer* 124(13): 2785-2800:

"This article is available under the terms of the Creative Commons Attribution Non-Commercial License CC BY-NC (which may be updated from time to time) and permits non-commercial use, distribution and reproduction in any medium, provided the original work is properly cited.

For an understanding of what is meant by the terms of the Creative Commons License, please refer to Wiley's Open Access Terms and Conditions.

Permission is not required for non-commercial reuse."

- https://s100.copyright.com/AppDispatchServlet#formTop

2) Permission to reuse NCI SEER*Explorer Database content for **Figure 2** and **Figure 3** from *https://seer.cancer.gov/explorer/*:

"Graphics explicitly credited to NCI are copyright-free and may be used without our permission. Please credit the National Cancer Institute as the source. Visit NCI Visuals Online to find copyright-free images you may download and use."

-https://www.cancer.gov/policies/copyright-reuse

3) Permission to reuse cBioPortal content for Figure 5 from *https://www.cbioportal.org/results/cancerTypesSummary?Action=Submit&cancer_study_list=msk_impact_2017&case_set_id=msk_impact_2017_all&clinicallist=NUM_SAMPLES_PER_PATIENT&gene_list=FGFR3&genetic_profile_ids_PROFILE_COPY_NUMBER_ALTERATION=msk_impact_2017_cna&genetic_profile_ids_PROFILE_MUTATION_EXTENDED=msk_impact_2017_mutations&show_samples=false&tab_index=tab_visualize* :

"Can I use figures from the cBioPortal in my publications or presentations?

Yes, you are free to use any of the figures from the portal in your publications or presentations (many are available in SVG or PDF format for easier scaling and editing). When you do, please cite Cerami et al., Cancer Discov. 2012, and Gao et al., Sci. Signal. 2013 (see the previous question for full citations)."

-https://www.cbioportal.org/faq#can-i-use-figures-from-the-cbioportal-in-my-publications-or-presentations

4) Permission to reuse Springer Nature content for **Figure 6** and **Figure 7** from *Wang, Bi-Dar et al. 2017. "Alternative Splicing Promotes Tumour Aggressiveness and Drug Resistance in African American Prostate Cancer." Nature Communications 8(15921): 1–14*:

"The author of articles published by Springer Nature do not usually need to seek permission for re-use of their material as long as the journal is credited with initial publication.

Ownership of copyright in in original research articles remains with the Author, and provided that, when reproducing the contribution or extracts from it or from the Supplementary Information, the Author acknowledges first and reference publication in the Journal, the Author retains the following non-exclusive rights:

To reproduce the contribution in whole or in part in any printed volume (book or thesis) of which they are the author(s)."

- https://www.nature.com/reprints/permission-requests.html

5) Permission to reuse unmodified content from Promega Corporation for **Figure 24** from *https://www.promega.com/-/media/files/resources/protocols/kinase-enzyme-appnotes/fgfr1-kinase-assay-protocol.pdf?la=en (Figure 1)*:

Thomas Contreras thomas.contreras@promega.com
To: "olenderj@gwu.edu" olenderj@gwu.edu
Subject: Promega Website Image Usage Permission
Wed, Apr 10, 2019 at 1:14 PM

Hi Jacqueline,
So I got my answer, for dissertations and other educational materials that will not be sold, our policy is to allow use of the figure as long as Promega Corporation is credited in the figure legend (and where possible a link to the original is included). I hope that helps and let me know if you need anything else.

Thank You

Thomas Contreras

Customer Service Representative

Phone: 1.800.356.9526 Ext. 3506 (USA & Canada)

Phone: 1.608.274.4330 Ext. 3506 (Toll)